CHARACTERISTICS OF AFRP BARS FOR PRESTRESSING APPLICATIONS

A Thesis

by

JOSE CARLOS MEDINA JR.

Submitted to the Office of Graduate Studies of
Texas A&M University
in partial fulfillment of the requirements for the degree of

MASTER OF SCIENCE

December 2011

Major Subject: Civil Engineering

Characteristics of AFRP Bars for Prestressing Applications

CHARACTERISTICS OF AFRP BARS FOR PRESTRESSING APPLICATIONS

A Thesis

by

JOSE CARLOS MEDINA JR.

Submitted to the Office of Graduate Studies of
Texas A&M University
in partial fulfillment of the requirements for the degree of

MASTER OF SCIENCE

Approved by:

Chair of Committee,	Monique Head
Committee Members,	John Mander
	Stefan Hurlebaus
	Yong-Joe Kim
Head of Department,	John Niedzwecki

December 2011

Major Subject: Civil Engineering

ABSTRACT

Characteristics of AFRP Bars for Prestressing Applications.

(December 2011)

Jose Carlos Medina Jr., B.S., Texas A&M University

Chair of Advisory Committee: Dr. Monique Head

Aramid fiber reinforced polymer (AFRP) composite materials show promise for prestressed concrete bridge applications. However, there are still some knowledge gaps due to lack of sufficient data to assess the long-term performance and therefore sustainability of beams prestressed with AFRP composite materials. The objective of this research is to effectively characterize the material properties based on the short-term and long-term characteristics of AFRP bars. Tensile, creep-rupture, and relaxation tests are experimentally conducted using AFRP bars to validate testing procedures and expand an existing limited database. Previous results from tensile tests show that the stress-strain behavior of Arapree® AFRP bars is linear until failure with tensile strength of approximately 210 ksi (1448 MPa) and strain of 2.1%. For the creep-rupture tests, three specimens are tested and monitored at four different load levels (50, 60, 75 and 85% of maximum tensile strength) throughout a period of 14 days (short-term evaluation) and 42 days (long-term evaluation). From these tests, it is expected that for a 100-year life span, 55% of the ultimate load, $F_{u,}$ must be applied as an initial stress to obtain a long-term residual strength of 0.80 F_u. For the relaxation tests, six specimens at

four different strain levels (50, 60, 75 and 85% of maximum tensile strain) are tested and monitored throughout a period of 14 days and 42 days. Relaxation loss profiles of the AFRP bars are developed based on the experimental data collected from prestressed AFRP bars, which have been less well understood given lack of sufficient experimental data. Overall, the results of this study provide more insight as to the reliability and potential long-term performance of AFRP bars embedded within prestressed bridge structures.

DEDICATION

To my family who has never doubted my ability to succeed regardless of any obstacles. My greatest appreciation extends to all of them for always supporting me.

ACKNOWLEDGEMENTS

I would like to acknowledge the support and guidance of my advisor, Dr. Monique Head. I would like to recognize all of my committee members, Dr. Hurlebaus, Dr. Mander, and Dr. Kim, and fellow researcher Shobeir Pirayeh Gar for their gracious help. This study was sponsored by the National Science Foundation (NSF) Project 0927333.

Finally, thanks to my mother and father for their encouragement, and to my wife for being extremely supportive, patient and loving.

NOMENCLATURE

P	Axial Tensile Load on AFRP Bar
P_u	Ultimate Tensile Load Capacity of AFRP Bar
m	Relaxation Rate or Slope
T	Time
FRP	Fiber Reinforced Polymer
AFRP	Aramid Fiber Reinforced Polymer
CFRP	Carbon Fiber Reinforced Polymer
GFRP	Glass Fiber Reinforced Polymer
BRC	Reinforced Concrete Beam
FRP RC Beam	Fiber Reinforced Polymer Reinforced Concrete Beam
M	Moment
M_{cr}	Cracking Moment
I_{cr}	Crack Moment of Inertia
I_e	Effective Moment of Inertia

TABLE OF CONTENTS

Page

LIST OF FIGURES

Page

LIST OF TABLES

Page

1. INTRODUCTION

1.1 Motivation

Reinforced concrete structures have been known to deteriorate in part due to corrosion of reinforcing steel that has the potential to weaken structures and decrease its durability. Furthermore, critical infrastructure of the United States, particularly roadways and bridges, are deteriorating due to cracking, being overloaded, and lack of needed repair. This is a major concern as the economy of the U.S. is greatly tied to its transportation system, where bridges are an integral part of that network that connects people and businesses. Therefore, it is important to make the inspection, maintenance, and repair of these structures a high priority for life safety and for advancing the art and practice of bridge design.

1.2 Problem Statement

Some methods that have been used to address these issues but have not successfully nor economically solved this dilemma are galvanization, stainless steel rebar, cathodic additions, and epoxy coated steel, to name a few. One alternative has been the development of fiber reinforced polymers (FRP) such as, aramid FRP (AFRP), carbon FRP (CFRP), and glass FRP (GFRP) bars, which have been used to replace conventional reinforcing steel. These materials have been previously used in military and aerospace applications. However, application of these materials for prestressed bridge structures has been limited in the U.S. although some attempts for deployment have been made abroad (Shahaway et al. 2007). FRP bars, in particular, have

---

This thesis follows the style of ASCE *Journal of Composites for Construction©.*

advantageous material properties such as corrosion resistance to de-icing salts, high strength, high fatigue resistance, non-conductivity, easy to handle, significant reduction in maintenance, and lightweight. Corrosion resistant materials assist in preventing premature spalling or corrosion-induced cracking, where longitudinal cracks and leakage between deck slabs and beams are of major concern (Shahaway et al. 2007). But, FRP materials have a low modulus of elasticity, about 3 times less than conventional reinforcing steel, resulting in larger deflections, in post-cracking regions. AFRP bars show promise as an emerging FRP with an ultimate strain capacity of approximately 2-4.6% when compared to an ultimate strain capacity of less than 3% for CFRP and GFRP bars. Consequently, further research on the material characterization and mechanical properties as well as predicting the structural behavior of AFRP bars embedded in concrete is needed to better improve the implementation of these materials into design practice.

Given the limited use and potential for beneficial use of AFRP bars in prestressed concrete bridge applications, there is a need to establish a performance-based design methodology that accurately reflects the response of a bridge system prestressed with AFRP bars and subjected to service and ultimate loads. But first, the material characteristics of the AFRP bars need to be evaluated, where the focus of the research presented herein is to determine the Arapree® AFRP bar's short-term and long-term mechanical behavior. The data from tensile tests, the modulus of elasticity, axial tensile capacity, and failure strain will be recorded. By conducting short-term and long-term relaxation tests, the prestress losses can be better understood, concrete effect on

relaxation will be observed, and prediction of relaxation losses will be shown. Furthermore, data from short-term and long-term creep-rupture tests will also reveal the effects of creep in the AFRP bars from high and low stress conditions as well as the effects of creep on the concrete needed to predict the 100-year design life.

2. LITERATURE REVIEW

2.1 State-of-the-Art

This section focuses on the evaluation of the current state-of-the-art of AFRP bars that have been previously used in prestressed concrete and reinforced concrete structures to assess their behavior and identify performance concerns.

2.1.1 Material Properties of AFRP Bars

Quantifying the material properties of AFRP bars has presented several challenges given the ability of these composite materials to creep and relax over time. Tests on pre- and post-tensioned slabs using Kevlar (a type of aramid material) reinforced bars have been conducted by Dolan (1989). Dolan's research consisted of six bars each having a diameter ø ⅛" (3 mm) and 5000 Kevlar fibers. A vinyl ester resin was applied for the fabrication of the rod. Dolan also conducted one-quarter scale tests on 7'-10" (2.38 m) long, 4" (10 cm) deep, and 6" (15 cm) wide beams. The results from his one-quarter scale beam tests using the Kevlar bars showed considerable ductility and virtually complete recovery after the removal of the load (Dolan 1989). Although the failure of AFRP bars is sudden, they have high tensile strengths up to 300 ksi (2068 MPa), and show sufficient strain (2-3% strain) and have a specific gravity more than 6 times less than steel. Moreover, the modulus of elasticity of AFRP bars, which is about 4 times less than steel, is beneficial in that a longer extension of the tendon is required during initial stressing and losses from creep and shrinkage of the concrete are less (Dolan 1990). However, more research is needed to justify using prestressed AFRP bars

given their failure mode and tendency to creep and relax over time with dependence on temperature and environment.

McKay and Erki (1992) found that the relaxation losses of AFRP tendons are higher than conventional steel with losses of 10-12% for a 50-year duration. McKay and Erki (1992) also found that the design theory for pre-tensioned steel beams was adequate for predicting cracking behavior, development length, transfer length, and ultimate moment of an AFRP pre-tensioned beam. However, post-cracking deflections were found to be overly conservative (McKay and Erki 1992). Furthermore, McKay and Erki (1992) found that the fatigue strength of 0.24 in (6.0 mm) nominal diameter AFRP rods is at least equal to that of steel strands under service stresses as noted in the two beams that they tested. These results, however, are highly dependent on the assumed material properties. Therefore, accurate material characterization is a critical part of accurately predicting this behavior, and therefore the focus of the research results presented in this thesis.

Mukae (1993) worked on material characterization of AFRP rods and conducted tensile, creep-rupture and fatigue tests. Using 0.24 in (6.0 mm) diameter rods like McKay and Erki (1992), he concluded that the average tensile strength of these AFRP rods was 274 ksi (1890 MPa). The creep-rupture test was conducted at stress level of 70-95% of ultimate, where it was concluded that the estimated stress level that produces a lifetime expectancy of 100 years is approximately 61% or 154 ksi (1060 MPa).

Previous studies of creep-rupture phenomena of AFRP bars have revealed the need for further investigation in different environments such as being embedded in

concrete, alkaline solution, and acidic solution, and exposed to varying temperatures (Bludelmann and Rostasy (1993). In order to effectively assess the reliability of the creep-rupture behavior of AFRP bars embedded in concrete, Scheibe and Rostasy (1996) suggested that long-term tests be conducted to failure to predict the life expectancy of AFRP bars, which is addressed in this thesis.

AFRP bars may exhibit good recovery like CFRP bars as revealed by Grace and Sayed (1997), where small residual displacements can be beneficial, especially during an earthquake. Previous work conducted by Grace and Sayed (1997) from the Lawrence Technological University in Southfield, Michigan has demonstrated that the use of carbon fiber reinforced polymer (CFRP) composite prestressing tendons can be designed to perform in a ductile manner. This ductility found in a concrete structure such as when prestressed with steel strands is defined by the structure's ability to sustain inelastic deformation without loss in their load carrying capacity prior to failure as shown in Figure 1 (Grace and Sayed 1997). Figure 2 shows this ductility of CFRP tendons in a prestressed concrete girder conducted by Grace and Sayed (1997).

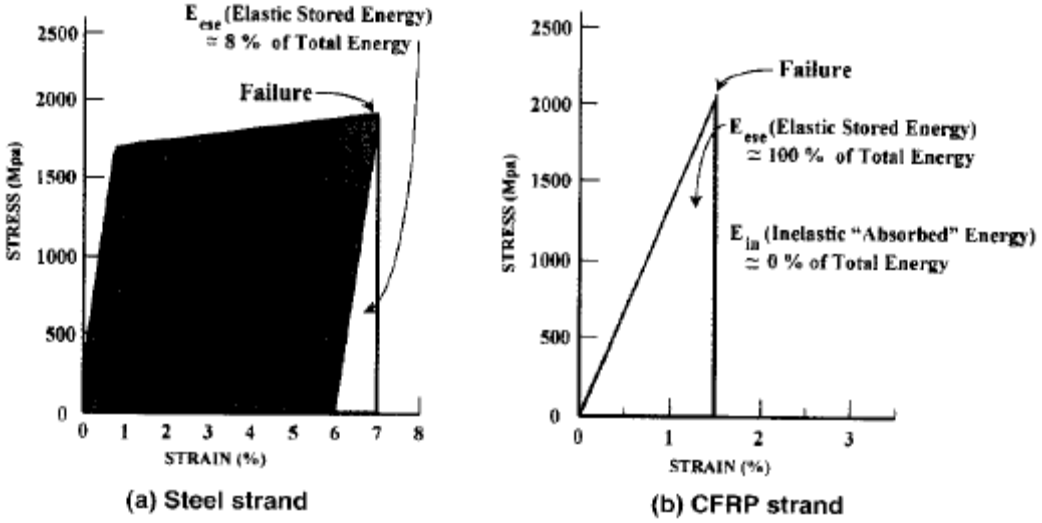

Figure 1 Percentage of stored and absorbed energies of steel and CFRP strands (Grace and Sayed 1997)

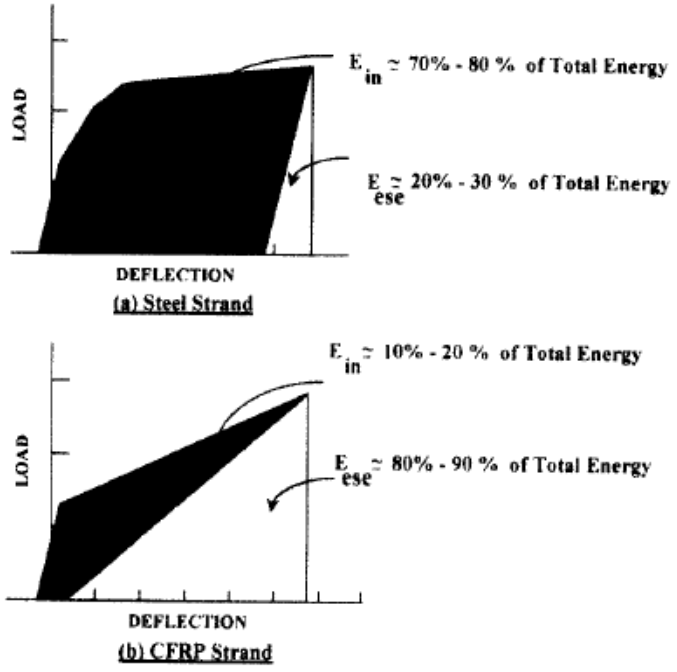

Figure 2 Stored and absorbed energies in prestressed concrete girders (Grace and Sayed 1997)

Creep-rupture test on AFRP bars (Arapree, ø 0.30 in (7.5 mm)) were conducted by Sheibe and Rostasy (1998). The tests were conducted at 75% of ultimate stress level of the Arapree® AFRP bars. Five specimens were tested at each of the following conditions: (1) dry air 68°F (20°C)/65% relative humidity, sealed 68°F (20°C), alkaline solution 68°F (20° C), alkaline solution 140°F (60°C), water 140°F (60° C). The lifetimes for each of the various environments tested were different and the moisture content of concrete seemed to play a vital role in the damage. Scheibe and Rostasy (1998) also tested AFRP bars which had been subjected to a long-term static axial stress of 0.7 to 0.8 of ultimate for one and two year of exposure in concrete, which were retrieved from tested slabs. Then, they were subjected to stress-rupture tests in alkaline solution having a temperature of 68°F (20°C). These tests showed that while embedded in concrete and exposed to outdoor weather conditions, a certain loss of long-term strength had occurred. However, if the loading was preceded by pre-loading the bars, then the lifetimes roughly correspond to the stress-rupture lines in dry air Sheibe and Rostasy (1998). Further research is needed to model the behavior of AFRP in concrete elements stored outdoors (Sheibe and Rostasy, 1998).

Saadatmanesh and Tannous (1999) also worked with AFRP bars and investigated their long-term behavior. From their relaxation tests, they analyzed Arapree® AFRP bars having a diameter of 0.39 in. (10 mm), and tested at -22°F (-30°C), -4°F (25°C), and 140°F (60°C) in air. They also tested at a pH of 12 for 77°F (25°C) and 140°F (60°C) and salt solution for 77°F (25°C) and 140°F (60°C). In order to eliminate slippage and grip settling from their data, testing was conducted one hour after initial loading.

Also a preliminary investigation of creep of the AFRP bars in air and alkaline solutions ($Ca(OH)_2$ pH=12,HCl pH=3, and NaCl) were also conducted by Saadatmanesh and Tannous (1999). From their results they concluded that relaxation losses increase with increase in temperature and relaxation losses in air were lower than those in solutions. The creep behavior was observed to be good in air (0.025% creep for 3000 hours) and alkaline solutions (0.04% creep for 3000 hours), but at a lower level for acidic solutions (0.027% creep for 3000 hours) when stressed to 40% of ultimate strength.

In other creep-rupture experiments conducted by Dolan et al. (2001), partial failure of a tendon occurred from the possibility of a manufacturing defect, which suggests another concern about these materials that must be resolved before full commercial development of material tendons (Dolan et al. 2001). Likewise, similar defective testing should be conducted to detect defects in the AFRP materials before conducting experimental testing.

2.1.2 Flexural Behavior of AFRP Bars

Additional research has experimentally evaluated the flexural behavior of AFRPs prestressed in concrete to show that the performance of AFRP bars is adequate for implementation. Toutanji and Saafi (1999) conducted a series of flexural tests in order to determine the best prestressing technique (either pre-tensioning, post-tensioning unbonded, or post-tension bonded) that would provide the most ductile failure versus the expected brittle failure of AFRP composites. From these tests, Toutanji and Saafi (1999)

found that brittle failure of prestressed bonded AFRP bars could be avoided in three ways as shown in Figure 3: 1) using unbonded rather than bonded bars, 2) using a combination of bonded and unbonded bars, and 3) adding non-prestressed bars. The results from these three cases are shown in Figure 4. The combination of bonded tendons with unbonded bars, as illustrated in Figure 4, when tested showed more ductile behavior using a ductility index, which was not evident when only bonded bars were present. Again, the ductility index can be defined as the ratio of total deformation at ultimate load to the elastic limit deformation. More results from an investigation conducted by Lees and Burgoyne (2000) concluded that the use of partially-bonded AFRP bars could be incorporated into the design of prestressed beams as their behavior shows large rotations, which would provide significant warning prior to collapse. The results to these experiments are quantified in Table 1, which show the prestressing force, bond property, reinforcing method, cracking load, ultimate load, deflection at ultimate, ultimate deflection and failure mode observed from the tests by Lees and Burgoyne (2000).

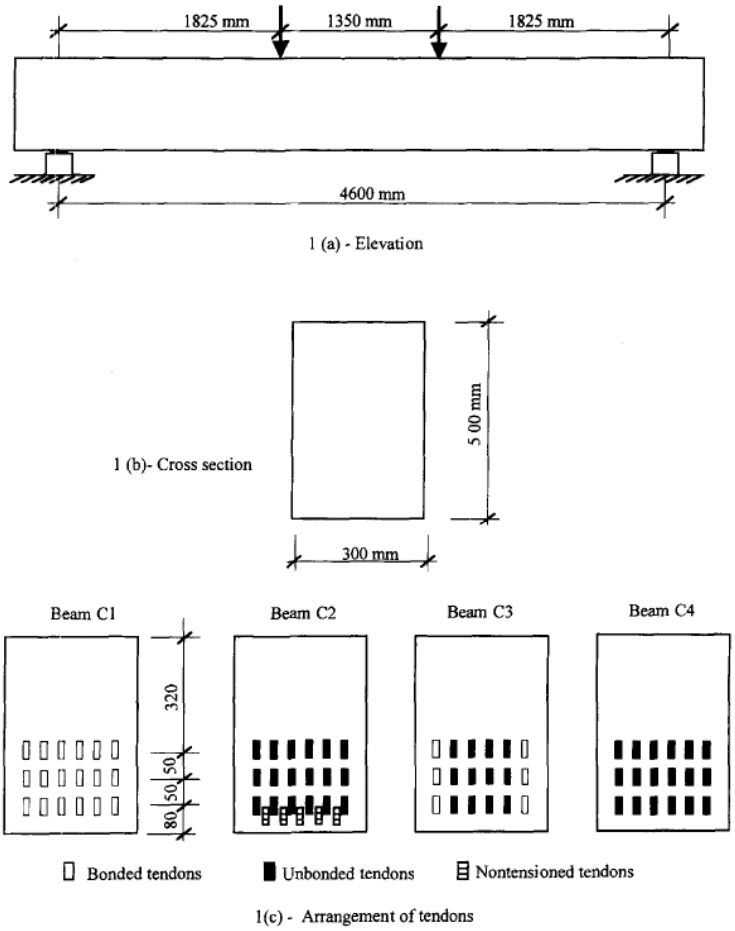

Figure 3 Beam configurations (Toutanji and Saafi 1999)

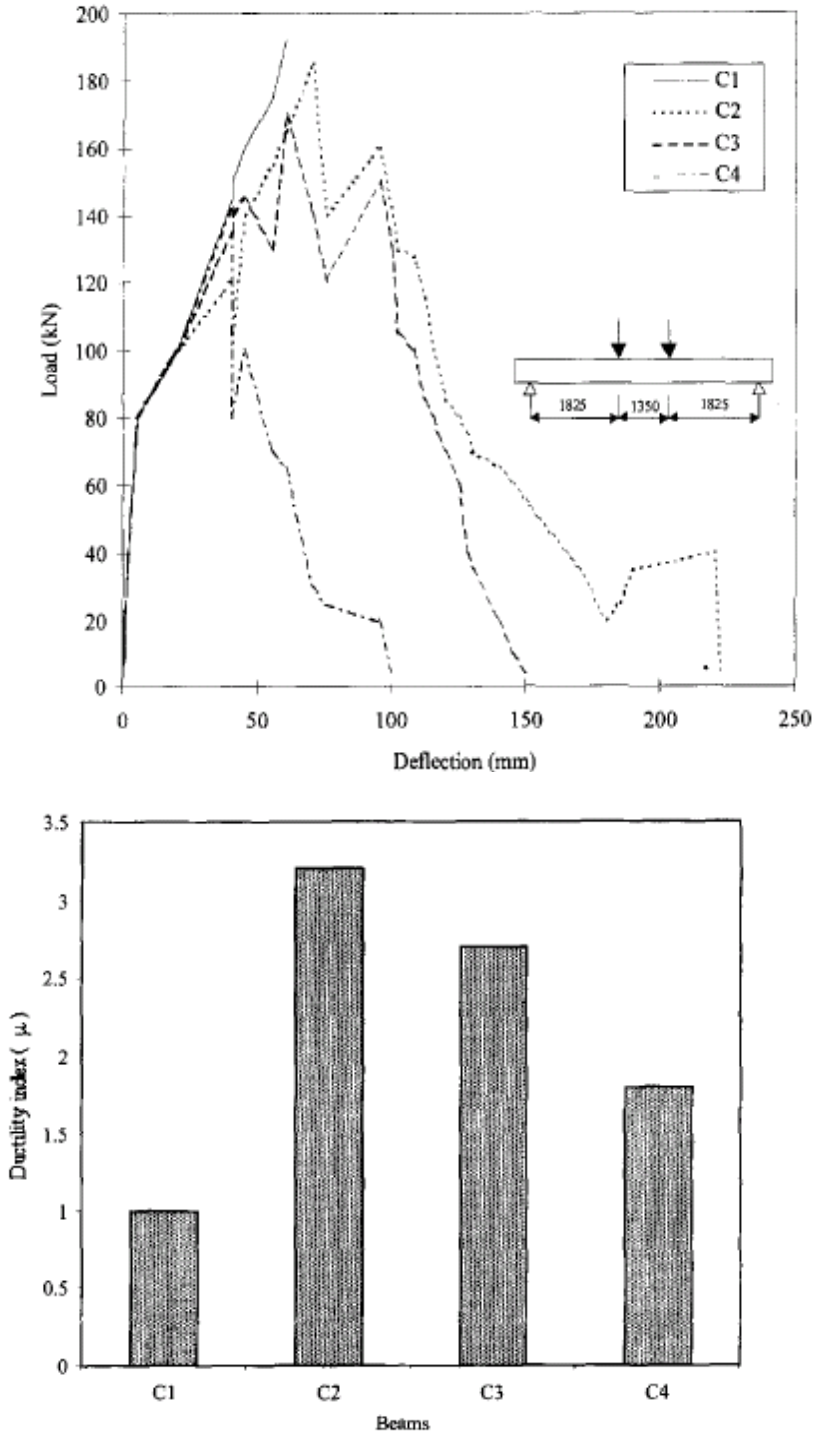

Figure 4 Load-deflection relationship and ductility index of beams (Toutanji and Saafi 1999)

Table 1 Testing methods and experimental results (Lees and Burgoyne 2000)

Beam	Tensioning force (kN per bar)	Bond property	Reinforcement method	Reinforcement ratio (%)
C1	20	Bonded	Prestressed	0.48
C2	20	Unbonded	Prestressed/reinforced	0.68
C3	20	Bonded and unbonded	Prestressed	0.48
C4	20	Unbonded	Prestressed	0.48

Beam	Cracking load (kN)	Ultimate load (kN)	Deflection at ultimate load (mm)	Ultimate deflection (mm)	Observed mode of failure
C1	85	195	59	59	Rupture of tendon
C2	85	185	70	230	Rupture of tendon
C3	86	155	65	155	Rupture of tendon
C4	84.7	143	50	99.5	Rupture of tendon

2.1.3 Bond Behavior and Development

Bond behavior of FRP rebar embedded in concrete has presented some challenges and needs for future research because the current research does not effectively characterize this behavior, which is necessary for determining prestressing losses. Some studies were conducted on the bond behavior of AFRP, CFRP, and GFRP rebar in concrete compared to steel (Okelo et al. 2005) and understanding the flexural behavior of FRP prestressed in concrete. Stress-strain curves, load-deflection modes of failure, load capacity, and cracking patterns were obtained by Dolan et al. (2001) and Shahaway et al. (2007). Okelo et al. (2005) tested the bond strength of AFRP, CFRP and GFRP bars, and found that on average the bond strength was in the range of 40-100% of steel. Following this, average bond strengths for any FRP (AFRP, CFRP and GFRP) straight rebar were proposed based on the concrete compressive strength and rebar diameter (Okelo et al. 2005). Some suggested bond improvements including sand coating and stressing external indentions. However, for AFRP bars, the usability of

AFRP bars in prestressed concrete girders using the bond strength of FRP bars at various structural depths have been explored by Okelo et al. (2005). Some of their models included flexural stresses and strains of prestressed concrete beams in compression, which were compared to previous flexural test data of AFRP tendons embedded in high strength concrete beams. The average bond strength was found to decrease as the diameter of bar increase just like in the case of steel. Also, the average bond strength, as shown in Figure 5, for AFRP bars is 40-100% of average bond strength of steel. Due to this large variation it will be important to accurately characterize the average bond strength of the specimen that we will be using in order to accurately predict the prestress losses. Shahaway et al. (2007) evaluated a double-tee concrete girder post-tensioned with aramid tendons for evaluations on flexure, shear and fatigue behavior. The results indicated satisfactory bond behavior until failure, implying that aramid tendons could be used. Linear and non-linear analyses of the beam were performed and compared to the experimental results. Analytical results correlated well with those observed in the experiment.

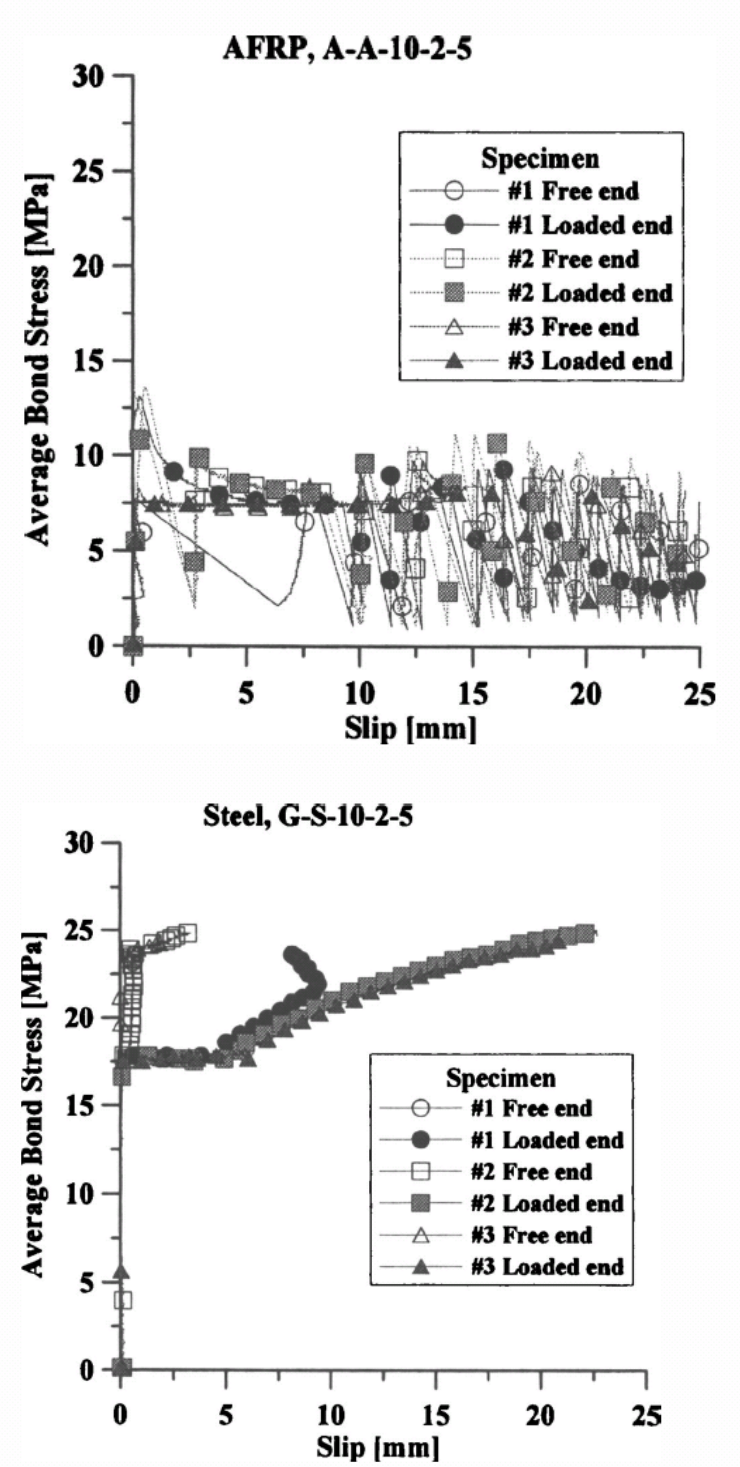

Figure 5 Average bond stress for AFRP bars and steel rebar (Okelo et al. 2005)

2.1.4 Calculation of Effective Moment of Inertia

It is very important to predict the deflections for FRP designed structures, which heavily rely on the calculation of the effective moment of inertia. Since FRPs have a typically lower modulus of elasticity compared to conventional steel, the deflections prior to cracking of concrete are larger than that of steel. Hence, the serviceability region of design will govern for FRPs. For this reason, it is essential to accurately predict the deflections for FRPs. For instance, Rafi et al. (2009) conducted work involving FRP bars as a replacement to steel in reinforced concrete and prestressed concrete structures, including methods for calculating theoretical deflections of beams but are not satisfactory for all types of FRP when compared to experimental data, because GFRP, CFRP and AFRP all have different mechanical properties. Rafi et al. (2009) proposed a method for calculating the effective moment of inertia, I_e, for any FRP reinforced concrete beam to aid with design, which was intended as proposed modifications to ACI 440. The effective moment of inertia of the CFRP reinforced concrete beams (referred to as BRC) was over-estimated by the ACI method for FRP reinforced concrete (RC) structures (Rafi et al. 2009). The analysis conducted by Rafi et al. (2009) showed that the ACI (2006) equation for I_e (Eq. (1)) where, M_{cr} is cracking moment, I_{cr} is the cracked moment of inertia and M is moment, can be used successfully for the deflection prediction of FRP RC beams reinforced with bars having a modulus between 5075 and 7250 ksi (35 and 50 GPa). The deflection, however, is overestimated for FRP bars with a modulus of elasticity, E_f , less than 5075 ksi (35 GPa) and underestimated for FRP bars with a modulus greater than 7250 ksi (50 GPa). Despite excellent deformation recovery

of large deformations in these tests, it was observed that there was a limit for these tendons during the serviceability limit state. At 80% of the theoretical ultimate load, the recovery of the deformation was 95% upon removal of load. Further improvement of I_e Eq. (1) would allow for more accurate predictions of deflections under monotonic loading.

$$I_e = I_{cr}\left[1 + 2.3\left[\frac{M_{cr}}{M}\right]^3\right] \quad (1)$$

2.1.5 Shear Behavior of AFRP Prestressed Beams

To fully characterize and have a complete design procedure, having experimental data and theoretical analysis to understand shear behavior of AFRP prestressed beams as shear failures can occur and result in catastrophic failure. In an experiment performed by Rashid et al. (2005), the performance of high strength concrete beams with AFRP bars as tensile reinforcement and steel bar as shear and compression reinforcements was investigated. It was found that the load-deflection response of these beams significantly differs from that of a steel-reinforced beam in terms of cracking behavior, post-cracking stiffness, magnitudes of deflections and crack widths, and mode of failure. Cracks in AFRP reinforced beams form in quick succession and, upon formation, penetrate deep into the compression side of the beam straight away (Rashid et al. 2005). It was determined that the usual shear design procedure may not be adequate for AFRP prestressed beams, especially when shear is associated with a high bending moment. These findings have led to reducing the maximum spacing of stirrups when large shear and bending moment have been identified in a high strength concrete beam reinforced with AFRPs.

In summary, the evaluation of the state-of-the-art highlighted some other potential failure areas and knowledge gaps that have not been addressed yet but will be addressed in this research, including the ability of AFRP bars to sustain high tensile stresses under service load conditions. As noted by previous investigators, more experimental data is needed for the development of nonlinear stress-strain models for concrete members reinforced with AFRP bars to improve prediction of these structures at large deformations (Bakis 2001), which will be addressed herein.

2.2 State-of-the-Practice

One reason for using AFRP tendons as a high performance material over prestressing steel is due to its high corrosive resistance, high tensile strength, high impact resistance, lightweight, high thermal stability, and insensitivity to electric fields. Corrosion resistant materials assist in preventing premature spalling or corrosion-induced cracking, where longitudinal cracks and leakage between deck slabs and beams are of major concern. Therefore, AFRP bars show promise as an emerging FRP with an ultimate strain capacity of approximately 2-4.6% when compared to an ultimate strain capacity of less than 3% of CFRP and GFRP, AFRP bars are the chosen material for this research. Therefore, further research on the material characterization and mechanical properties as well as predicting the structural behavior of AFRP bars embedded in concrete is needed to better improve the implementation of these materials into design practice.

Large deformations are desirable before failure as AFRP materials have been known to fail in a brittle manner. In prestressing applications, the tendons' durability

and long-term performance are important areas that will be investigated due to the lack of research work involving long-term performance and durability (Shahaway et al. 2007). The importance of determining long-term performance and durability will help in predicting the life expectancy of a structure as well as its serviceability. To arrive at guidelines for transfer lengths, more experimental data is required (Shahaway et al. 2007). In an experiment conducted by Dolan et al. (2001), partial failure of a tendon occurred with possible tie to a manufacturing defect that suggests this issue must be resolved before full commercial development of material tendons (Dolan et al. 2001). Likewise, similar defective testing should be conducted to detect defects in the AFRP material before conducting experimental testing.

Other potential failure areas that have not been addressed yet but will be addressed in this research, which include the ability of AFRP bars to sustain high tensile stresses under service load conditions. More experimental data is needed for the development of nonlinear stress-strain models for concrete members reinforced with AFRP rebar to improve prediction of these structures at large deformations (Bakis 2001).

2.2.1 Epoxy-Coated Rebar

Epoxy-coated rebar has been used in the field for corrosion protection of rebar Sagues et al. (1994). However, the long-term behavior is uncertain, and in some studies the results are only marginally better than conventional rebar. “The Texas Department of Transportation (TxDOT) uses approximately 18 million pounds of epoxy-coated reinforcing steel annually in bridge structures with additional use in concrete pavements and retaining wall systems (Wolf and Sarcinella 1999).” A seven year study conducted

at the University of Texas at Austin sponsored by TxDOT reported that epoxy-coated rebar perform better than black bar, however, certain limitation exists and imperfections in coating as well as damage while installation may result in localized corrosion (Wolf and Sarcinella 1999)." Therefore, epoxy-coated rebar seems to only "patch-up" the corrosion issue while not completely solving the problem. Hence, there is a need to find a permanent solution to address the issue corrosion with the use of fiber reinforced polymer (FRP) bars.

2.2.1.1 Long-Term Behavior of Epoxy-Coated Rebar

A project conducted by Sagues et al. (1994) in Florida was to assess the current performance of epoxy-coated reinforced (ECR) concrete bridges in harsh environmental conditions such as sea water. A major conclusion of this project was that ECR cannot be used as the only method of corrosion resistance for a marine substructure in Florida (Sagues et al. 1994). This work later lead to FDOT suspending all ECR projects permanently in 1992. Some of the reported problems were epoxy coating disbondment in almost all structures examined. The analysis conducted on the epoxy-coated rebar showed that after initiation of corrosion, the speed of corrosion was equivalent to that of normal rebar. Furthermore, one third of all the bridges examined showed service life without significant repair of several decades, while another third showed need of repair within a decade time frame and the remaining third showed need of frequent monitoring for need of immediate repairs (Sagues et al. 1994). Some solutions to simple spalling repairs found by Sagues et al. (1994) were to spray zinc sacrificial anodes to ECR

structures. In addition, Sagues et al. (1994) suggest that having a 4 in. (10 cm) minimum cover is a key parameter for long term durability.

In 1980, Oregon DOT placed six concrete beams reinforced with epoxy-coated rebar and place in Yaquina Bay Bridge in Newport, Oregon (Griffith and Laylor 1999). Some of the findings on this tested beam included under-film corrosion, separation of coating and cathodic disbondment (Griffith and Laylor 1999).

In Minnesota, Pincheria et al. (2008) assessed the corrosion of 30-35 year old bridge decks reinforced with epoxy coated rebar. Researchers in this study found generally good condition of the bridge deck with light cracking, few delaminated areas and modest corrosion (Pincheria et al. 2008). It was determined that bars away from crack and under at least 3.5 in. (9 cm) of overlay should not corrode until after 20 to 25 years. It was also found that increasing the overlay can improve the performance and extend the service life of bridge decks (Pincheria et al. 2008).

2.2.1.2 Special Handling of Epoxy-Coated Rebar

The handling of epoxy-coated rebar has been found to be very critical as damage will result in detrimental effects on the performance of these bars. The handling requirements described by Epoxy Interest Group (2010) includes storage, cutting, bar placement, bar supports & tie wires, loading and securing, and field repair patching lifting. For storage bars, they must be placed on timber and the timber must be placed in a position to minimize sagging. If bars will be stored for longer than 30 days outdoors then a cover, which minimizes condensation, should be placed over them. Coated bars and uncoated bars need to be stored separately. For cutting bars flame cut should not be

done. Bar supports and tie wires should also be coated. When placing bars in position, these bars should not be dragged because a 2% damage of bar will result in rejection of bar. After bending, cutting, or any other damage process patching must be done to a maximum of 5% if more than the bar should be rejected. Finally when lifting, bundles this process must be done in a manner that minimizes sag and should be done with a spreader bar or strongback (Epoxy Interest Group 2010).

2.3 Current Research Approach

The current research approach will focus on the material characterization of Arapree® AFRP bars for assessing the long-term performance and durability of the AFRP composite material prestressed in concrete. By focusing on the material properties of the studied AFRP bars, material property inconsistencies can be limited.

In order to characterize the properties of 0.51 in. (13 mm) AFRP bars, tensile, creep-rupture, relaxation and fatigue strength tests will be conducted. Figure 6 illustrates the set up for the tensile test. The purpose will be to determine the modulus of elasticity, ultimate strength and ultimate strain of the studied AFRP bars. As stated in Table 2, the AFRP bar will be conditioned at 73.4 ±3.6 °F (23±2°C) and 50±10% relative humidity for at least 48 hours before testing (ASTM D638-2008). Measurements of the diameter of rod specimen will be measured to the nearest 0.0001 in. (0.025 mm) at a minimum of two points 90° apart (and/or at three points along the test length with the average value recorded) (Dolan et al. 2001). After this, the specimens are ready for testing and an extension indicator, i.e. a linear variable displacement transducer (LVDT) will be attached to the specimen while using the grip fixtures to grip the specimen, which will

then be loaded to a rate of 7.2 ksi per min (350 N/mm^2 per minute) or failure of less than 5 minutes (ASTM D638-2008). The data will be recorded continuously. Similarly, for the creep-rupture test, the specimens will be conditioned, and then proper diameter measurements will be conducted. However, testing will take a minimum of 42 days or 300 hours. The test will be controlled by a constant stress with changing strain, and will be monitored at least for each of the stated times in Appendix I. Figure 7 shows the experimental test set up for the rectangular creep-rupture specimen encased in concrete. The goal for this creep-rupture test will be to plot a curve of stress-at-rupture versus time-to-rupture. Therefore, from a given stress, the long-term strain will be recorded until failure. Furthermore, the main purpose of the relaxation test, which is illustrated by Figure 8, will be to determine the change in stress in our AFRP bars under constant strain. This test will require the specimen to be conditioned and properly measured and then will be strained to a level producing failure at a minimum of 120 hours or 5 days. More details of the specimen setup, loading protocol and results will be presented in the subsequent chapters. In Table 2 and Table 3, the testing plan for creep-rupture and relaxation is presented. It is important to obtain material characteristics in the load level that is expected to be used in implementation (60%) as well as load level less than (50%) and greater than (75-85%). This will validate the reasons of selecting a particular load level as well as provide useful characteristics to better understand long-term behavior.

Table 2 Creep-rupture testing plan

Creep-rupture Testing Matrix		
Load levels (percent of ultimate)	Initial Forces	Test Time
50	13 kips	6 weeks
60	15.5 kips	6 weeks
75	19.4 kips	14 days
85	22 kips	14 days

Table 3 Relaxation testing plan

Relaxation Testing Matrix		
Load levels (percent of ultimate)	Initial Force	Test Time
50	13 kips	6 weeks
60	15.5 kips	6 weeks
75	19.4 kips	14 days
85	22 kips	14 days

Figure 6 Tensile test setup

Figure 7 Creep-rupture test setup

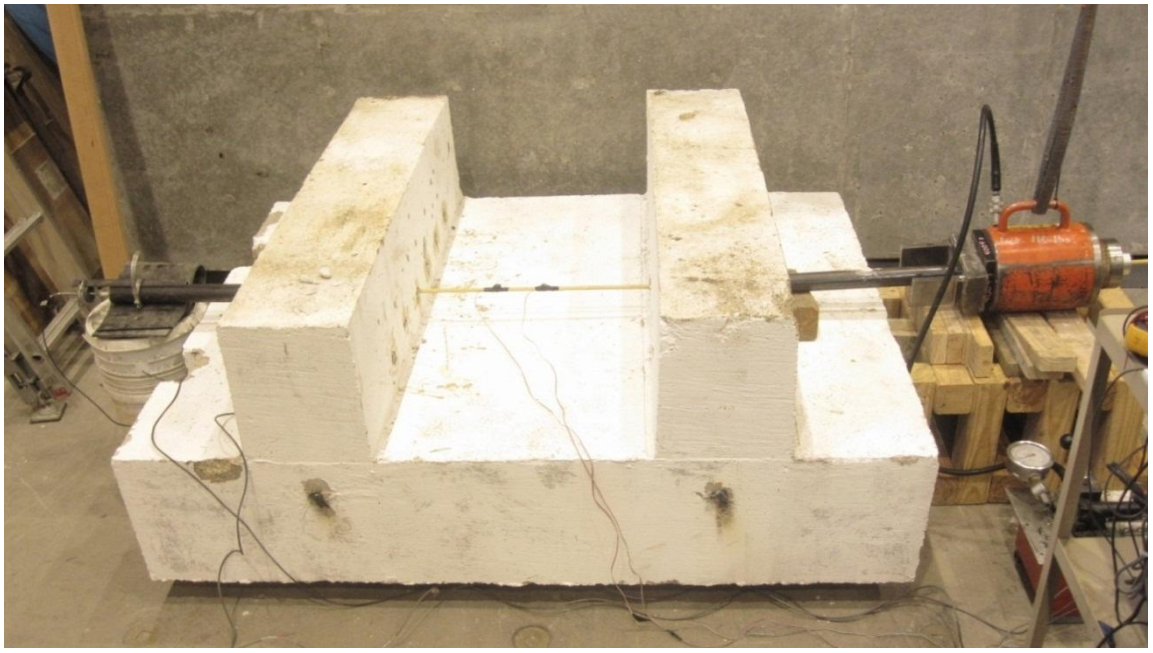

Figure 8 Relaxation test setup

3. EXPERIMENTAL TESTING AND MATERIAL CHARACTERIZATION

3.1 Introduction

Experimental tests are needed to accurately characterize the material properties of AFRP bars for application in prestressed concrete structures. However, limited data is available to show the reliability of such materials that have the potential to sustain load and be suitable for long-term performance. Therefore, there is a need to 1) validate material properties of Arapree® AFRP bars, 2) measure strain increase (or % creep, which is determined to be the increase in strain in percentage from the initial instantaneous strain found when the bar was originally stressed) in AFRP bars when under constant load, 3) measure stress losses (relaxation) while under constant strain, and 4) develop a method to predict prestress losses.

3.2 Preliminary Tests

3.2.1 Description of Preliminary Tensile Tests of Arapree® AFRP Bars

Preliminary tensile tests were conducted to reveal various unknown parameters vital to ensure reliable test data. First six 60 in. (152 cm) specimens were tested using the manufacturer's conventional anchorage system (shown in Figure 9). To determine the maximum tensile load that the manufacturer's conventional anchorage system can achieve, the most suitable strain gauges and effect of slippage on anchorage while loading need to be determined. Oiling the wedges' outer surface and roughening the inner surface of the anchorage system were applied to determine their effects on the maximum load capacity (Figure 10). Another parameter that was tested was the effect of preloading to 7.5 kips (33.4 kN) or 5 kips (22.2 kN). Following, a step loading of 4 kips

(17.8 kN) was applied, then a hold for 15 seconds, and then the specimen was loaded for another 4 kips (17.8 kN) with a hold for 15 seconds. This procedure was followed until failure.

Figure 9 Conventional anchorage system tensile test setup

Figure 10 Plastic wedge roughened surface and regular surface

In order to determine a testing technique to reach the tensile failure of the AFRP bars without slippage or failure near the anchorage, two specimens were testing using grouted ends. The preparation included using an 18 in. (45.7 cm) and 16 in. (40.6 cm) steel pipe on both ends of specimen that were filled with grout (Shepler's Shep Rock).

3.2.2 Instrumentation

For preliminary tensile tests, the following instrumentation was used: strain gauges, MTS axial precision machine, manufacturer's anchorage system (consisting of steel housing and plastic wedges), steel pipes and grout. For preliminary relaxation tests, the following instrumentation was used: hydraulic jack (shown in Figure 11), steel pipe

(shown in Figure 12), grout (shown in Figure 13), plastic stoppers (shown in Figure 14), LVDTs (shown in Figure 15), and strain gauges (shown in Figure 16).

Figure 11 Hydraulic jack and pump

Figure 12 Steel pipes used for anchorage

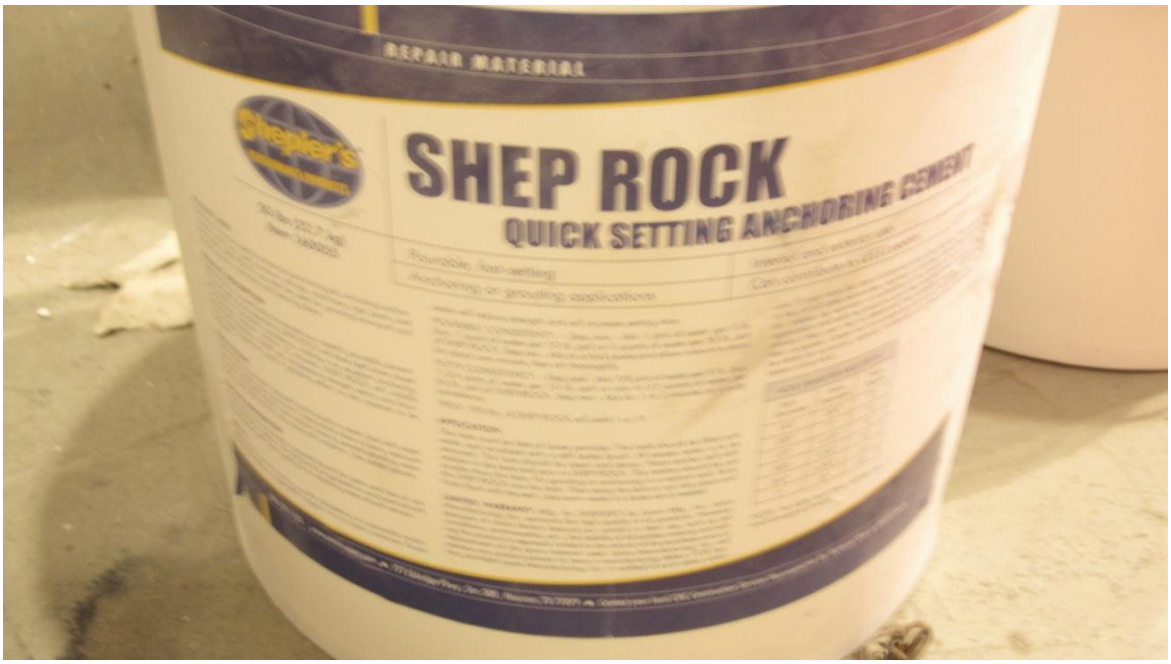

Figure 13 Shepler's shep rock grout

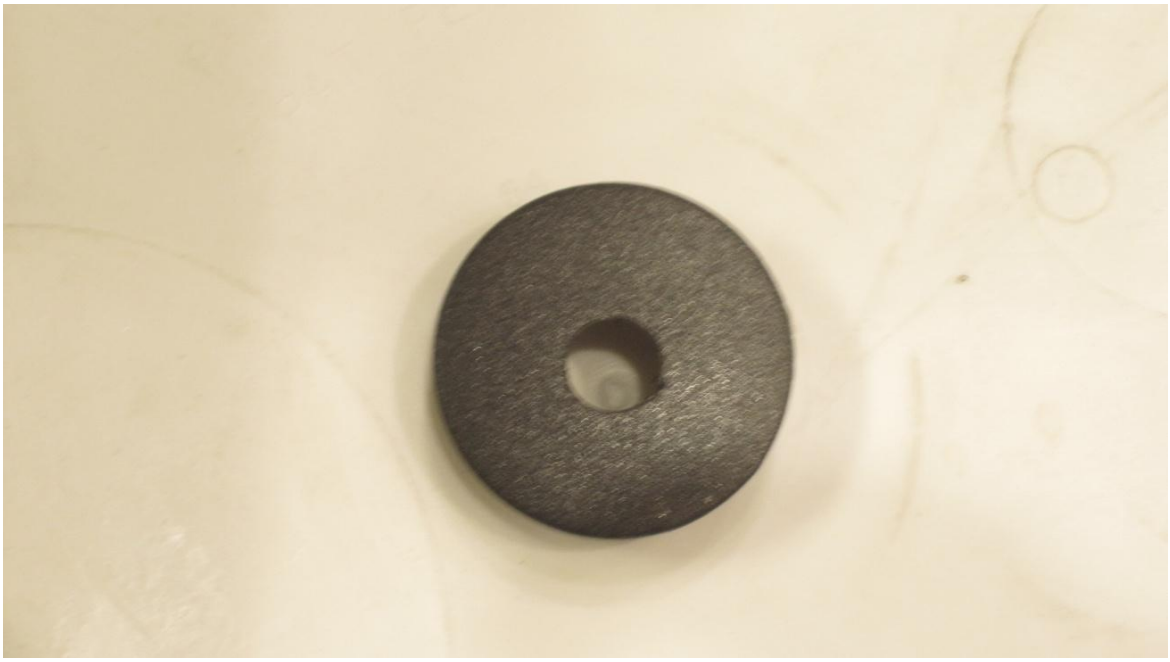

Figure 14 Plastic stopper

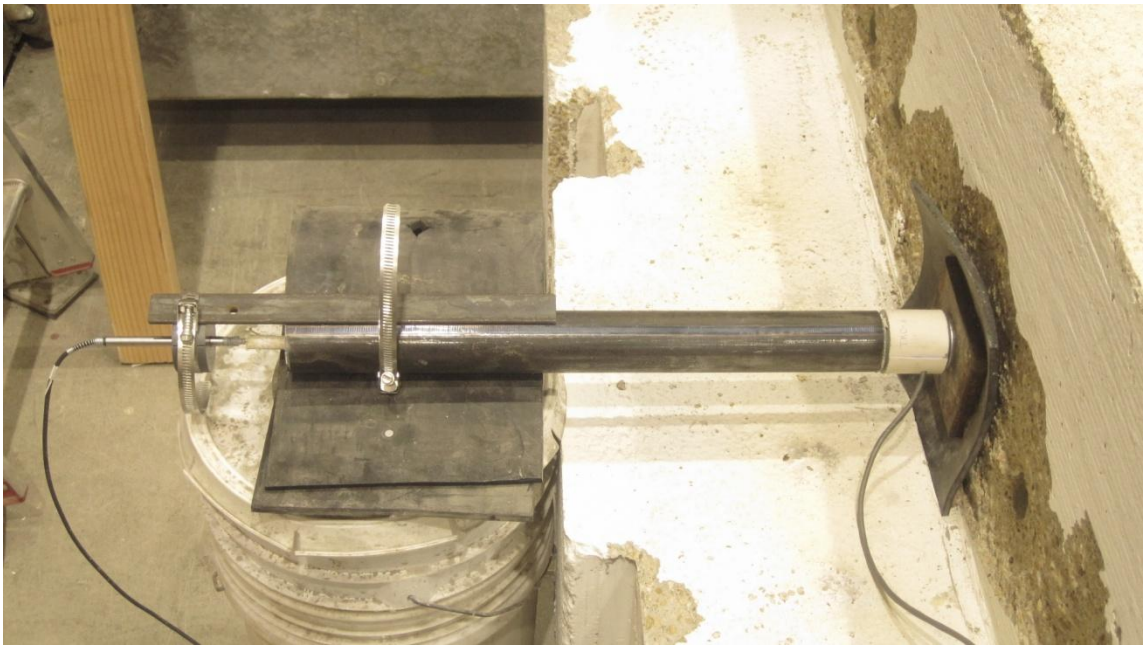

Figure 15 LVDT and load cell on dead end

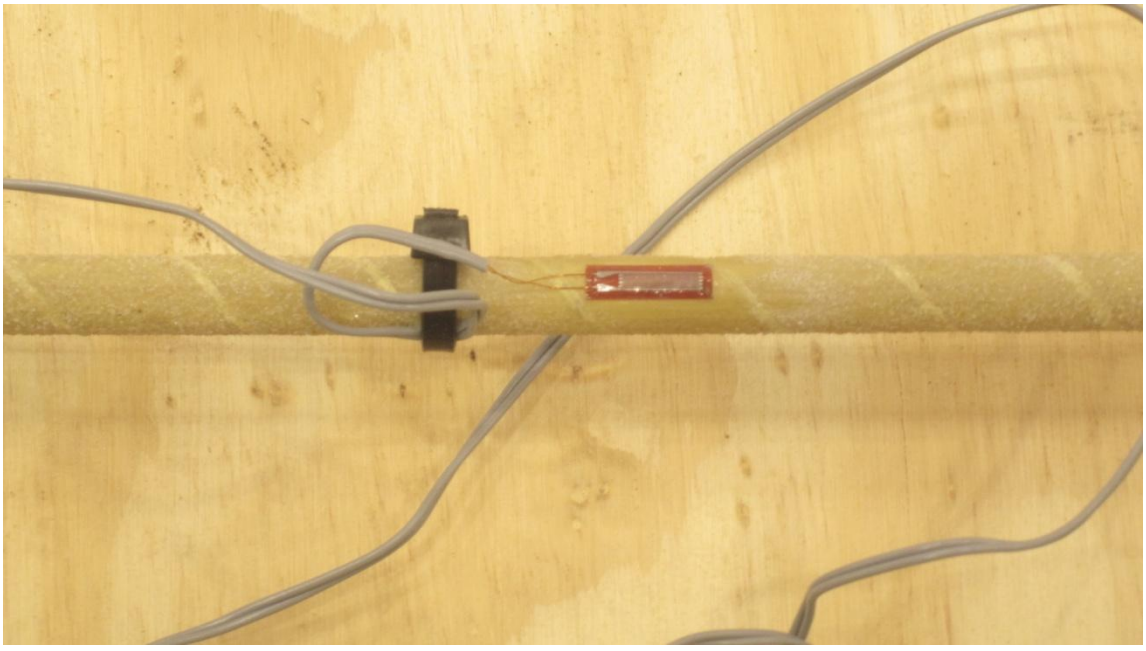

Figure 16 Strain gauged AFRP bar

3.2.3 Experimental Results

To determine the effects from oiling the wedges' outer surface and roughening the inner surface, different specimens were tested to evaluate the benefit, if any, of altering the surface of the anchorage system. For example, the specimens were preloaded to 7.5 kips (33.4 kN) or 5 kips (22.2 kN). Followed by a step loading with a loading rate of 4 kips per minute (17.8 kN per minute) and stopping at 4 kips (17.8 kN), holding for 15 seconds, loading for another 4 kips (17.8 kN) stop, and then holding for 15 seconds. This loading pattern was applied until failure.

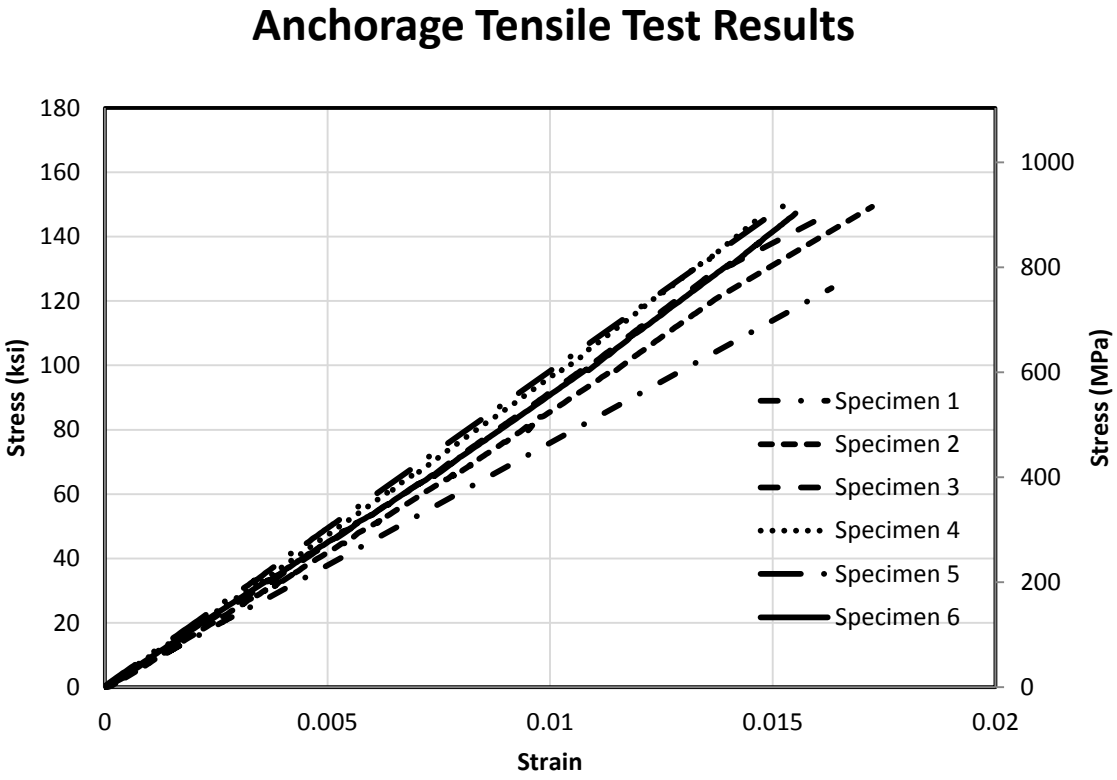

Figure 17 Anchorage system tensile test results

The first specimen tested was loaded monotonically at 4 kips per minute (17.8 kN per minute). Results can be seen in Figure 108 in Appendix II. A comparison of all anchorage tests are shown in Figure 17. The wedges inside the anchorage were simply placed in position. While conducting this test, it was noted that continuous sudden slipping points. The failure mode for this specimen was slippage from anchorage at 15 kips (66.7 kN) shown in Figure 18. The diameter of the AFRP bar was crushed at the anchorage, and significantly decreased in size causing failure.

The second specimen tested was loaded using an incremental, stepped (or ramped) loading process. The results are shown in Figure 109 in Appendix II. A comparison of all anchorage tests are shown in Figure 17. The wedges inside the anchorage were oiled on the contact surface with the anchorage itself and roughened on surface in contact with AFRP bar shown in Figure 10 then placed in position. The slippage seen in this test was still considerably sudden, but not as violent. The failure mode for this specimen was slippage from anchorage at 18.2 kips (81.0 kN). Oiling the bars helped decrease the sharp slippage that cause damage to the first specimen and allowed us to reach a high load.

The third specimen tested was loaded using step loading, but was first preloaded to 7.5 kips (33.4 kN) as shown in Figure 110 in Appendix II. A comparison of all anchorage tests are shown in Figure 17. The purpose of preloading was to allow the anchorage to settle and remove some of the slippage for the continuous test. After preloading the specimen was then tested. The wedges inside the anchorage were oiled on the contact surface with anchorage were roughened on surface in contact with AFRP bar

just like the previous specimen then placed in position. The slippage seen in this test did not occur until about 10 kips and was also less violent. The failure mode for this specimen was crushing near anchorage at 17.85 kips (79.4 kN) shown in Figure 18. The modulus was also higher for this case because most of the sharp slippage was decreased compared to the continuously damage of the specimens observed in the previous tests.

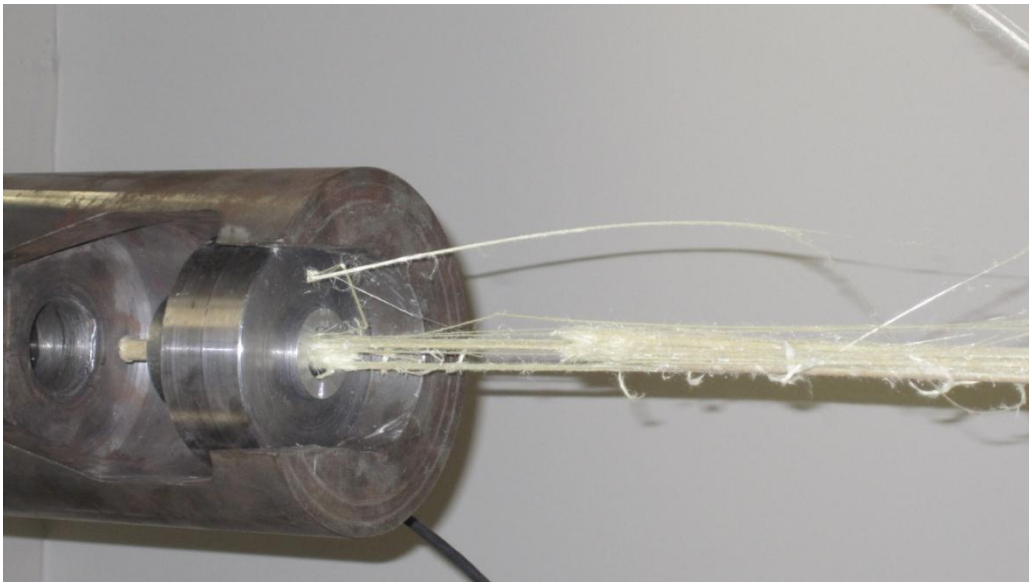

Figure 18 Failure of specimen near anchorage zone

The fourth specimen tested was loaded using a similar step loading, but was first preloaded to 7.5 kips (33.4 kN) as shown in Figure 111 in Appendix II. A comparison of all anchorage tests are shown in Figure 17. After preloading the specimen was then tested. The wedges inside the anchorage were oiled on the contact surface with anchorage were not roughened on surface in contact with AFRP bar in order to determine if roughening the surface of the wedges had any impact in testing. The failure

mode for this specimen was rupture near anchorage at 17.72 kips (78.8 kN) as shown in Figure 19. Roughening the surface proved to have little to no effect.

Figure 19 Failure induced by anchorage stress concentration

The fifth specimen tested was loaded using step loading, but was first preloaded to 5 kips (22.2 kN) shown in Figure 112 in Appendix II. A comparison of all anchorage tests are shown in Figure 17. Preloading was decreased to see if preloading as high as

7.5 kips (33.4 kN) caused any deterioration to the material. The wedges inside the anchorage were oiled on the contact surface with anchorage and were also not roughened on surface in contact with AFRP bar as it was determined that had little effect on the test. The failure mode for this specimen was slippage at anchorage at 18.7 kips (83.2 kN). Preloading to 5 kips (22.2 kN) instead of 7.5 kips (33.4 kN) showed that preloading to 7.5 kips (33.4 kN) caused some damage that did not allow the specimen to reach loads higher than 17 kips (75.6 kN).

The sixth specimen tested was loaded using step loading, but was not preloaded shown in Figure 113 in Appendix II. A comparison of all anchorage tests are shown in Figure 17. The wedges inside the anchorage were oiled and well as the inside of anchorage. The failure mode for this specimen was slippage at anchorage at 17.8 kips (79.2 kN). Figure 20 shows the conventional anchorage after the tensile test. Clearly, the plastic wedge is fully embedded in the steel housing leading to anchorage failure. Preloading proved to not be as important as oiling. The modulus calculated from the data was very close that reported by the manufacturer. It was concluded that oiling both wedges and anchorage along with step loading would allow anchorage system to achieve 17.5 kips (77.8 kN) of load on AFRP bars with 1.5% strain.

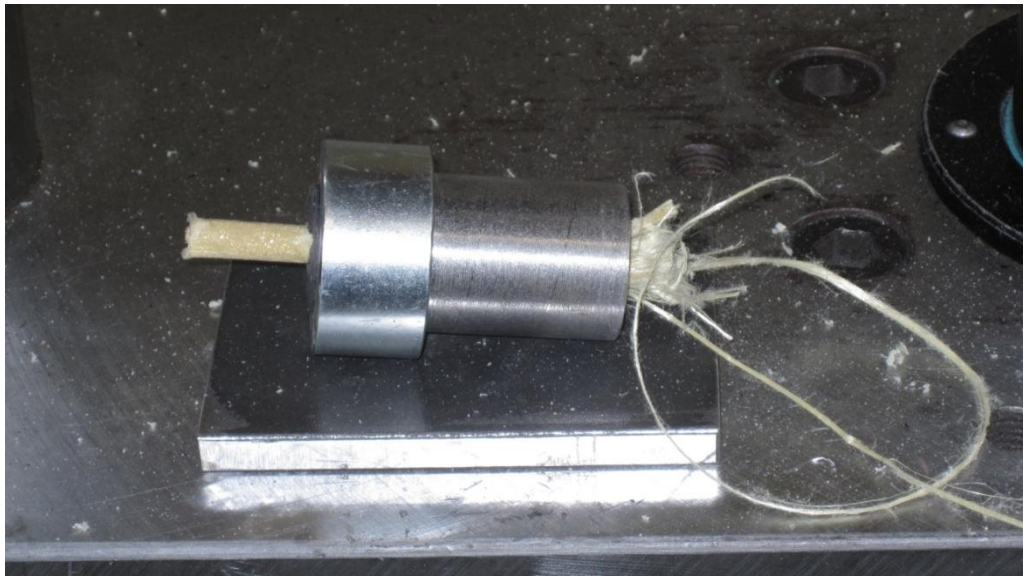

Figure 20 Conventional anchorage system after tensile test

The first specimen tested with grouted ends shown in Figure 21 was monotonically loading at 4 kips per minute (17.8 kN per minute). The pipe used for this test consisted of two 16 in. (40.6 cm) pipes with two different outer diameter of 1.9 in. (4.8 cm) and 1.5 in. (3.8 cm), respectively. The test setup is shown in Figure 22. The failure mode for this specimen was slippage (19 kips (84.5 kN)) in fixture due to lack of friction on the 1.5 in. (3.8 cm) diameter pipe and lack of bolts in fixture. The results are shown in Figure 114 in Appendix II. A comparison of all grouted steel pipe test are shown in Figure 23. The modulus observed in this test was much higher than the test conducted using the anchorage system. It was concluded that that longer pipe (18 in. (45.7cm)) and 1.9 in. (4.8 cm) diameter pipe would be needed to reach failure.

Figure 21 Wooden frame holding grouted AFRP specimens

Figure 22 Grouted steel pipe anchorage system tensile test

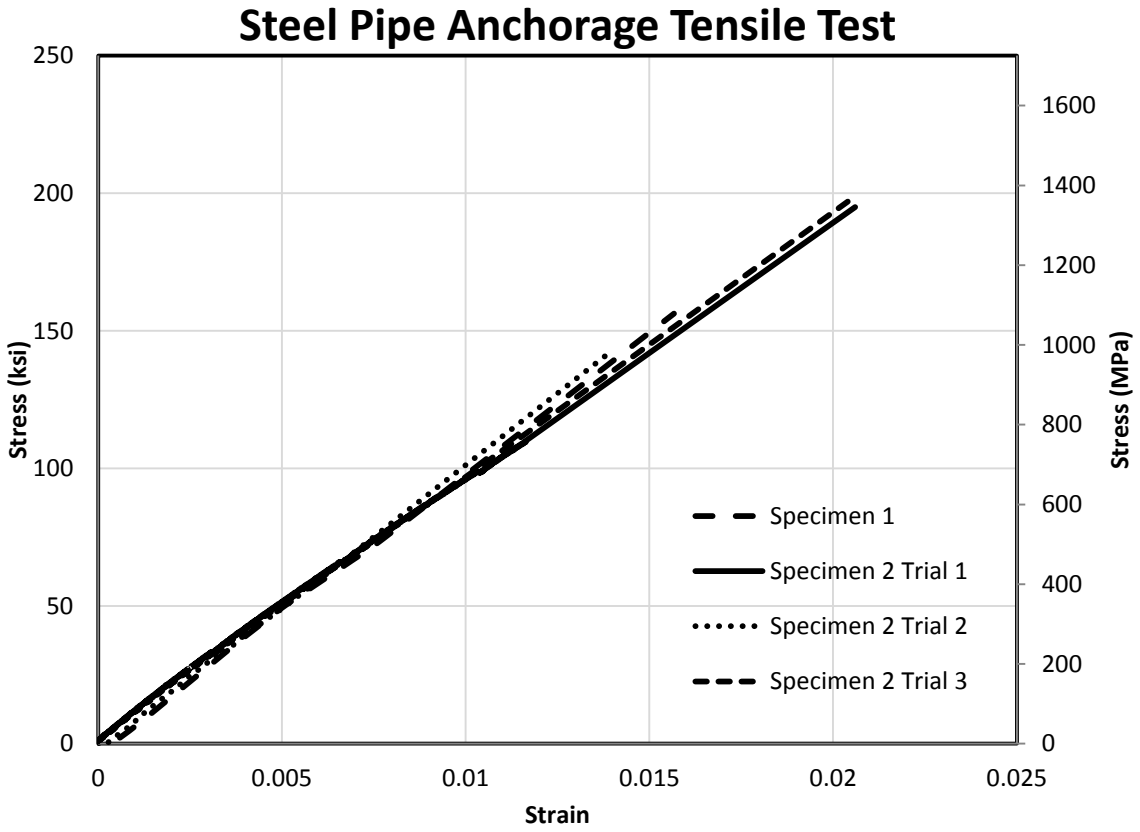

Figure 23 Grouted steel pipe anchorage system tensile test results

The second specimen tested with grouted ends was loaded using monotonic loading at 4 kips per minute (17.8 kN per minute). The pipe used for this test consisted of two 18 in. (45.7 cm) pipes with outer diameter of 1.9 in. (4.8 cm). The specimen was tested three times due to unexpected slippage failures. The first trial, shown in Figure 115 in Appendix II, was not adequately tightened and slipped inside fixture at 19 kips (84.5 kN). The second trial, shown in Figure 116 in Appendix II was effectively tightened, but slipped at 24 kips (106.8 kN) due to lack of bolt in fixture. Finally for the third trial, shown in Figure 117 in Appendix II, the bolts were rearranged in order to

distribute force evenly throughout the anchorage, configuration led to tensile rupture. A comparison of all grouted steel pipe test are shown in Figure 23. For the third trial, failure was tensile rupture at 23.7 kips (105.4 kN) as shown in Figure 24. It was concluded that multiple loading on the same specimen affected the modulus of elasticity as it was shown to decrease it every time. Also the ultimate capacity was clearly affected as the specimen failed at a lower load on the third trail compared to the second.

Figure 24 Tensile failure of AFRP bar using grouted steel pipe anchorage system

3.2.4 Description of Preliminary Relaxation Test of Arapree® AFRP Bars

Relaxation tests were conducted to reveal anchorage performance in a 1 week period as well as prestress losses during this timeframe. Two 87 in. (221 cm) specimens were tested using two grouted steel tubes, conventional anchorage and a hydraulic jack with hand pump. One specimen was stressed to 50% and the other to 60% of ultimate tensile stress.

3.2.5 Instrumentation

For the preliminary relaxation tests, the following instrumentation was used: strain gauges, load cell, 2 steel washers, 2-18 in. (46 cm) long, 1.9 in. (5 cm) outer diameter steel pipe, 4 plastic stoppers, 2 steel plates, conventional anchorage system, and Shepler's Shep Rock expansive grout shows the hydraulic jack with hand pump that was used.

Two 87 in. (221 cm) Arapree® AFRP bars were cut using a rotating steel wheel found in Appendix III Figure 125. Once the bars were cut the dead end of each bar was grouted. The steel pipe's ends were closed using plastic stoppers. After the grout set for 2 hours on the dead end, strain gauges were attached. After installing the strain gauges, the bars were placed in the concrete block with load cell (2 washers top and bottom) and then a steel plate. On the live end, a steel plate followed by steel pipe with two plastic stoppers was placed. Once the pipe was placed, the hydraulic jack was placed in position with conventional anchorage at end. The strain gauge cable was then soldered to DAQ and was calibrated along with load cell and LVDT. On the dead end, an LVDT was installed. At this point, the AFRP bar is ready for prestressing. The grout was prepared

once the bar has been prestressed to 80% of the desired load. Once the prestressing load reached the desired load grout is poured using a plastic stopper in the hole within the steel pipe. The grout in the live end was allowed to set for 2 hours and then the hydraulic jack was released. The bar section extending was also cut. The LVDT for the live end was then attached to the live end as shown in Figure 25.

Figure 25 Live end LVDT

3.2.6 Experimental Results

After testing the grouted (steel) pipes and conventional anchorage for ultimate short-term performance, there was a need for sustained load performance evaluation such that a prestressing method was tested while also evaluating the effects due to relaxation. To address this, three specimens were tested, one at 50% of ultimate tensile

stress as shown in Figure 26, another at 60% as shown in Figure 27, which reflects the stress level that is desired for prestressing and finally one at 50% as shown in Figure 28.

The results showed that the largest percentage of prestressing load loss occurred during the first 100 hours. These experiments also revealed that little to no slippage occurred at the dead end during a 180 hour test for grout steel pipe case. On the live end, there was a 4 percent load loss due to slippage.

Using the conventional (or wedge) anchorage after about 18 hours, localized damage to the bar resulted in a sudden drop in stress. Relaxation behavior prior to this sudden drop was consistent with results observed from the grouted steel pipe case. However, at 72 hours, the specimen failed near the anchorage due to local stress concentration on bar. Therefore, it was concluded that using the conventional anchorage system provided by the manufacturer for prestressing at 50% stress level is unreliable and failure can be expected.

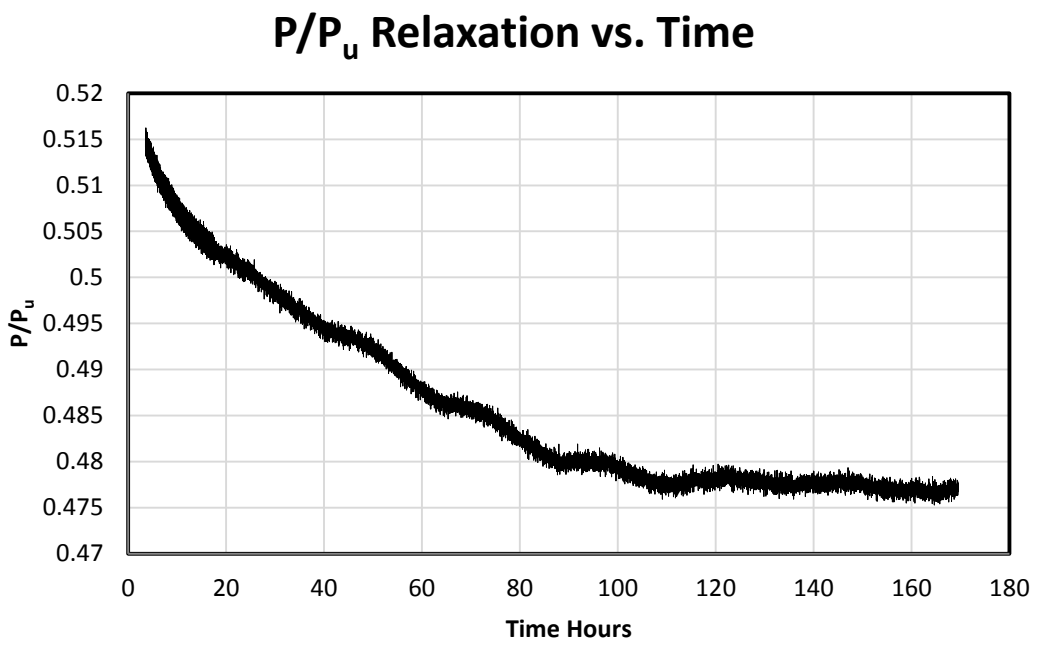

Figure 26 Preliminary relaxation test specimen 1 at 50% stress level

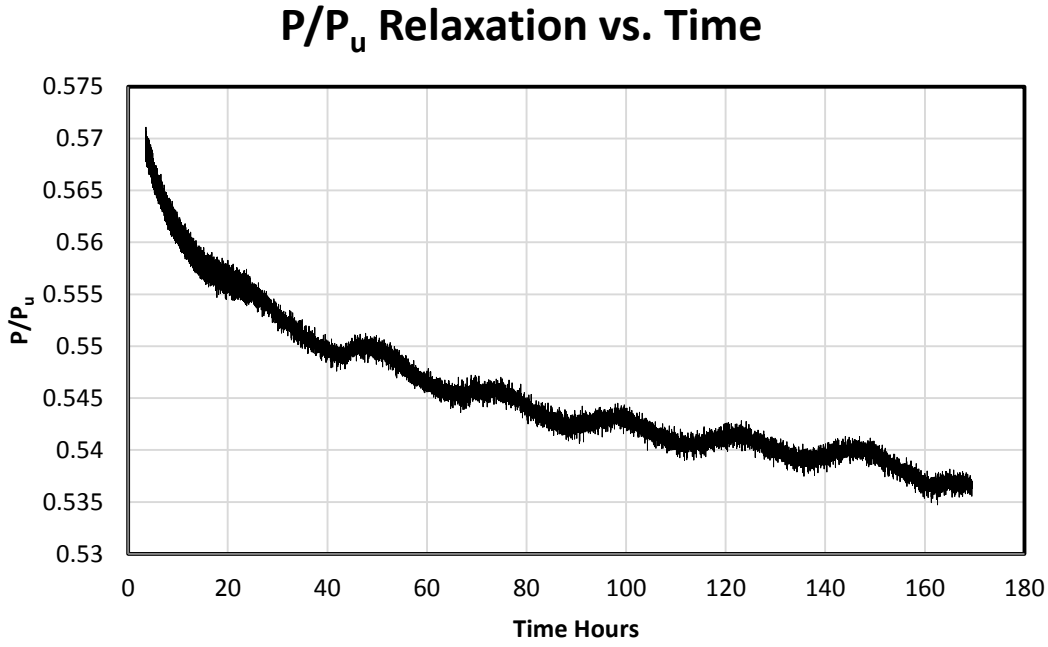

Figure 27 Preliminary relaxation test specimen 2 at 60% stress level

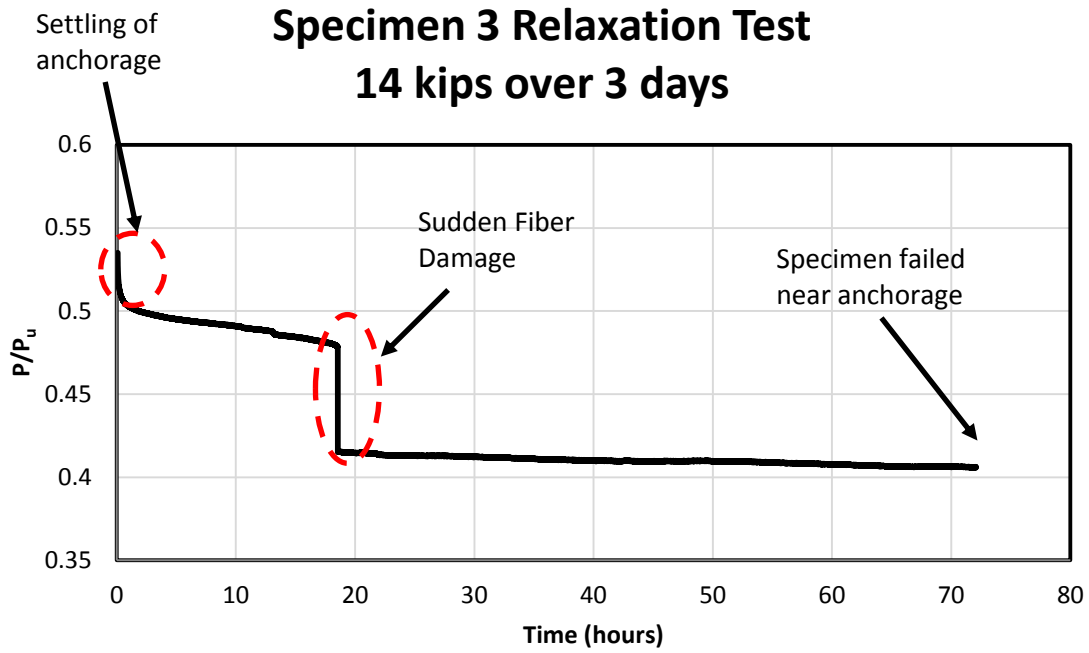

Figure 28 Preliminary relaxation test specimen 3 at 55% using wedge anchorage system

3.3 Tensile Test

3.3.1 Description of Preliminary Tensile Tests of Technora AFRP Bars

Tensile tests were conducted on Technora AFRP bars in order to validate their tensile strength and evaluate them for this research. The test specimens were stored in an environment of 77°F (25°C) and 50% relative humidity for at least forty-eight hours. Then, the diameter of each rod specimen was measured with a micrometer to the nearest hundredth of an inch at a minimum of two points at 90° apart in five sections of the rod. The average value was recorded. Table 4 contains the measurement data for each rod specimen.

After the AFRP rods were measured, each rod specimen is placed in the grips of the testing machine and properly aligned along its longitudinal axis as shown in Figure 29. The extensometer is attached to the rod specimen and the testing machine is set to run at a rate of 50.7 ksi per minute (350 MPa per minute). The loading was to continue until the specimen failed. Measurements were to continue recording until strain reached at least 60% of the tensile capacity. Specimen 2 was not tested because the first and third specimens tested did not reach failure when failing in slippage. Specimen 1 was tested first and then specimen 3 because specimen 3 and specimen 1 were the first two specimens prepared to be tested. After testing, no tensile failure occurred as slippage was the failure mechanism so further testing was discontinued.

Table 4 Diameter measurements of rod specimens

Specimen 1 in (mm)	**Specimen 3 in (mm)**
0.31 (7.91)	0.31 (7.88)
0.32 (8.16)	0.32 (8.21)
0.31 (7.86)	0.31 (7.85)
0.33 (8.32)	0.33 (8.28)
0.31 (7.95)	0.31 (7.93)
0.33 (8.36)	0.33 (8.34)
0.31 (7.86)	0.31 (7.83)
0.32 (8.24)	0.32 (8.23)
0.31 (7.88)	0.31 (7.90)
0.32 (8.22)	0.33 (8.36)
Avg. = 0.32 (8.08)	**Avg. =0.32 (8.08)**

Figure 29 Tensile testing machine and rod specimen setup

3.3.2 Instrumentation

In this tensile test, an extensometer was attached to each bar. Two steel grips shown in Figure 30 were manufactured to grip to AFRP bar. Then the grips were inserted into MTS machine to prepare for tensile testing.

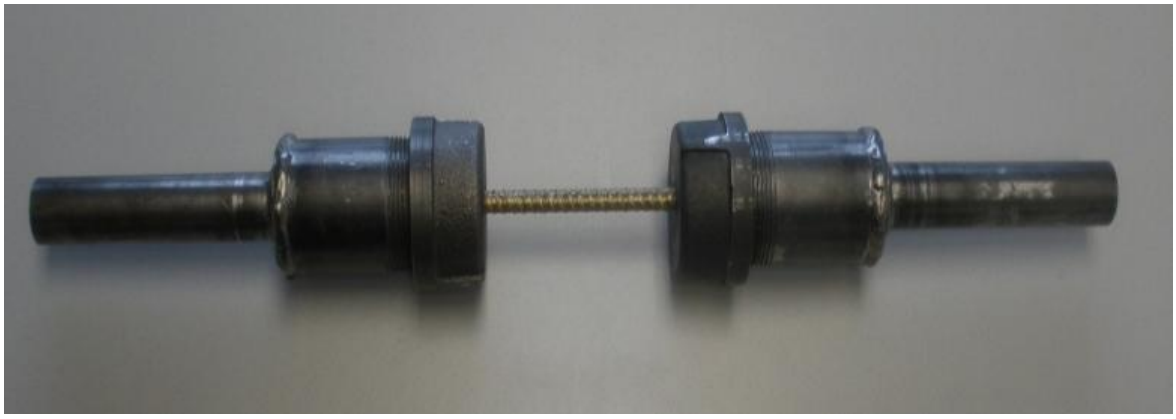

Figure 30 Rod Specimen 1

3.3.3 Experimental Results

The following are plots generated from the data collected by the MTS testing machine. Figure 31 and Figure 32 illustrate the relationship between stress vs. strain while Figure 33 and Figure 34 illustrate the relationship between force vs. displacement.

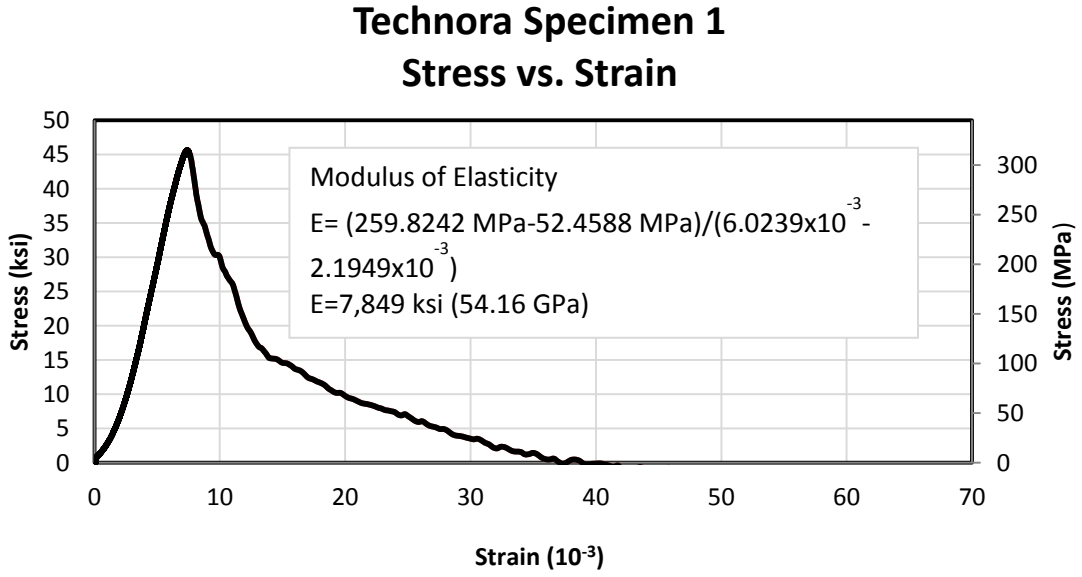

Figure 31 Technora Specimen 1 Stress vs. Strain

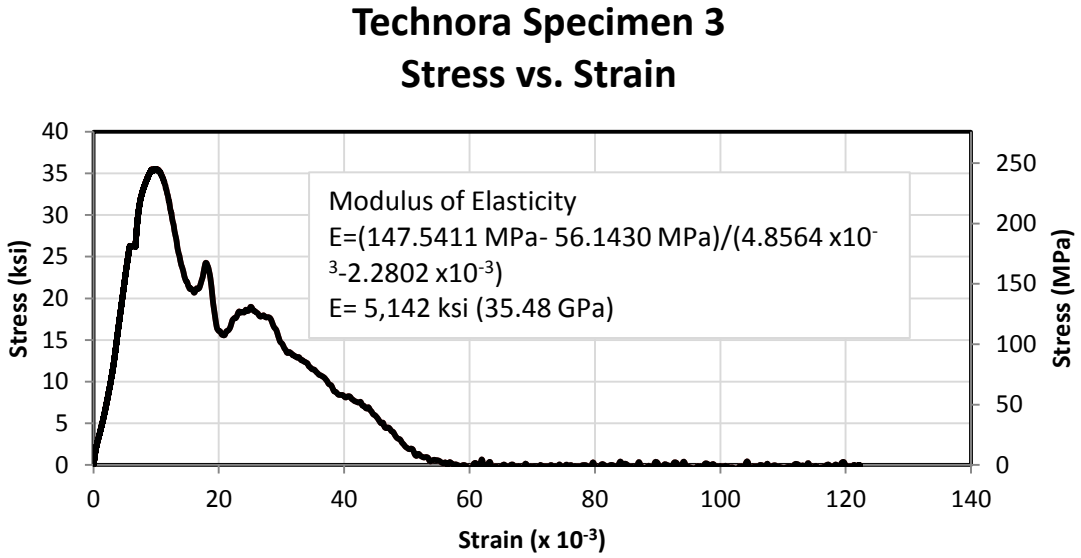

Figure 32 Technora Specimen 3 Stress vs. Strain

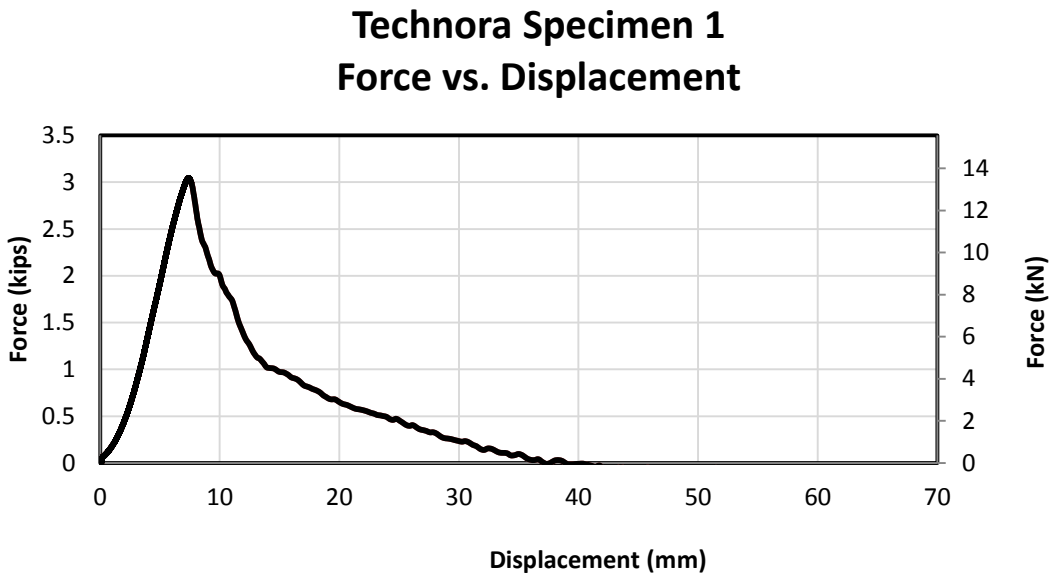

Figure 33 Technora Specimen 1 Force vs. Displacement

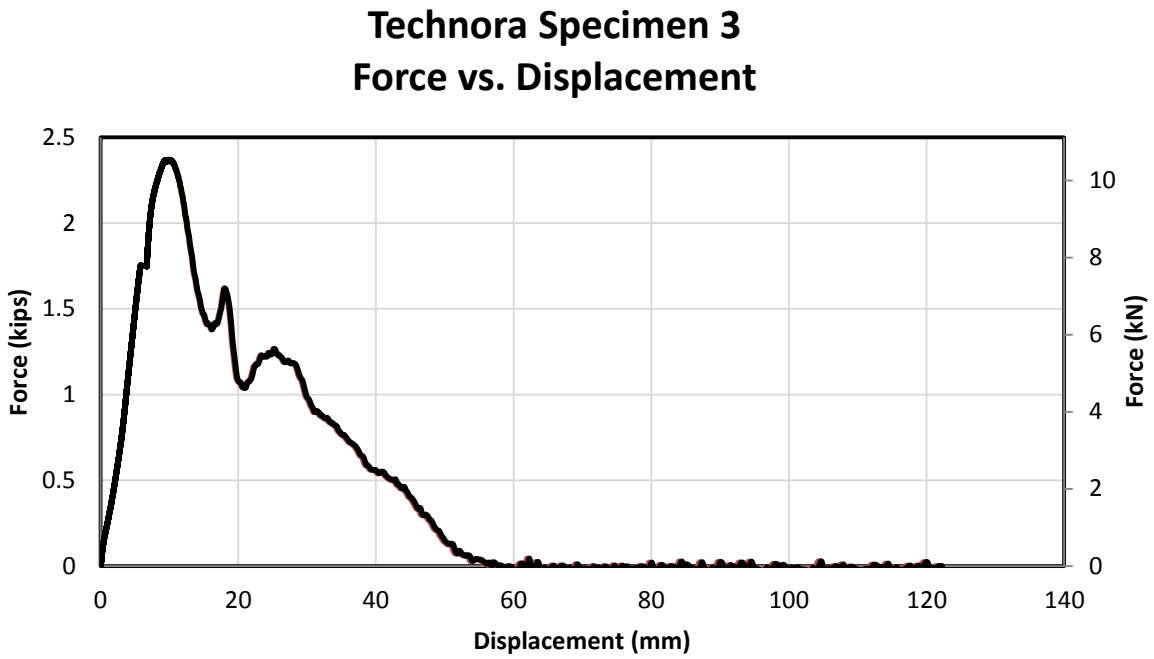

Figure 34 Technora Specimen 3 Force vs. Displacement

From our tensile testing, the research team concluded that the extensometer connected to the rod specimen was not working properly. Therefore, the data collected was a rough estimate of the strain for each specimen, where it was assumed that the strain is equal to the displacement divided by a 0.4 in. (1 mm) gauge length such that the displacement equals the strain. These assumptions are applied in the stress vs. strain plot in order to estimate the modulus of elasticity for each specimen.

The computed modulus of elasticity of the Technora rod from the tensile tests varied from the actual modulus of elasticity reported by the manufacturers of Technora, which was 7,971 ksi (55 GPa). The computed modulus of elasticity of the two specimens tested was about 7,849 ksi (54 GPa) and 5,142 ksi (36 GPa) for Specimens 1 and 3, respectively. The variation in modulus of elasticity is mainly due to slippage

between the interior of the grips and the actual exterior fiber of the rod during the testing process. The inability of the grips to maintain bond with the specimen is the reason for the difference in modulus of elasticity in specimen 1. Figure 30 shows a photo of the Technora rod (specimen 3) within the fabricated grips.

From specimen 3, it was also concluded that the application of epoxy on the two ends of the rod specimen caused greater slippage, resulting in a lesser value for the modulus of elasticity. The tensile testing of the rod specimen with epoxy indicated the possibility of limiting the slippage if the specimen were of greater length. Specimen 3 is illustrated in Figure 35 after the tensile testing, revealing the separation of the epoxy from the AFRP rod.

Figure 35 Rod Specimen 3

3.3.4 Description of Tensile Tests of Arapree®AFRP Bars

Researchers conducted tensile tests to determine ultimate stress, strain and modulus of elasticity of Arapree® AFRP bars once it was determined that Technora bars would not be available for the research project. Six 56 in. (142 cm) specimens (see Figure 36) were tested using two 18 in. (45.7 cm) grouted steel pipes (outer diameter 1.9

in. (4.8 cm) and inner diameter 1.5 in. (3.8 cm) at the ends for transferring load to bar. The specimens were taken from a 6 ft (1.8 m) diameter circular spool of 328 ft (100 m) provided by the manufacturer as shown in Figure 124; hence, the specimens showed some natural curvature. All specimens were loaded monotonically at 5 kips per minute (1.12 kN per minute) (ASTM 638-2008).

Figure 36 AFRP tensile specimens

3.3.5 Instrumentation

All specimens were strain gauged with Texas Instrument gauges as shown in Figure 16. The grout used was Shelper's Shep Rock quick setting grout. The bars were held in a vertical position using a wooden frame (Figure 21). The bars were placed in a steel pipe. Using a rigid plastic plug with a central hole, the bar was positioned in the

center of pipe. Two hours after the first end was cast, the second end was cast. One day after the specimens were prepared, the strain gauges were installed and then the specimens were tested.

3.3.6 Experimental Results

The first specimen tested was monotonically loaded at 4 kips per minute (see Figure 37). The failure mode of the bars was rupture also shown in Figure 37. The AFRP bar reached above 210 ksi (1450 MPa) and had 2.2% strain with a modulus of elasticity of 10,189 ksi (70.3 GPa). Results can be seen in Figure 118 in Appendix II and the compared results can be seen in Figure 38.

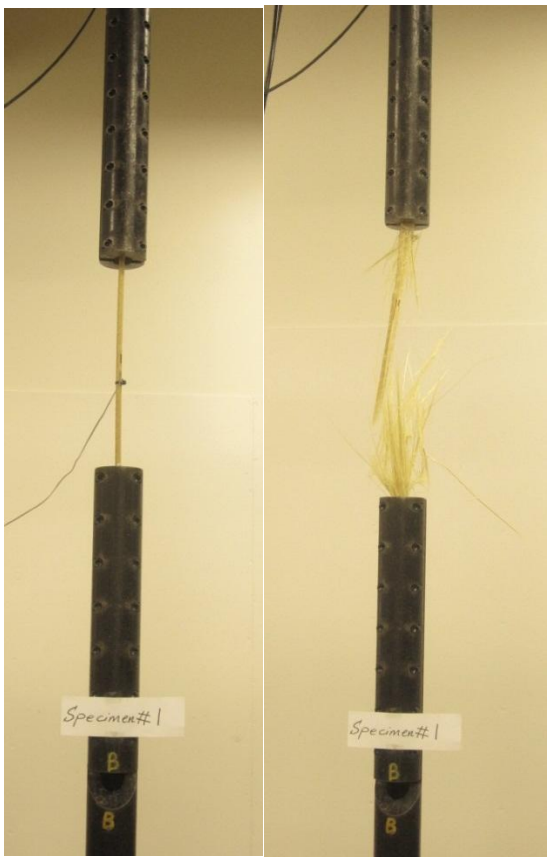

Figure 37 AFRP tensile specimen 1

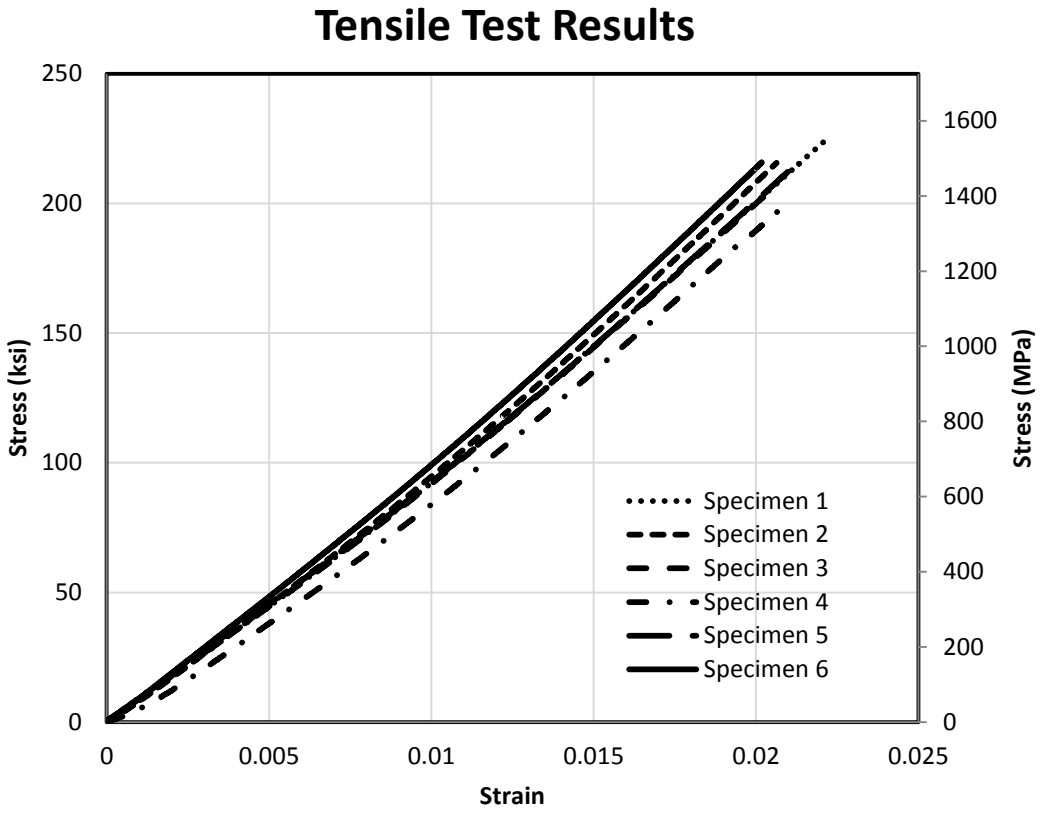

Figure 38 Arapree® AFRP tensile test results

The second specimen tested was monotonically loaded at 4 kips per minute (17.8 kN per minute) as seen in Figure 39. The failure mode of the bars was rupture also shown in Figure 39. The AFRP bar reached above 210 ksi (1450 MPa) and had 2.1% strain with a modulus of elasticity of 10,500 ksi (72.5 GPa). Results can be seen in Figure 119 in Appendix II and the compared results can be seen in Figure 38.

Figure 39 AFRP tensile specimen 2

The third specimen tested was monotonically loaded at 4 kips per minute as shown in Figure 40. The failure mode was bar rupture as seen in Figure 40. The AFRP bar reached above 210 ksi (1450 MPa) and had 2.1% strain with a modulus of elasticity of 10,071 ksi (69.5 GPa). Results can be seen in Figure 120 in Appendix II and the compared results can be seen in Figure 38.

Figure 40 AFRP tensile specimen 3

The fourth specimen tested was monotonically loaded at 4 kips per minute (17.8 kN per minute) as seen in Figure 41. The failure mode of the bars was rupture and is also shown in Figure 41. The AFRP bar reached just below 200 ksi (1380 MPa) and had 2.1% strain with a modulus of elasticity of 9,819 ksi (67.8 GPa). Results can be seen in Figure 121 in Appendix II and the compared results can be seen in Figure 38.

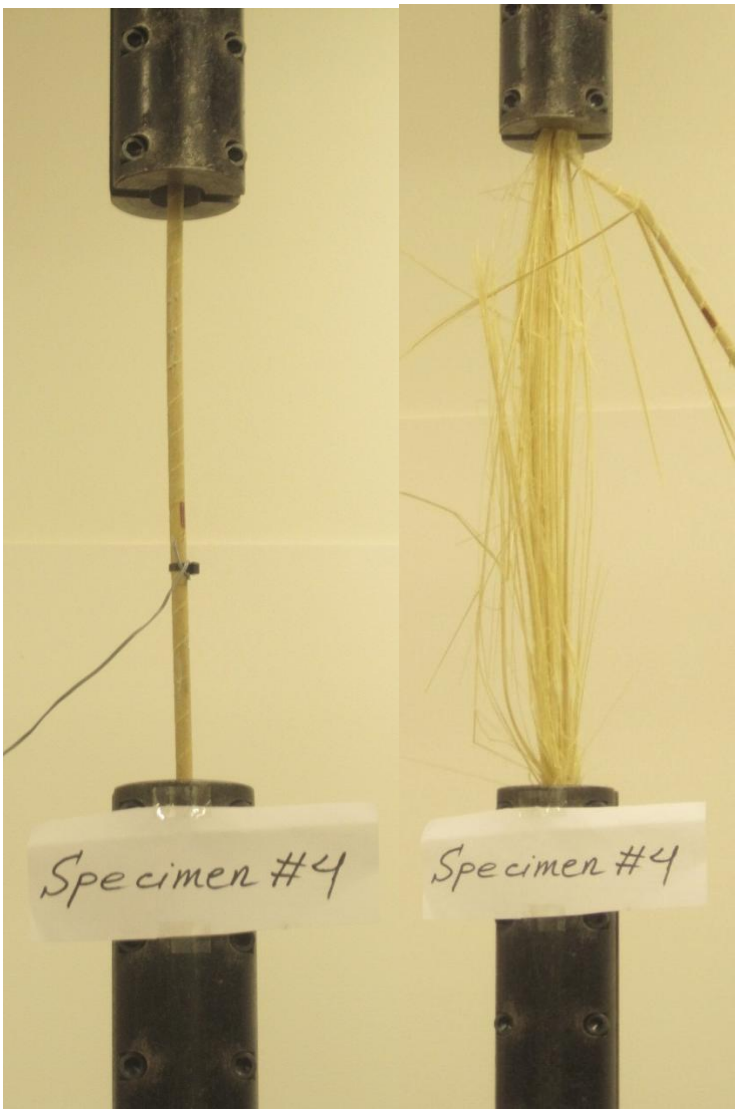

Figure 41 AFRP tensile specimen 4

The fifth specimen tested was monotonically loaded at 4 kips per minute (17.8 kN per minute) as seen in Figure 42. The failure mode of the bars was rupture and is also shown in Figure 42. The AFRP bar reached above 210 ksi (1450 MPa) and had 2.2%

strain with a modulus of elasticity of 10,092 ksi (69.6 GPa). Results can be seen in Figure 122 in Appendix II and the compared results can be seen in Figure 38.

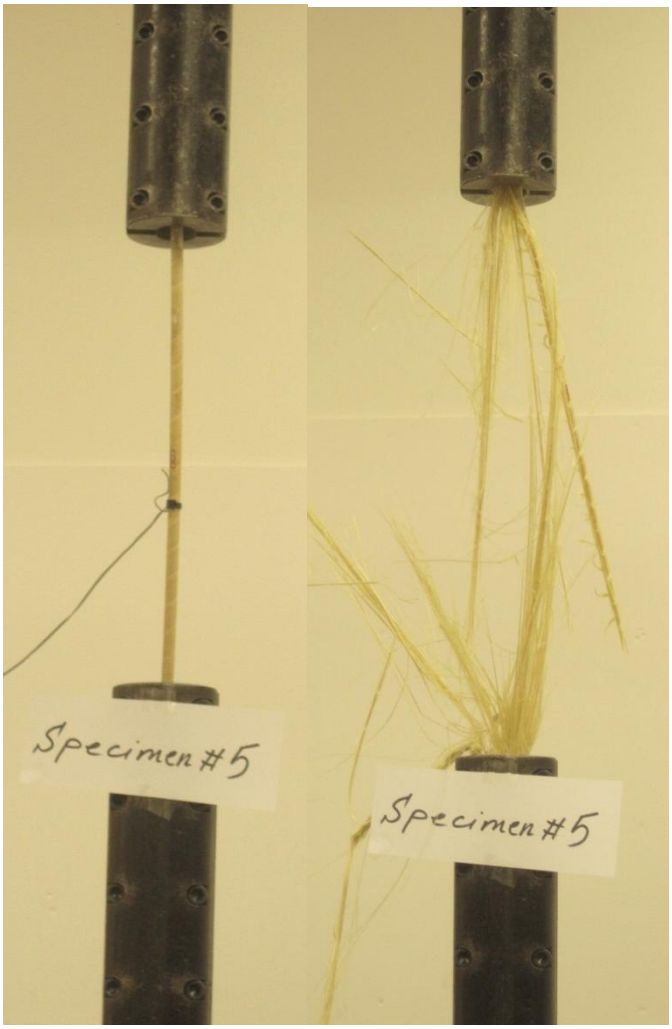

Figure 42 AFRP tensile specimen 5

The sixth specimen tested was monotonically loaded at 4 kips per minute (17.8 kN per minute) shown in Figure 43. The failure mode was bar rupture and is also shown in Figure 43. The AFRP bar reached above 210 ksi (1450 MPa) and had 2.2% strain with

a modulus of elasticity of 10,189 ksi (70.3 GPa). Results can be seen in Figure 123 in Appendix II and the compared results can be seen in Figure 38. Finally a summary of the results can be seen in Table 5.

Figure 43 AFRP tensile specimen 6

Table 5 Tensile test summary

Specimen	Ultimate Load kips (kN)	Ultimate Stress ksi (MPa)	Ultimate Strain	Modulus of Elasticity ksi (GPa)
1	27.39 (121.8)	224 (1550)	0.0222	10189 (70.3)
2	26.30 (117.0)	215 (1488)	0.0206	10500 (72.5)
3	25.29 (112.5)	207 (1431)	0.0207	10071 (69.5)
4	24.01 (106.8)	196 (1359)	0.0207	9819 (67.8)
5	25.87 (115.1)	212 (1464)	0.0210	10092 (69.6)
6	26.31 (117.0)	215 (1489)	0.0202	10717 (73.9)
Average	25.86 (115.0)	212 (1464)	0.0209	10231 (70.6)

3.4 Creep-Rupture Test

3.4.1 Description of Creep-Rupture Tests of Arapree®AFRP Bars

Creep-rupture tests on Arapree® AFRP bars consisted of prestressing bars to 4 different load levels of 50, 60, 75, and 85 percent of ultimate tensile strength, shown in Table 2. Three to bars were tested at each stress level until rupture of tendon or after a presumed period of time. The bars will be anchored on both end using expansive grout poured into steel pipe minimum length of 18 in. (45.7 cm) and an outer diameter of 1.9 in. (4.8 cm). The bars with 50 and 60 percent load level were embedded in concrete to better represent a prestress concrete condition. Strain gauges were embedded in the concrete on the AFRP bars. Bars were mounted on to a concrete block that will restrain the concrete by applying a compressive force while the bars were in tension.

3.4.2 Instrumentation

For the creep-rupture tests, the following instrumentation was used: strain gauges, load cell, 2 steel washers, 3-18 in. (45.7 cm) long 1.9 in. (4.8 cm) OD steel pipe,

6 plastic stoppers, 2 steel plates, 11 disc springs, expansive grout Shepler's Shep Rock, and hydraulic jack with a hand pump.

Six 94 in. (238.8 cm) Arapree® AFRP bar were cut using a rotating steel wheel found in Appendix III Figure 125 for long-term test and six 46 in. (116.8 cm) bars were also cut for short-term creep-rupture test. Once the bars were cut the dead end of each bar was grouted. The steel pipe's ends were closed using plastic stoppers. After the dead end grout set for 2 hours, strain gauges were attached. After installing the strain gauges the bars were placed in concrete block (Figure 44) with load cell (2 washers top and bottom) then steel plate followed by eleven disc springs shown in Figure 45. On the live end a steel plate followed by steel pipe with two plastic stoppers were placed. Once the pipe was placed, the hydraulic jack was placed in position with the conventional anchorage at its end as shown in Figure 46. The strain gauge cable is then soldered to DAQ and is calibrated along with load cell and LVDT. On the dead end an LVDT is installed. At this point the bars are ready for prestressing. Grout is prepared once the bar has been prestressed to 80% of the desired load. Once the prestressing load reached the desired load grout is poured using a plastic stopper in the hole in the steel pipe. In Figure 47, show how the disc springs compress when bar reaches the desired load. The grout in the live end is allowed to set for 2 hours and then the hydraulic jack is released and the bar section extending is cut. The LVDT for live end is then attached to the live end.

Figure 44 Creep-rupture setup before test

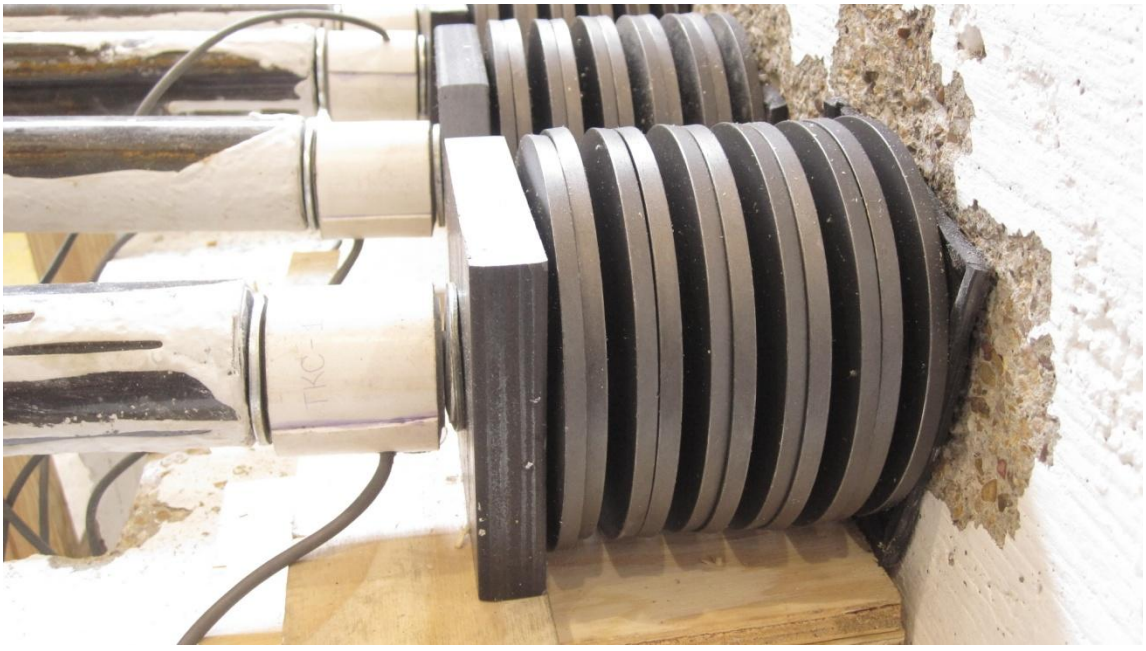

Figure 45 Uncompressed disc spring

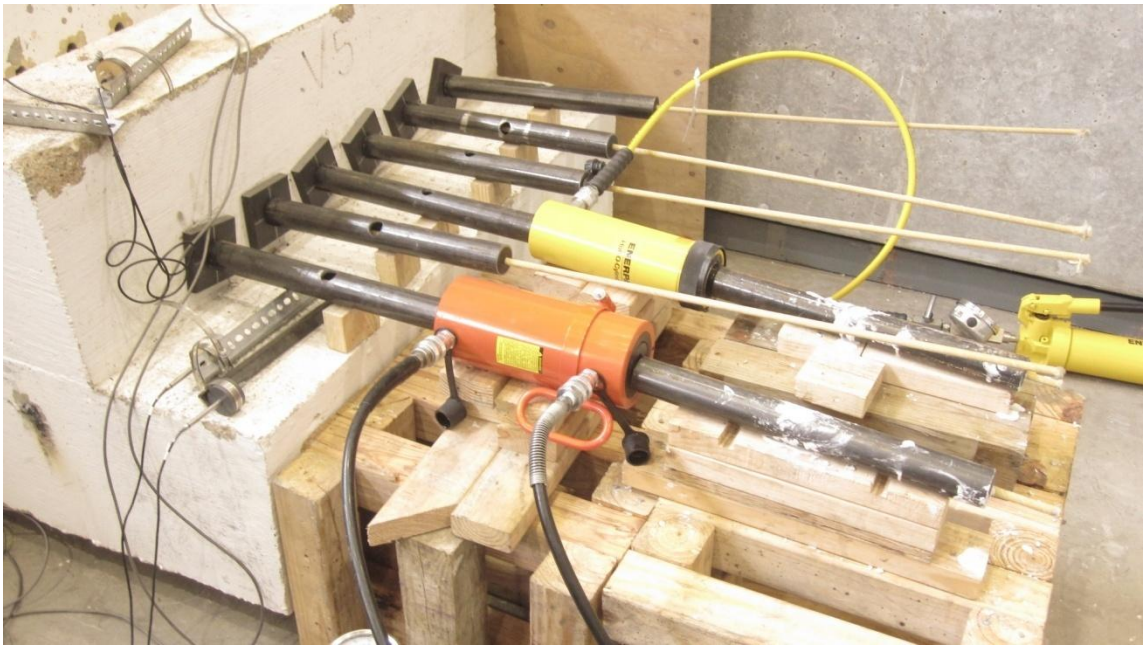

Figure 46 Hydraulic jacks and hand pumps for multiple prestressing

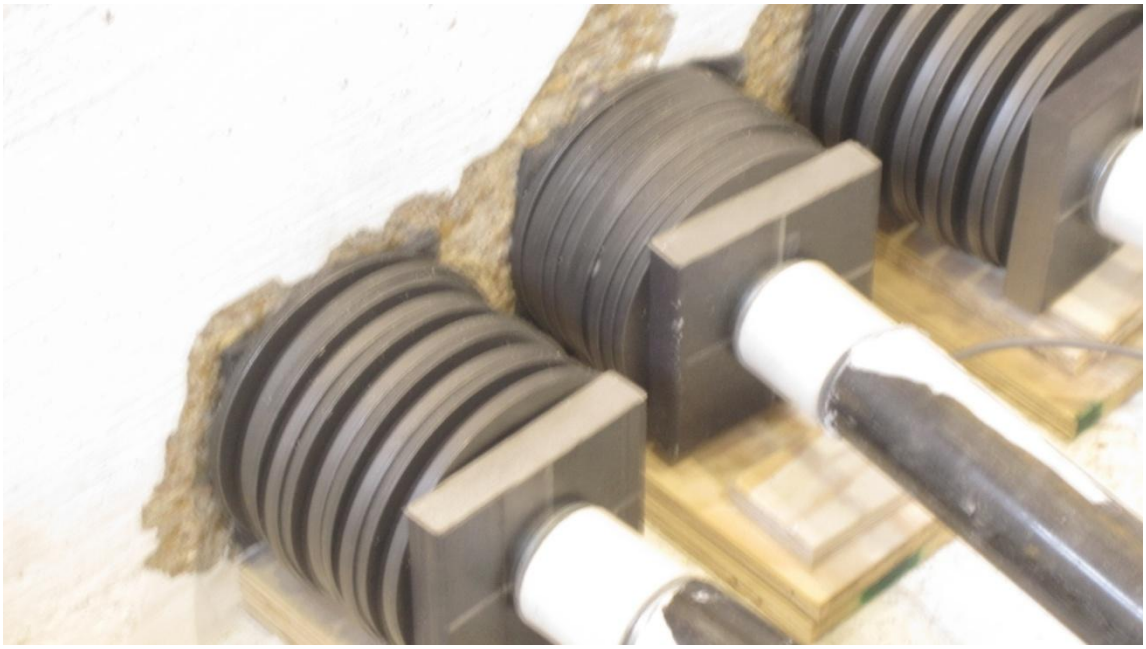

Figure 47 Compressed disc spring

3.4.3 Experimental Results

Short-term creep-rupture tests are necessary in order to better predict the 100-year life of the AFRP bars as rupture will occur in a range of time between a few hours and a few days (i.e., 5 hours to 14 days). These experiments are underway and will be documented in a journal paper to come, where the results will help determine the rupture time for AFRP when prestress to 60% by extrapolating the results obtained by testing at the 85% and 75% stress level.

3.4.3.1 Long-Term Creep-Rupture Tests

The first specimen tested was prestressed to 60% of ultimate stress of AFRP bar. Shown in Figure 48 is the measured stress level vs. time graph for specimen 1. The stress in the bar was determined using load cell reading and adding LVDT displacement by converting to strain and using modulus of elasticity to convert to stress in order to compensate for losses in load due to slippage. The bar was tested for 1000 hours; however, at 500 hours the bar failed due to slippage. The creep behavior can be seen in Figure 49. From this experiment it was noted that when concrete was poured and curing of concrete began there was a spike in the creep rate. After this time frame the creep rate returned to normal.

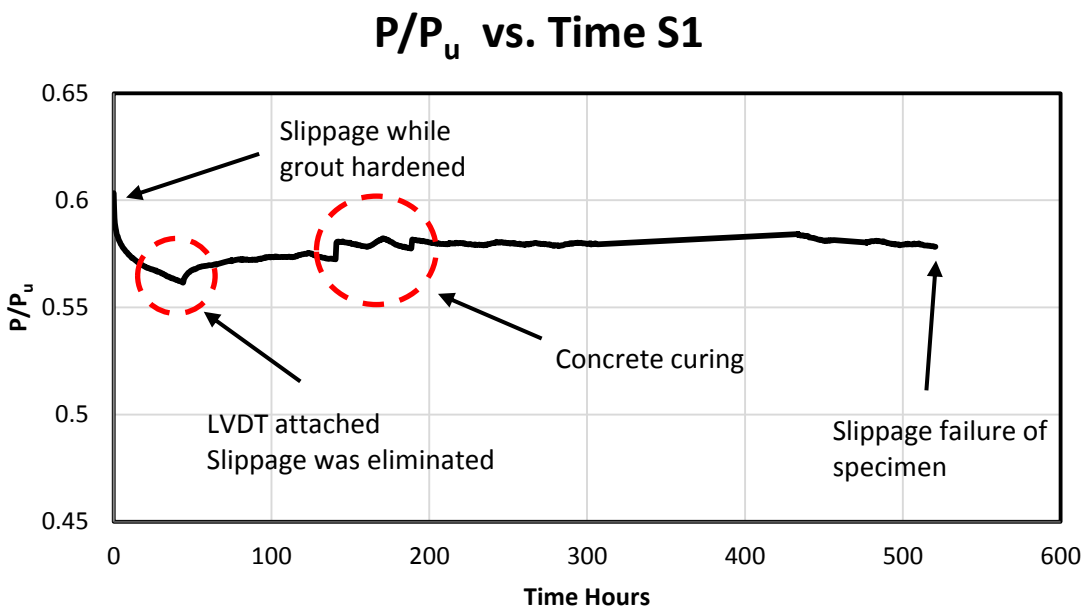

Figure 48 Long-term creep specimen 1 load level vs. time

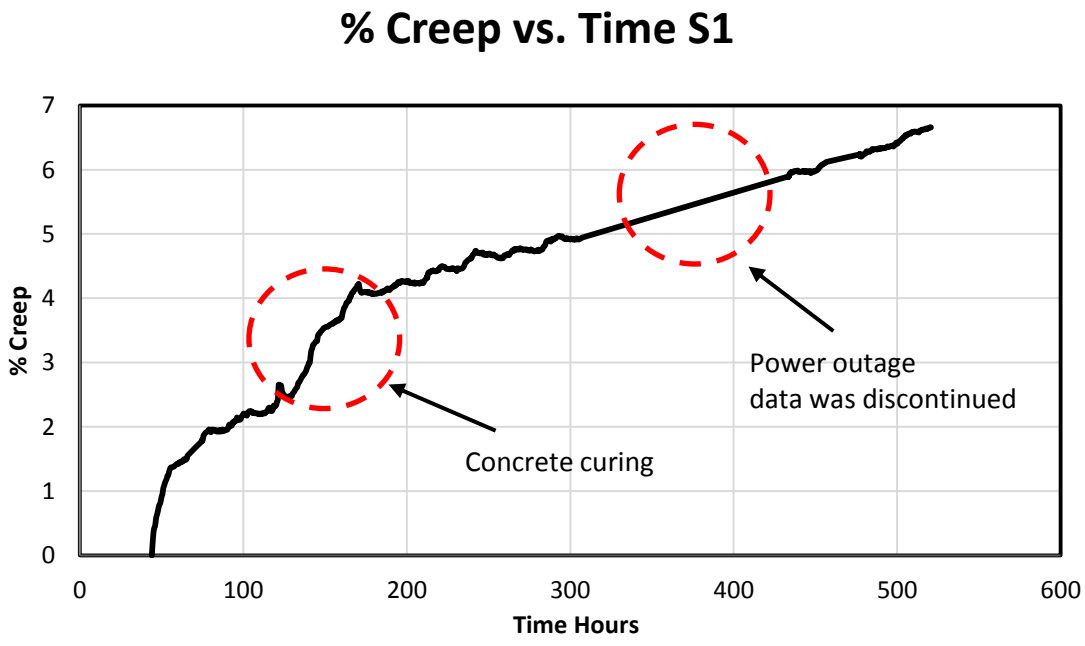

Figure 49 Long-term creep specimen 1% creep vs. time

The second specimen tested was prestressed to 50% of ultimate stress of AFRP bar. Shown in Figure 50 is the measured stress level vs. time graph for specimen 2. The stress in the bar was determined using load cell reading and adding LVDT displacement by converting to strain and using modulus of elasticity to convert to stress in order to compensate for losses in load due to slippage. The bar was tested for 1000 hours and experience about 12% loss due to slippage. The creep behavior can be seen in Figure 51.

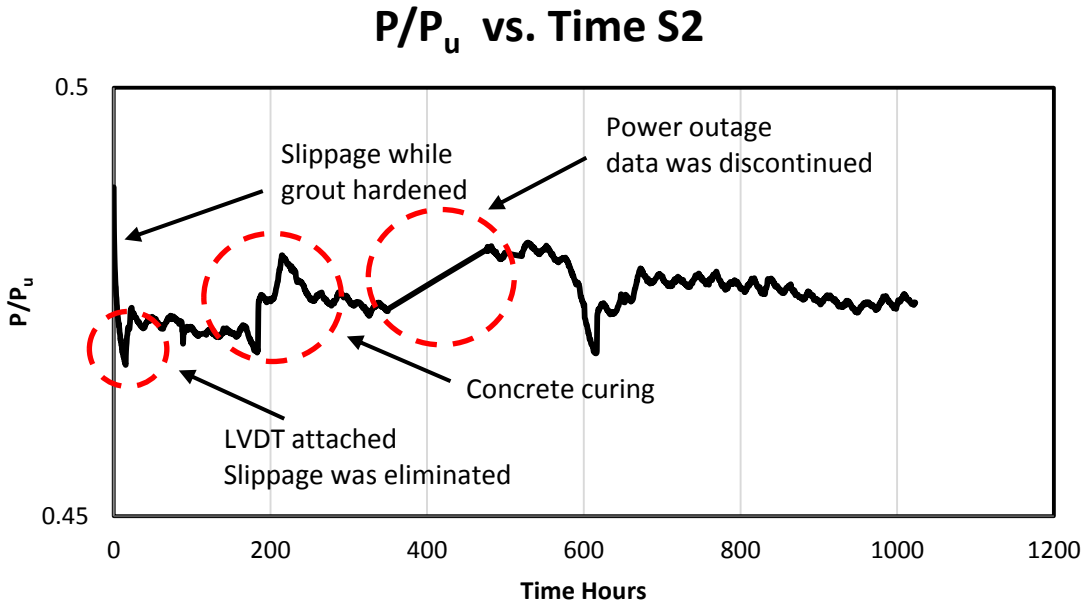

Figure 50 Long-term creep specimen 2 load level vs. time

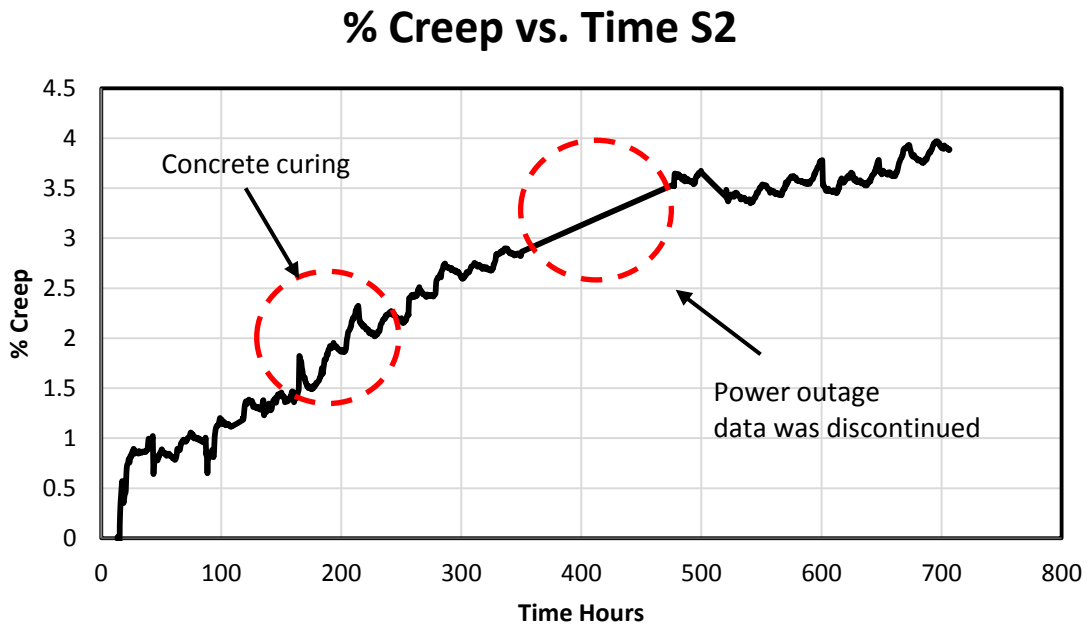

Figure 51 Long-term creep specimen 2% creep vs. time

The third specimen tested was prestressed to 60% of ultimate stress of AFRP bar. Shown in Figure 52 is the measured stress level vs. time graph for specimen 3. The stress in the bar was determined using load cell reading and adding LVDT displacement by converting to strain and using modulus of elasticity to convert to stress in order to compensate for losses in load due to slippage. The bar was tested for 1000 hours however, at 140 hours the bar failed due to slippage. The creep behavior can be seen in Figure 53. From this experiment it was noted that when concrete was poured and curing of concrete began there was a spike in the creep rate. After this time frame the creep rate returned to normal.

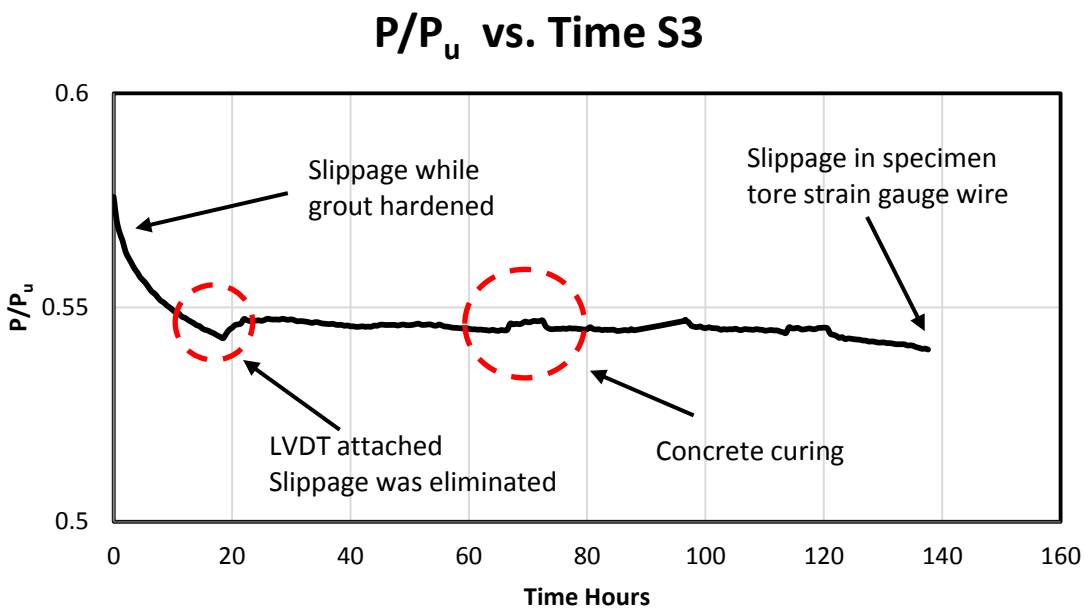

Figure 52 Long-term creep specimen 3 load level vs. time

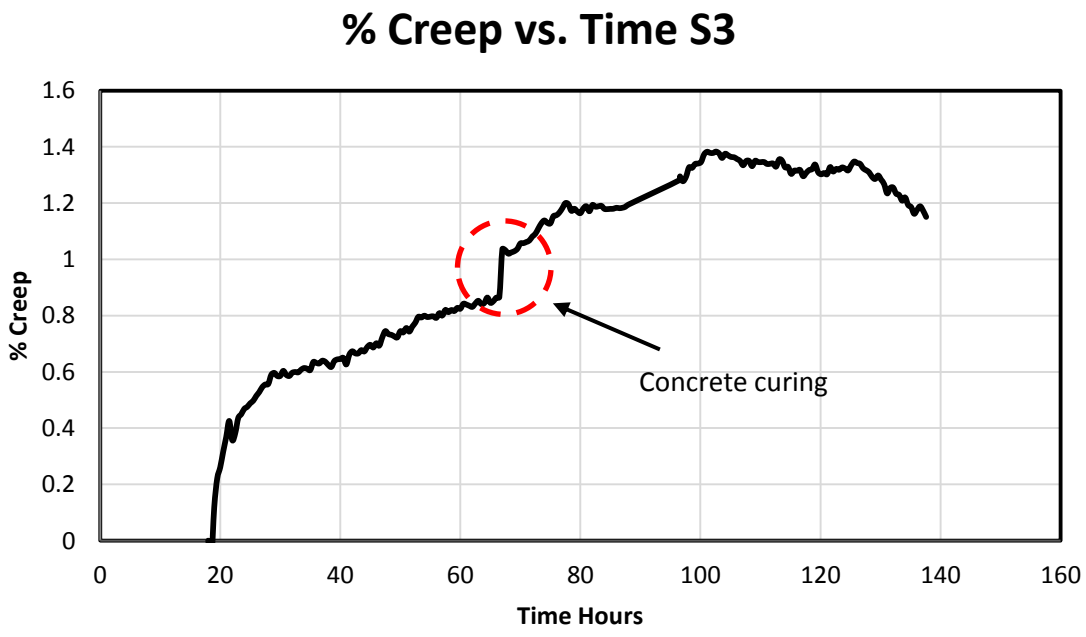

Figure 53 Long-term creep specimen 3% creep vs. time

The fourth specimen tested was prestressed to 50% of ultimate stress of AFRP bar. Shown in Figure 54 is the measured stress level vs. time graph for specimen 4. The stress in the bar was determined using load cell reading and adding LVDT displacement by converting to strain and using modulus of elasticity to convert to stress in order to compensate for losses in load due to slippage. The bar was tested for 1000 hours. The creep behavior can be seen in Figure 55. From this experiment it was noted that when concrete was poured and curing of concrete began there was a spike in the creep rate. After this time frame the creep rate returned to normal. The overall creep for this specimen at 1000 hours was 4%.

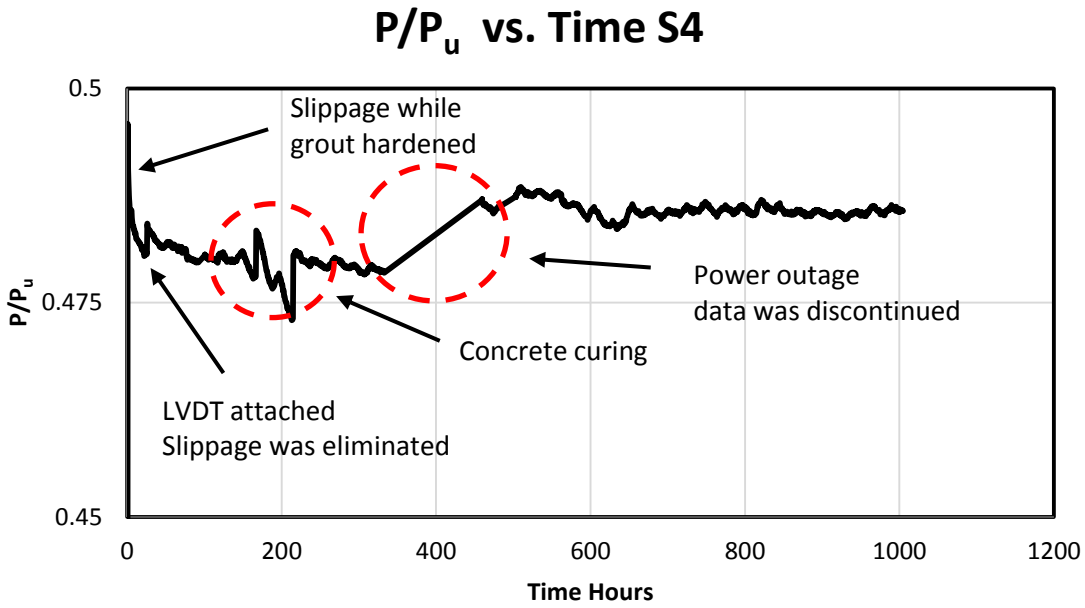

Figure 54 Long-term creep specimen 4 load level vs. time

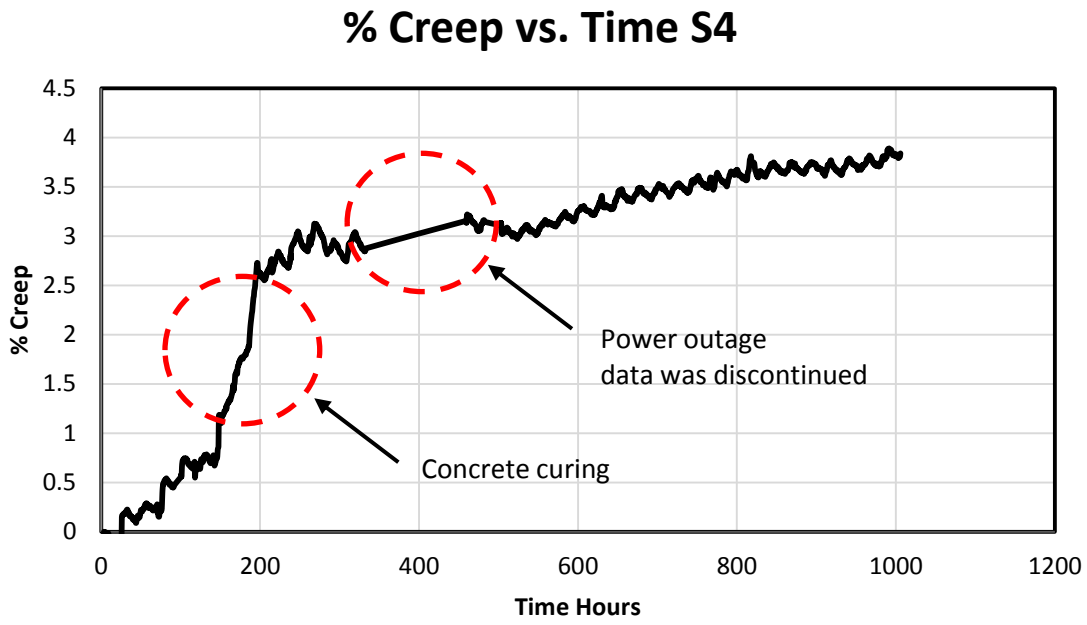

Figure 55 Long-term creep specimen 4% creep vs. time

The fifth specimen tested was prestressed to 50% of ultimate stress of AFRP bar. Shown in Figure 56 is the measured stress level vs. time graph for specimen 5. The stress in the bar was determined using load cell reading and adding LVDT displacement by converting to strain and using modulus of elasticity to convert to stress in order to compensate for losses in load due to slippage. The bar was tested for 1000 hours. The creep behavior can be seen in Figure 57. From this experiment it was noted that when concrete was poured and curing of concrete began there was a spike in the creep rate. After this time frame the creep rate returned to normal. The total creep recorded for 1000 hours was 3.5%.

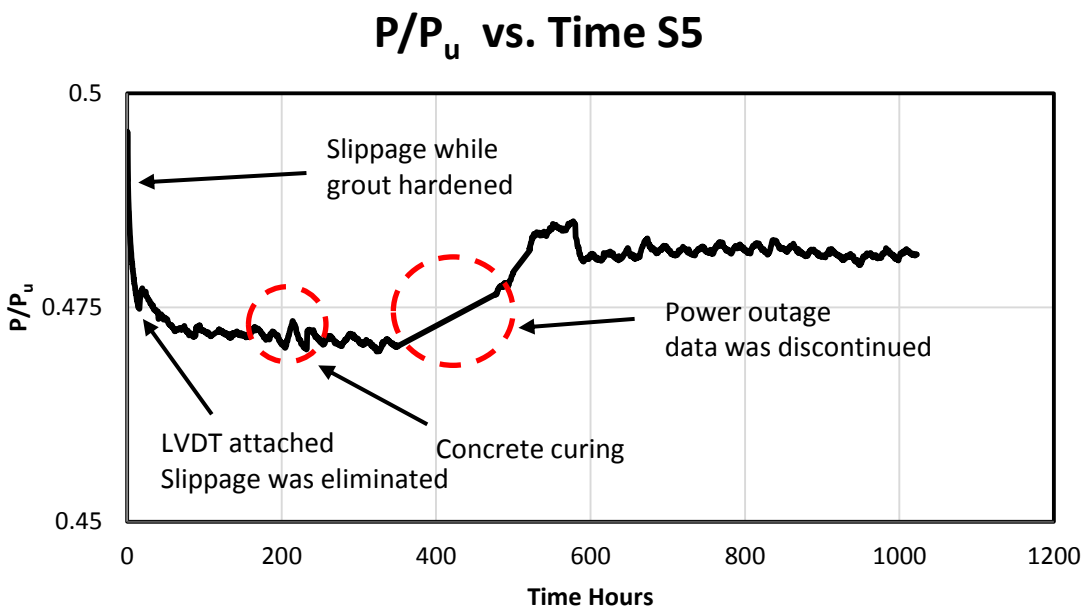

Figure 56 Long-term creep specimen 5 load level vs. time

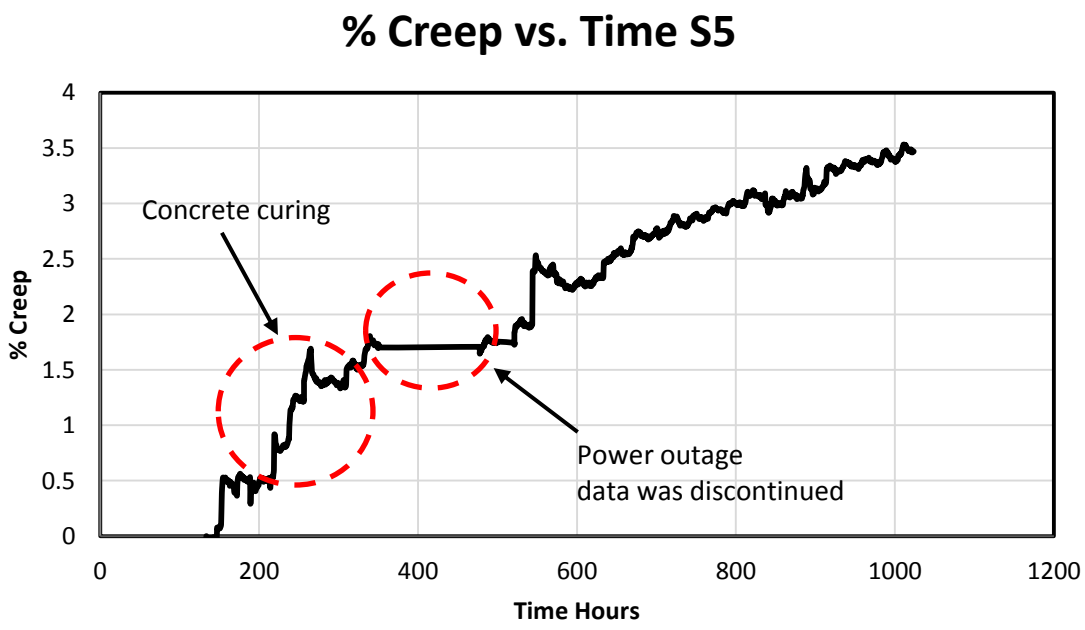

Figure 57 Long-term creep specimen 5% creep vs. time

The sixth specimen tested was prestressed to 60% of ultimate stress of AFRP bar. Shown in Figure 58 is the measured stress level vs. time graph for specimen 6. The stress in the bar was determined using load cell reading and adding LVDT displacement by converting to strain and using modulus of elasticity to convert to stress in order to compensate for losses in load due to slippage. The bar was tested for 1000 hours (42days); however, at 170 hours the bar began to slip from the dead end, hence the reason for dip in creep at 170 hours as can be seen in Figure 59. The reason that this slippage was not compensated was that previous test showed no slippage at dead end however, in this particular case bad grouting of dead end caused the anchorage to slip. Attention must be place on grouting for either live end or dead end as slippage can be intensified for higher load levels when grouting is not conducted well. From this experiment it was noted that when concrete was poured and curing of concrete began there was a spike in the creep rate. After this time frame the creep rate returned to normal. The maximum creep recorded before slippage at 170 hours was 4.5%.

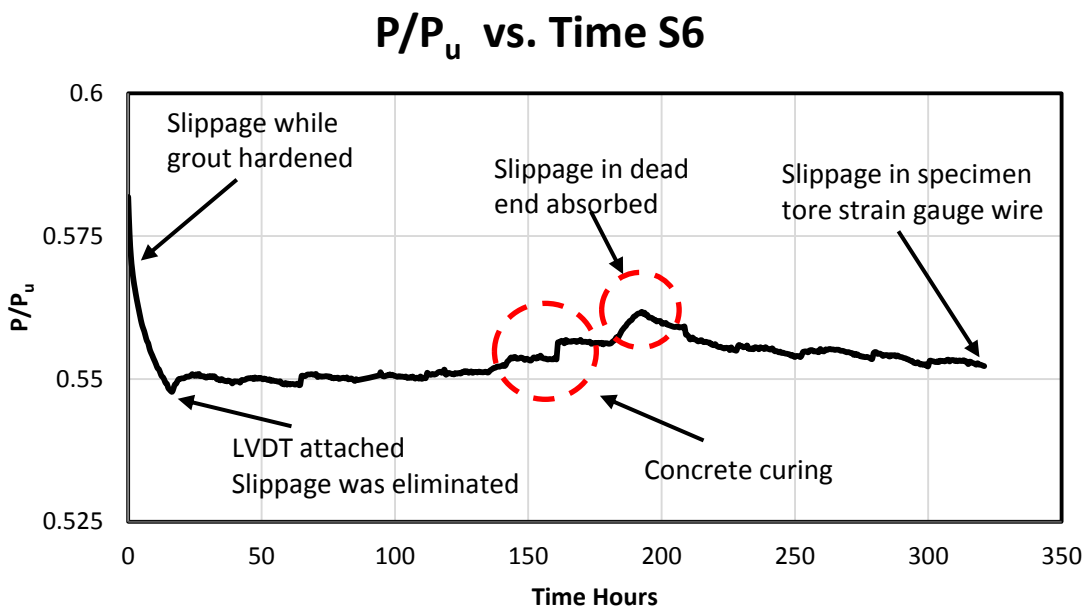

Figure 58 Long-term creep specimen 6 stress level vs. time

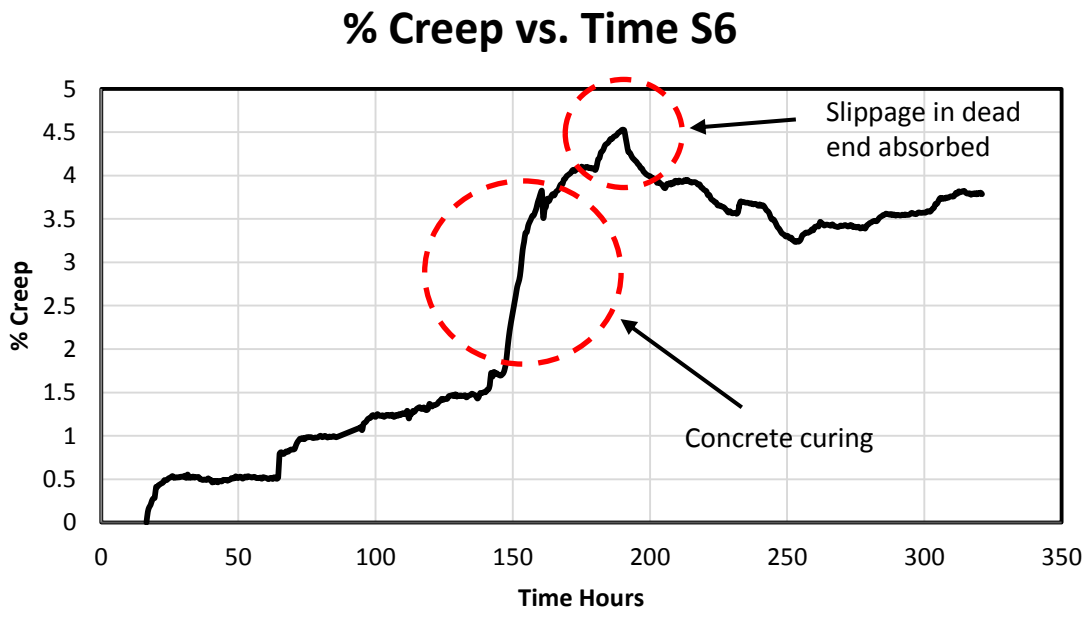

Figure 59 Long-term creep specimen 6% creep vs. time

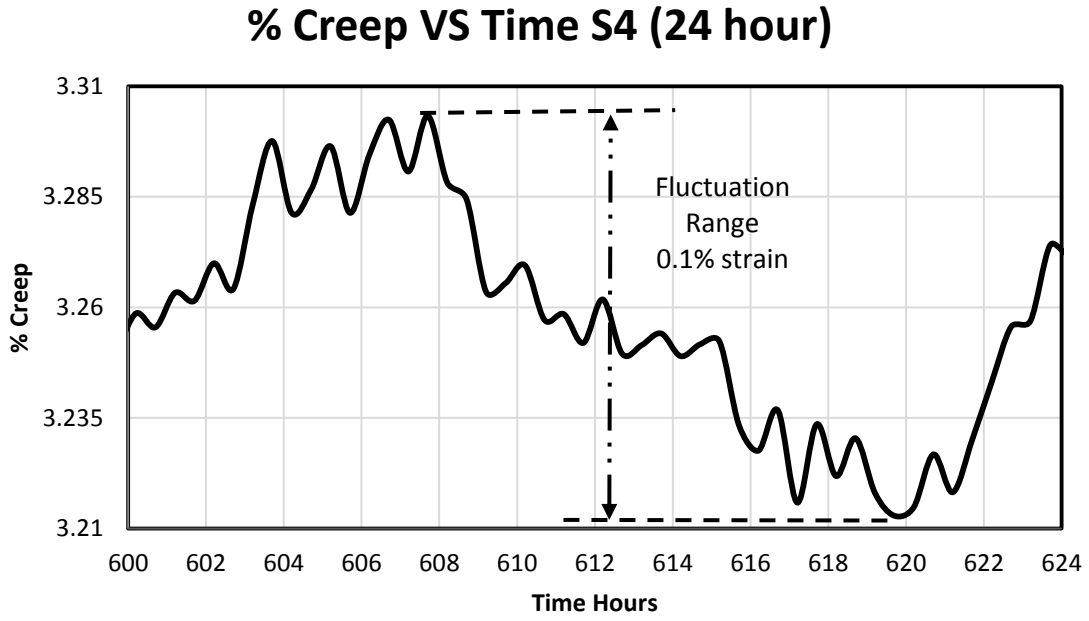

Figure 60 Creep-Rupture 24-hour plot

All creep-rupture curves showed noticeable fluctuation, for this reason a plotted snap shot of a 24 hour period was analyzed to determine the reason for this fluctuation. Shown in Figure 60, is this 24-hour period and clearly there is an overall sinusoidal pattern. At peak temperature the curve reached a max and at the lowest temperature the curve reached its min for the day. However, it is important to note that this fluctuation is between a plus or minus 0.05% strain change.

3.5 Relaxation Tests

3.5.1 Description of Relaxation Tests of Arapree® AFRP Bars

Short-term (2 weeks) and long-term (6 weeks) relaxation tests were conducted to revile the performance of Arapree® AFRP bars under constant strain. Twelve 87 in. (221 cm) specimens were tested three at each of 50, 60, 75, and 85% of ultimate tensile

capacity, shown in Table 3. The short-term tests were conducted with bars exposed to air and the long-term tests were conducted with bars embedded in concrete to mimic the effect of bars in prestressed concrete.

3.5.2 Instrumentation

For relaxation test the following instrumentation was used strain gauges, load cell, 2 steel washers, 3-18'' long 1.9'' OD steel pipe, 6 plastic stoppers, 2 steel plates, expansive grout Shepler's Shep Rock, and hydraulic jack with hand pump.

Twelve 87 in. (221 cm.) Arapree® AFRP bar were cut using a rotating steel wheel (Figure 125). Once the bars were cut the dead end of each bar was grouted. The steel pipe's ends were closed using plastic stoppers. After dead end grout set (2 hours) strain gauges were attached. After installing the strain gauges the bars were placed in concrete block with load cell (2 washers top and bottom) then steel plate. On the live end a steel plate followed by steel pipe with two plastic stoppers were placed. Once the pipe was placed the hydraulic jack was placed in position with conventional anchorage at end. The strain gauge cable was then soldered to DAQ (Figure 61) and is calibrated along with load cell and LVDT. On the dead end an LVDT is installed. At this point the bars are ready for prestressing. Grout is prepared once the bar has been prestressed to 80% of the desired load. Once the prestressing load reached the desired load grout is poured using a plastic stopper in the hole in the steel pipe. The grout in the live end is allowed to set for 2 hours and then the hydraulic jack is released and the bar section extending is cut. The LVDT for live end is then attached to the live end.

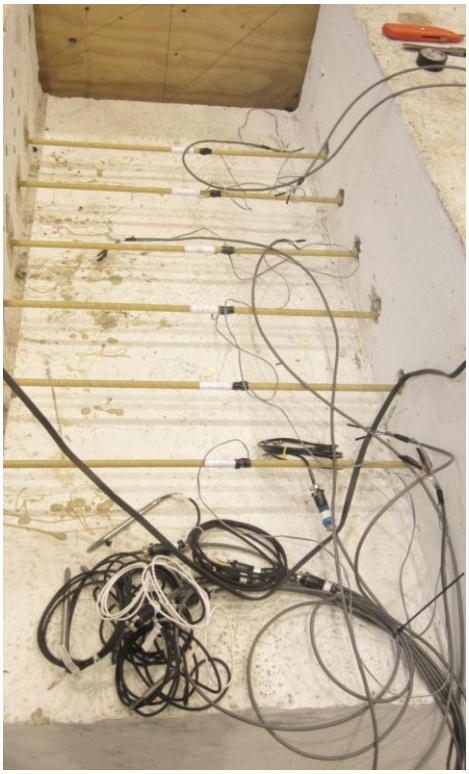

Figure 61 Strain gauge wiring

3.5.3 Experimental Results

3.5.3.1 Short-Term Relaxation

The first specimen tested was prestressed to 80% of ultimate stress of AFRP bar. Shown in Figure 62 is the relaxation curve for specimen 1. The stress in the bar was determined using load cell reading and adding LVDT displacement by converting to strain and using modulus of elasticity to convert to stress in order to compensate for losses in load due to slippage. The bar was tested for roughly 250 hours. The relaxation curve is also illustrated in Figure 63 in log scale clearly showing that the bar experienced 15% prestress loss in roughly 250 hours. From this experiment, it was noted that after 3

hours fiber damage to the bar cause a sudden drop in load and increased the rate of relaxation.

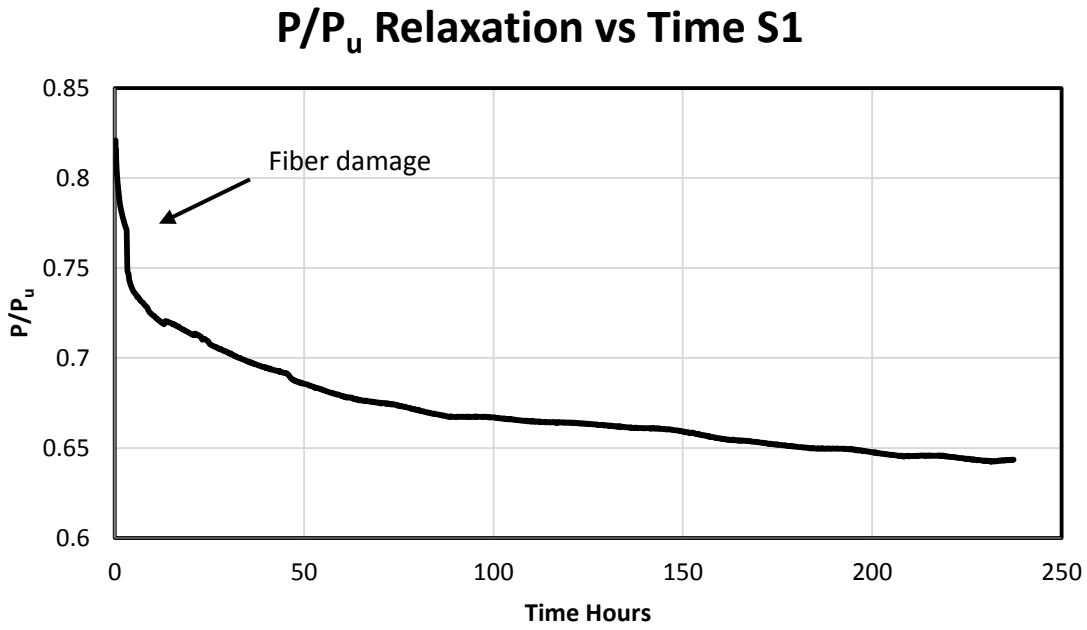

Figure 62 Relaxation stress level 80% specimen 1

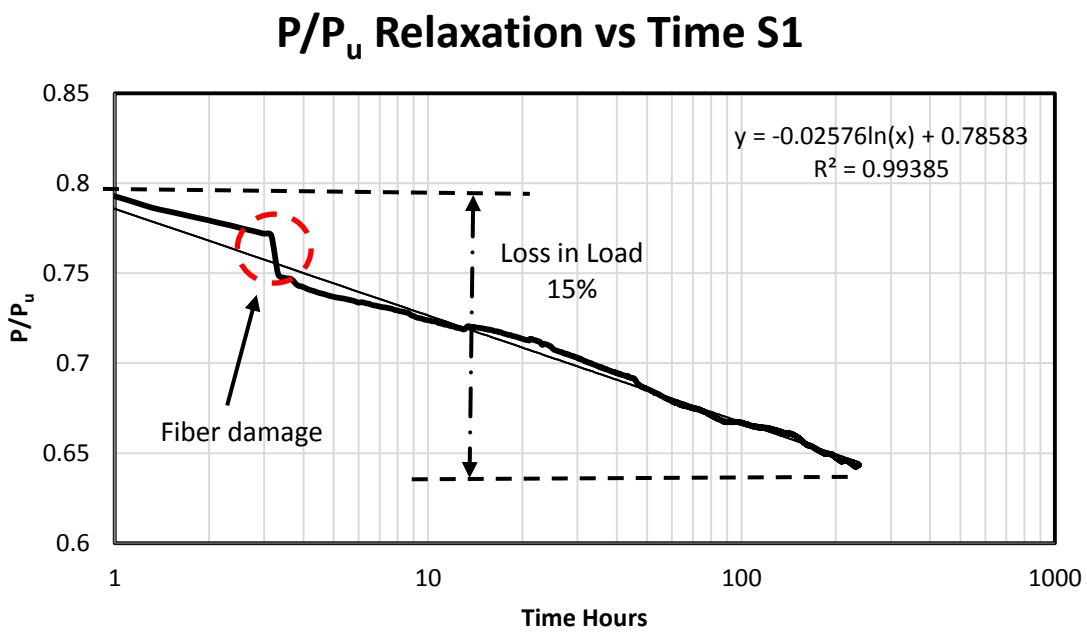

Figure 63 Relaxation stress level 80% specimen 1

The second specimen tested was prestressed to 65% of ultimate stress of AFRP bar initially however, after just 30 minutes of prestressing the bar failed near anchorage. It was determined after removing the specimen that the bar rubbed the concrete block and damage the bar leading the failure. The bar was later replaced and to avoid the same problem the bar was only prestressed to 65%. Shown in Figure 64 is the relaxation curve for specimen 2 redo. The stress in the bar was determined using load cell reading and adding LVDT displacement by converting to strain and using modulus of elasticity to convert to stress in order to compensate for losses in load due to slippage. The bar was tested for roughly 140 hours. The relaxation curve is also illustrated in Figure 64 in log scale clearly showing that the bar experience 3% prestress loss in roughly 100 hours much less than the specimen 1, which was prestressed to 80%. From this experiment it

was noted that the rate of relaxation is highly dependent on initial stress level and damage to bar.

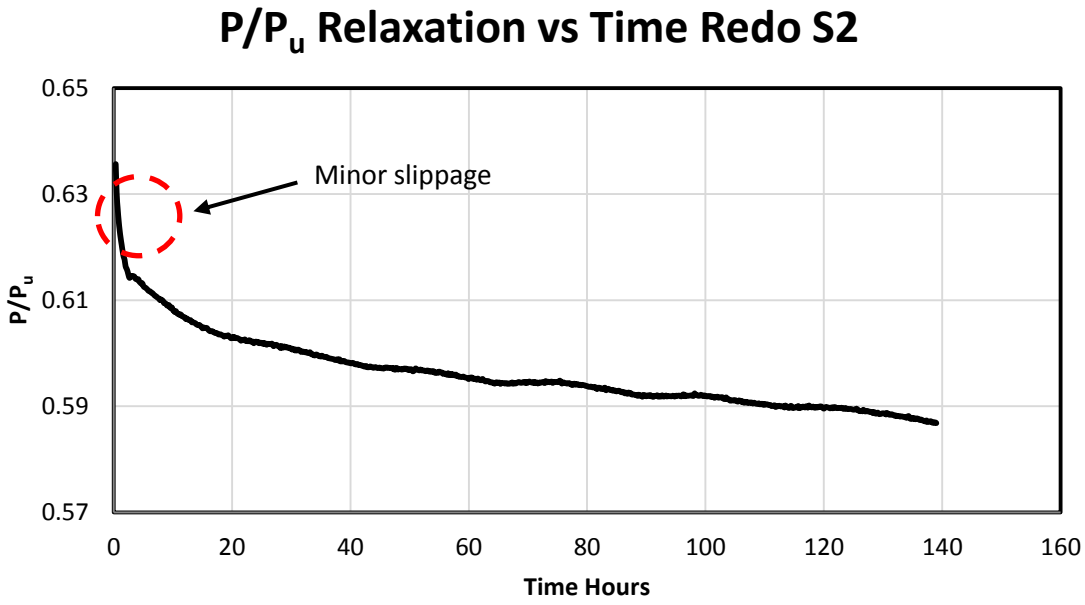

Figure 64 Relaxation stress level 65% specimen 2

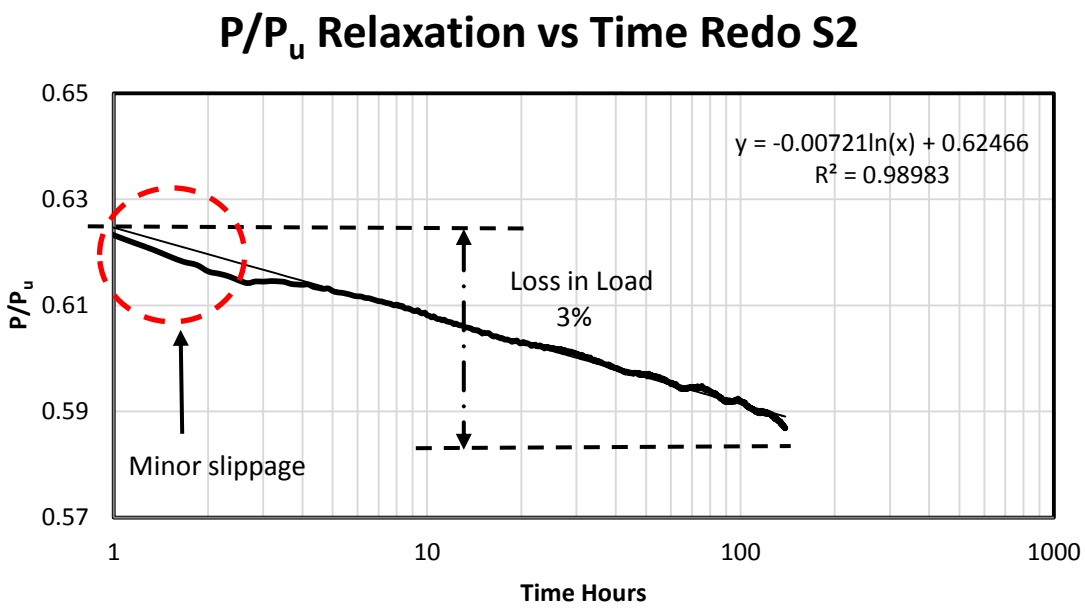

Figure 65 Relaxation stress level 65% specimen 2

The third specimen tested was prestressed to 75% of ultimate stress of AFRP bar. Shown in Figure 66 is the relaxation curve for specimen 3. The stress in the bar was determined using load cell reading and adding LVDT displacement by converting to strain and using modulus of elasticity to convert to stress in order to compensate for losses in load due to slippage. The bar was tested for roughly 250 hours; some fiber damage occurred at about 25 hours and clearly is shows a jump in stress level. The relaxation curve is also illustrated in Figure 67 in log scale clearly showing that the bar experienced 10% prestress loss in roughly 250 hours.

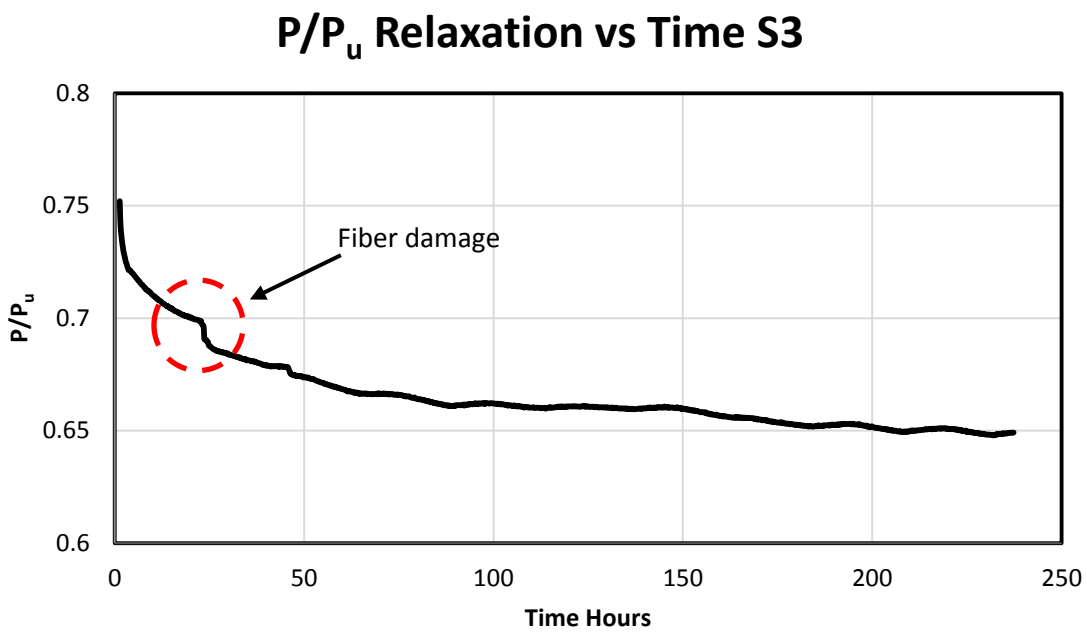

Figure 66 Relaxation stress level 75% specimen 3

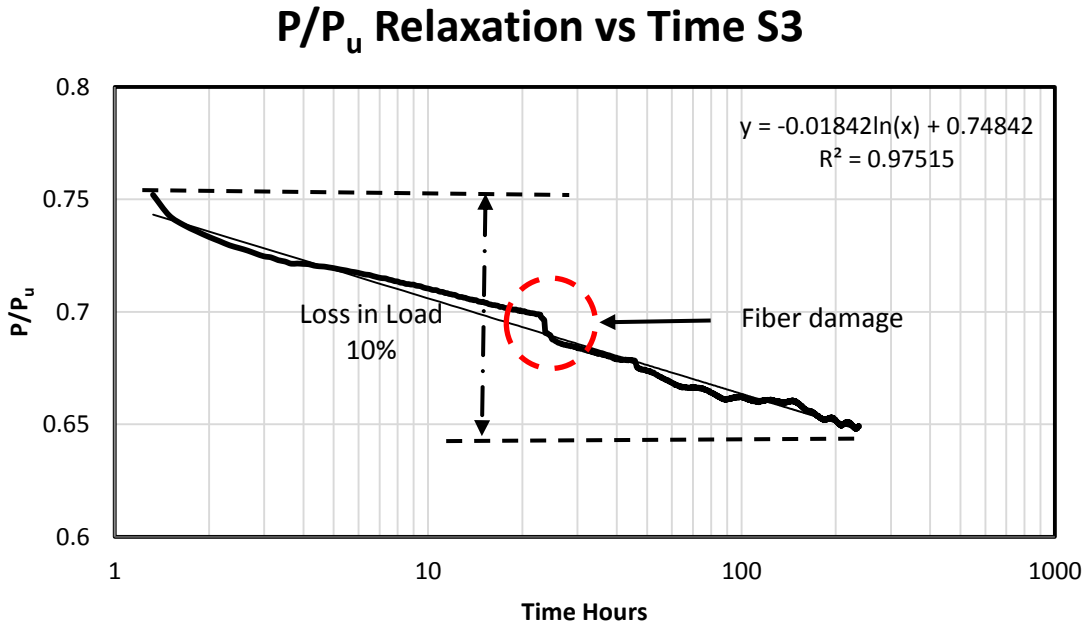

Figure 67 Relaxation stress level 75% specimen 3

The forth specimen tested was prestressed to 75% of ultimate stress of AFRP bar. Shown in Figure 68 is the relaxation curve for specimen 3. The stress in the bar was determined using load cell reading and adding LVDT displacement by converting to strain and using modulus of elasticity to convert to stress in order to compensate for losses in load due to slippage. The bar was tested for roughly 225 hours, some fiber damage occurred at about 2 hours and a sudden jump in stress level occurred. The relaxation curve is also illustrated in Figure 69 in log scale clearly showing that the bar experienced 13% prestress loss in roughly 225 hours.

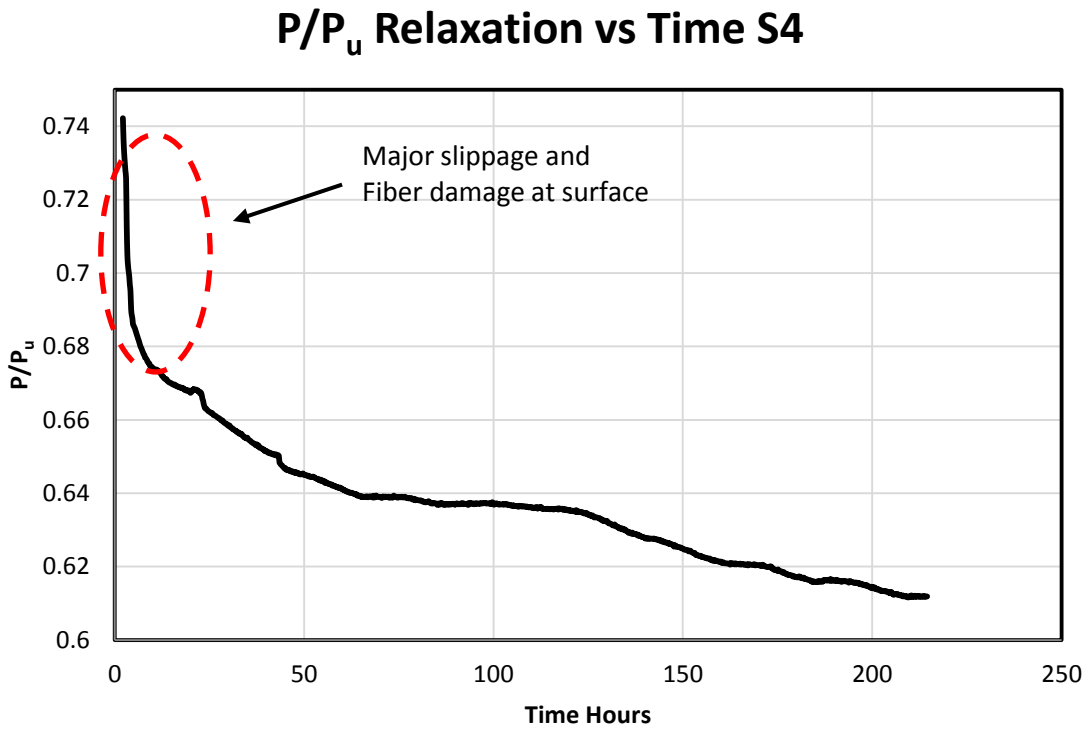

Figure 68 Relaxation stress level 75% specimen 4

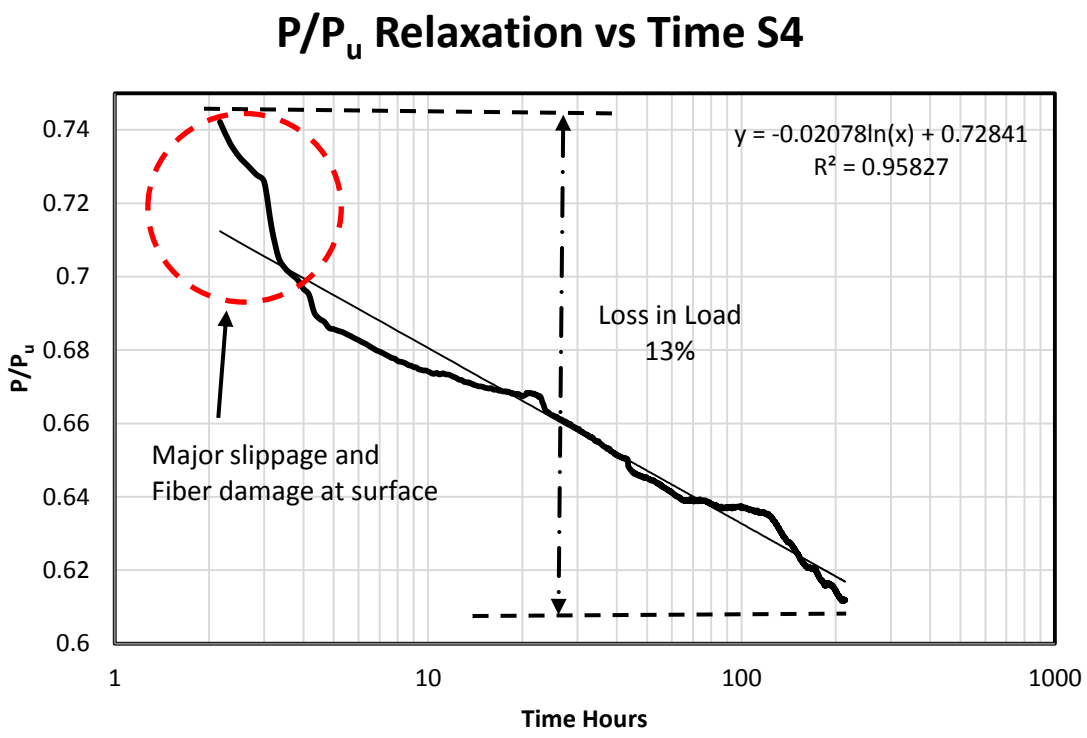

Figure 69 Relaxation stress level 75% specimen 4

The fifth specimen tested was prestressed to 75% of ultimate stress of AFRP bar. Shown in Figure 70 is the relaxation curve for specimen 5. The stress in the bar was determined using load cell reading and adding LVDT displacement by converting to strain and using modulus of elasticity to convert to stress in order to compensate for losses in load due to slippage, however, major slippage occurred in the bar and only a small portion was recoverable. The bar was tested for roughly 200 hours. The bar experienced nearly 37% prestress loss due mostly to slippage. From this experiment, it was noted that after that grouting of live end is very important and water to grout ratio will affect the strength of the grout after 2 hours.

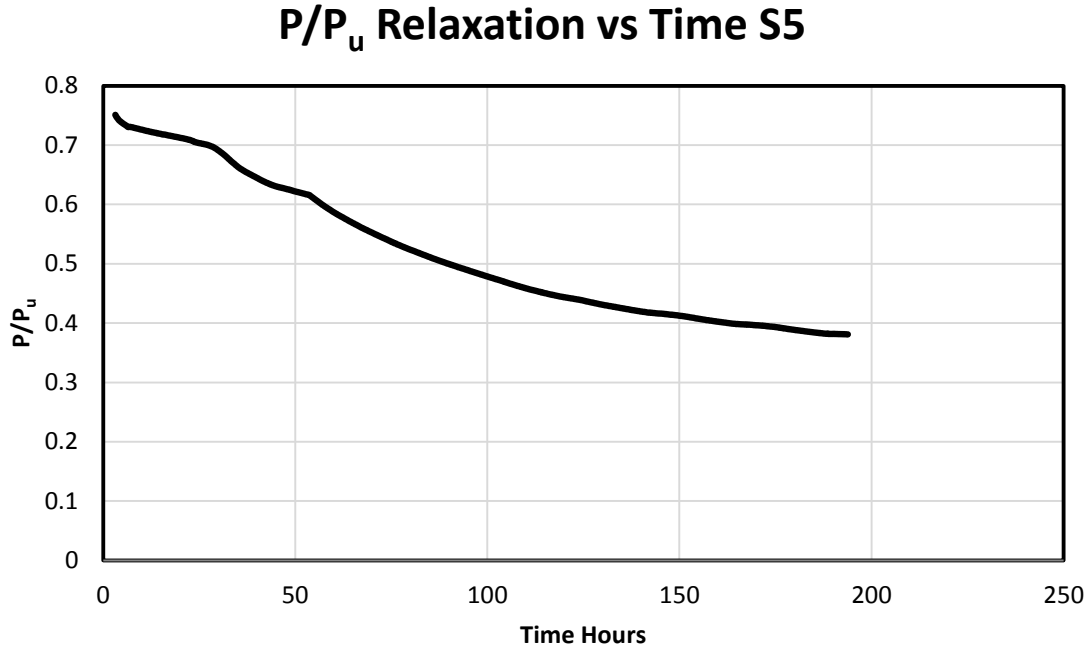

Figure 70 Relaxation stress level 75% specimen 5

The sixth specimen tested was prestressed to 80% of ultimate stress of AFRP bar. Shown in Figure 71 is the relaxation curve for specimen 6. The stress in the bar was determined using load cell reading and adding LVDT displacement by converting to strain and using modulus of elasticity to convert to stress in order to compensate for losses in load due to slippage. The bar was tested for roughly 200 hours. The relaxation curve is also illustrated in Figure 72 in log scale clearly showing that the bar experienced 14% prestress loss in roughly 200 hours.

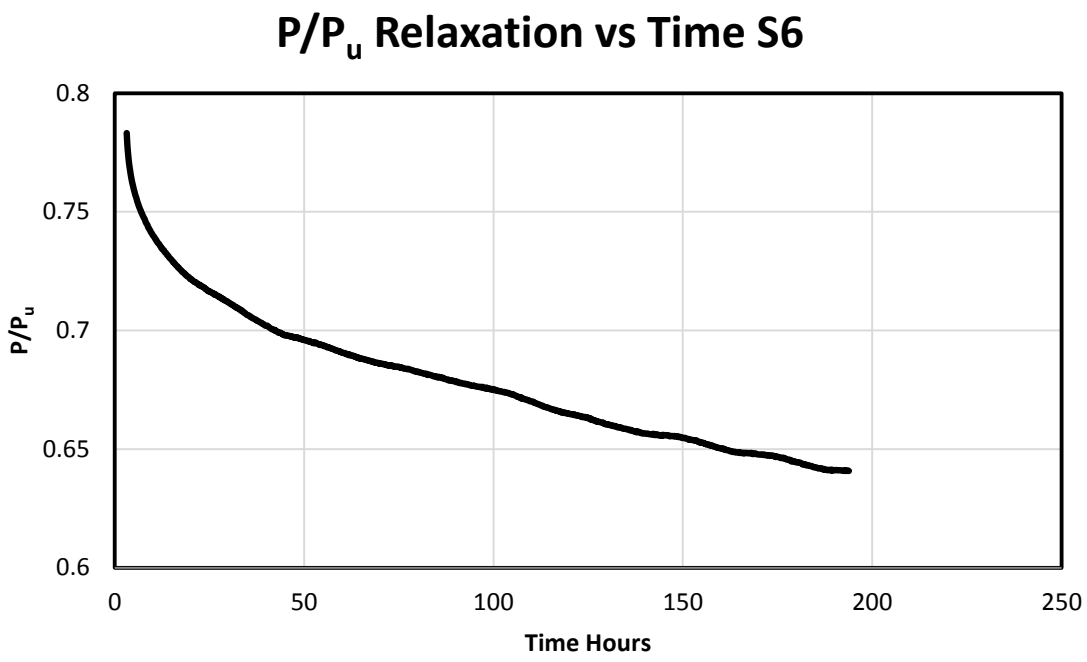

Figure 71 Relaxation stress level 80% specimen 6

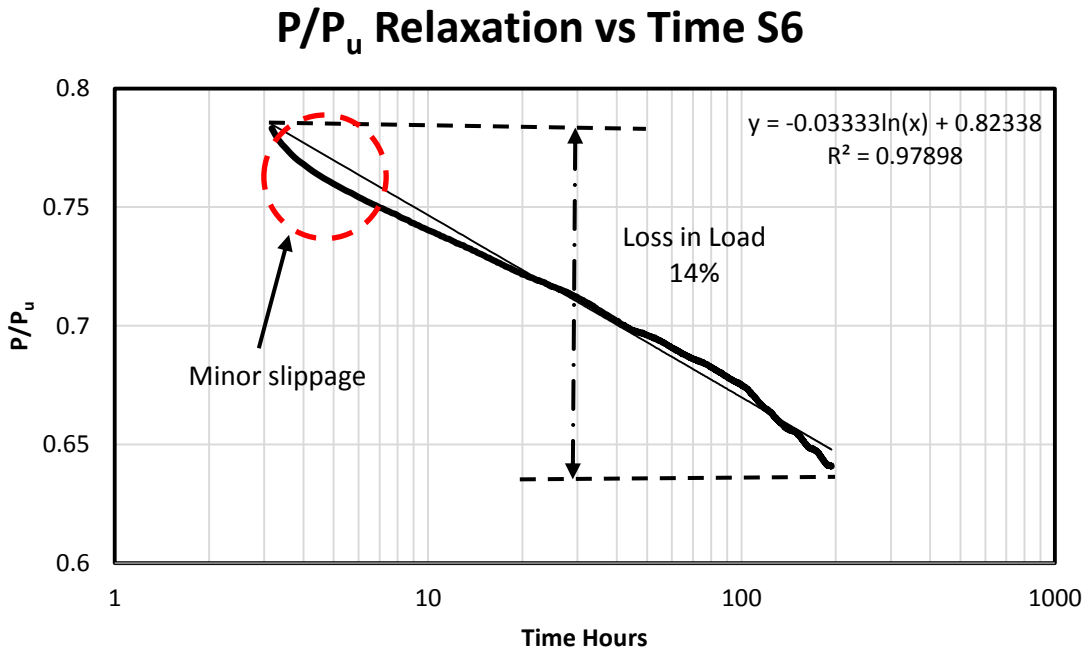

Figure 72 Relaxation stress level 80% specimen 6

3.5.3.2 Long-Term Relaxation

The long-term relaxation bars were tested for roughly 1000 hours. The strain gauges were coated with a protective wax and hardener which can be seen in Figure 73. Wooden form work, shown in Figure 74, was prepare around all the relaxation bars in order to pour concrete after all bars were prestress. Concrete was poured at about 70 hours after start of test shown in Figure 75. In the live ends of all bars a LVDT was attached see Figure 76. In Figure 77, it shows the angle and tie used to keep LVDT in position next to steel pipe. The dead end of bar can be seen in Figure 78.

Figure 73 Concrete protected coating on strain gauges

Figure 74 Formwork for concrete to encase bars

Figure 75 Long-term relaxation bars with concrete

Figure 76 Live ends with LVDTs

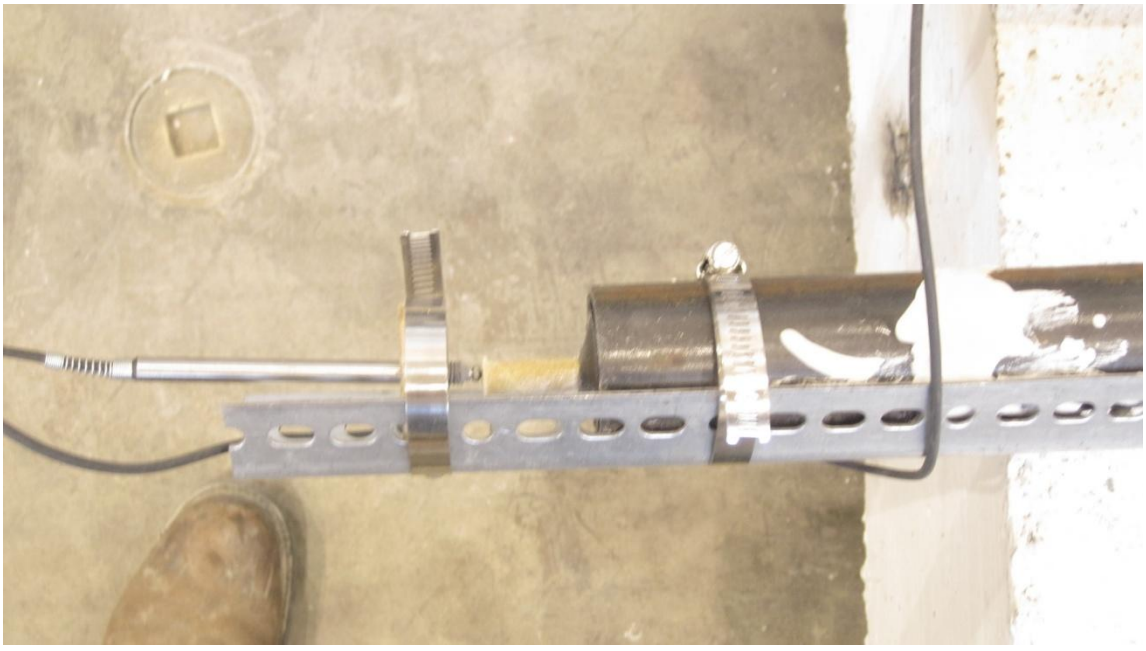

Figure 77 Live end LVDT for long-term test

Figure 78 Dead end relaxation specimens

The seventh specimen tested was prestressed to 50% of ultimate stress of AFRP bar. Shown in Figure 79 is the relaxation curve for specimen 7. The stress in the bar was determined using load cell reading and adding LVDT displacement by converting to strain and using modulus of elasticity to convert to stress in order to compensate for losses in load due to slippage. The bar was tested for roughly 1000 hours. The relaxation curve is also illustrated in Figure 80 in log scale clearly showing that the bar experienced 5% prestress loss in roughly 1000 hours. From this experiment, it was noted that curing of the concrete caused the rate of relaxation to accelerate.

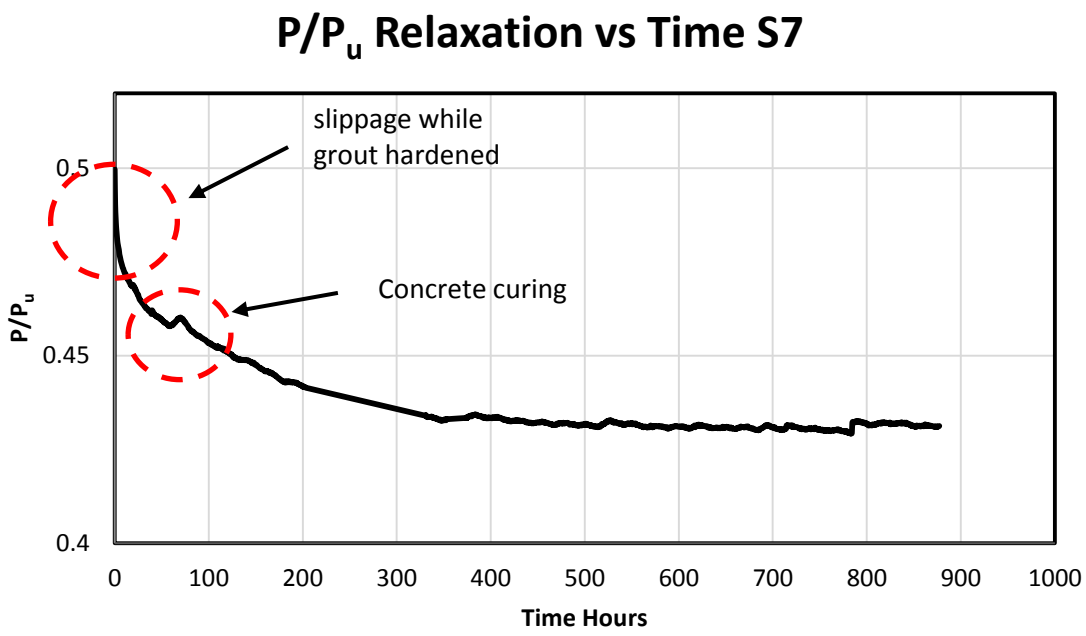

Figure 79 Relaxation stress level 50% specimen 7

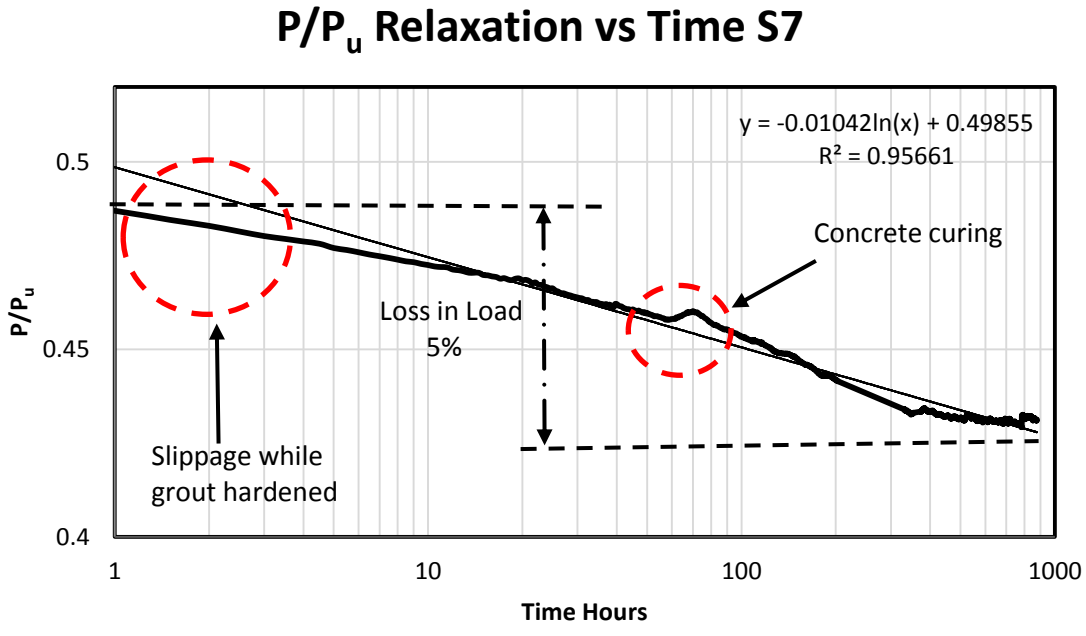

Figure 80 Relaxation stress level 50% specimen 7

The eighth specimen tested was prestressed to 50% of ultimate stress of AFRP bar. Shown in Figure 81 is the relaxation curve for specimen 8. The stress in the bar was determined using load cell reading and adding LVDT displacement by converting to strain and using modulus of elasticity to convert to stress in order to compensate for losses in load due to slippage. The bar was tested for roughly 1000 hours. The relaxation curve is also illustrated in Figure 82 in log scale clearly showing that the bar experienced 8% prestress loss in roughly 1000 hours. From this experiment, it was noted that curing of the concrete caused the rate of relaxation to accelerate.

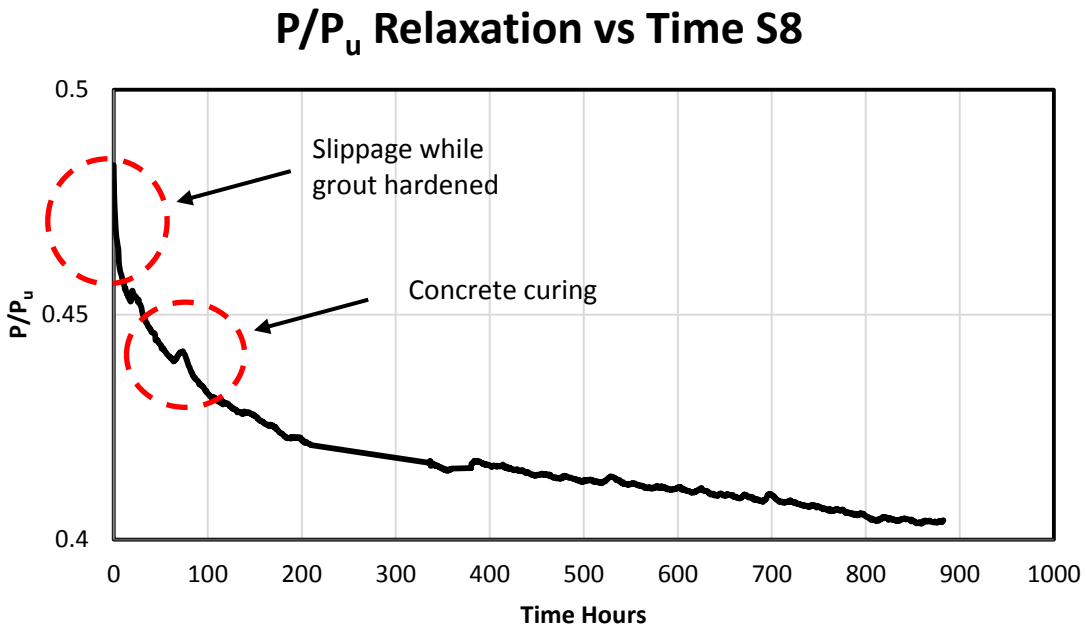

Figure 81 Relaxation stress level 50% specimen 8

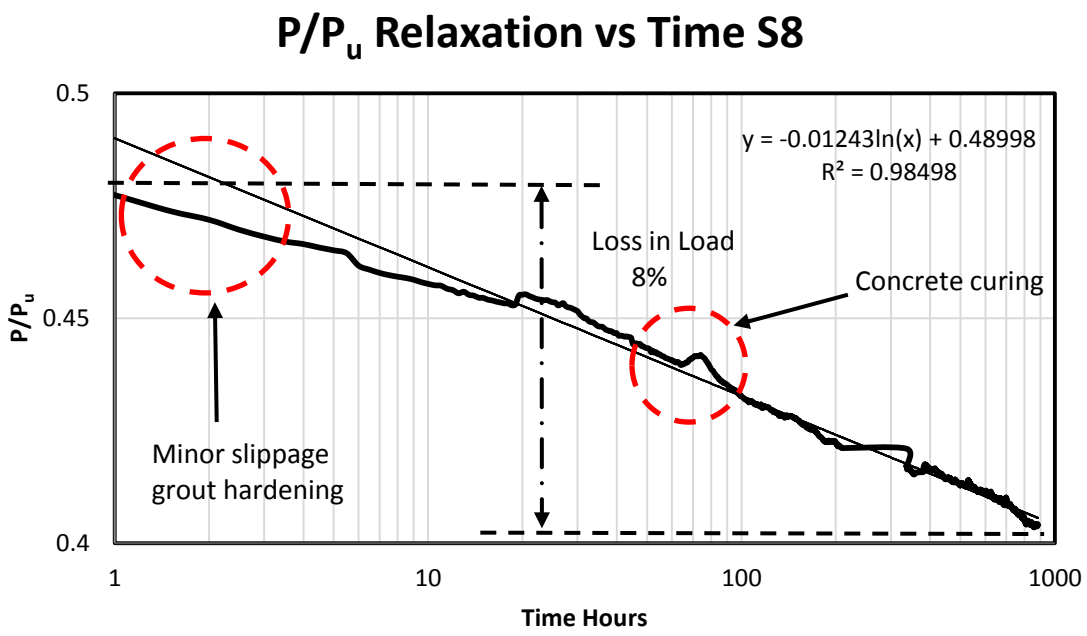

Figure 82 Relaxation stress level 50% specimen 8

The ninth specimen tested was prestressed to 60% of ultimate stress of AFRP bar. Shown in Figure 83 is the relaxation curve for specimen 9. The stress in the bar was determined using load cell reading and adding LVDT displacement by converting to strain and using modulus of elasticity to convert to stress in order to compensate for losses in load due to slippage. The bar was tested for roughly 1000 hours. The relaxation curve is also illustrated in Figure 84 in log scale clearly showing that the bar experienced 5% prestress loss in roughly 1000 hours. From this experiment, it was noted that curing of the concrete caused the rate of relaxation to accelerate.

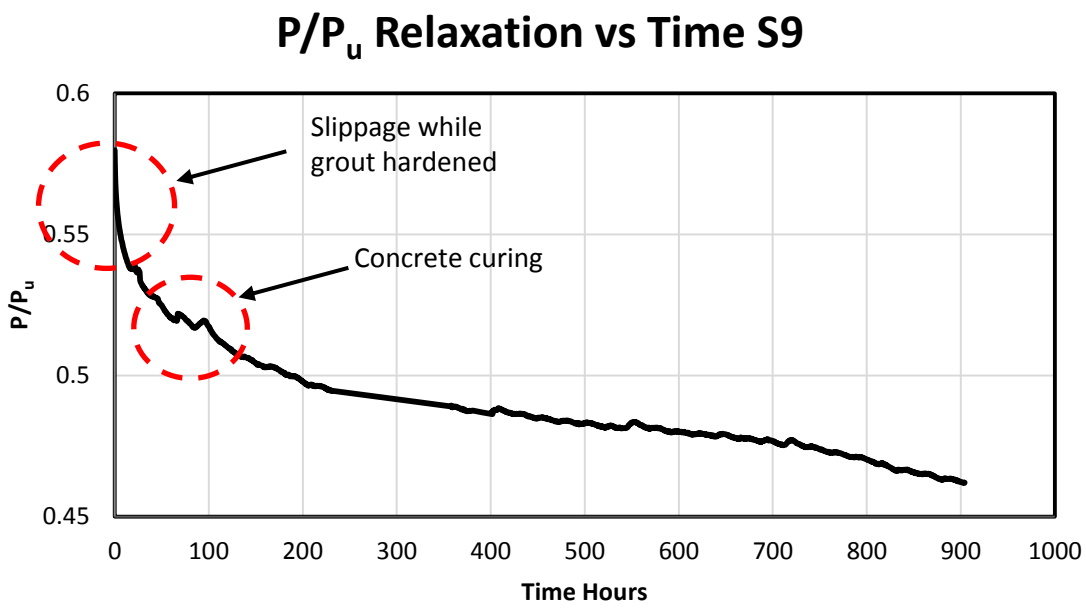

Figure 83 Relaxation stress level 60% specimen 9

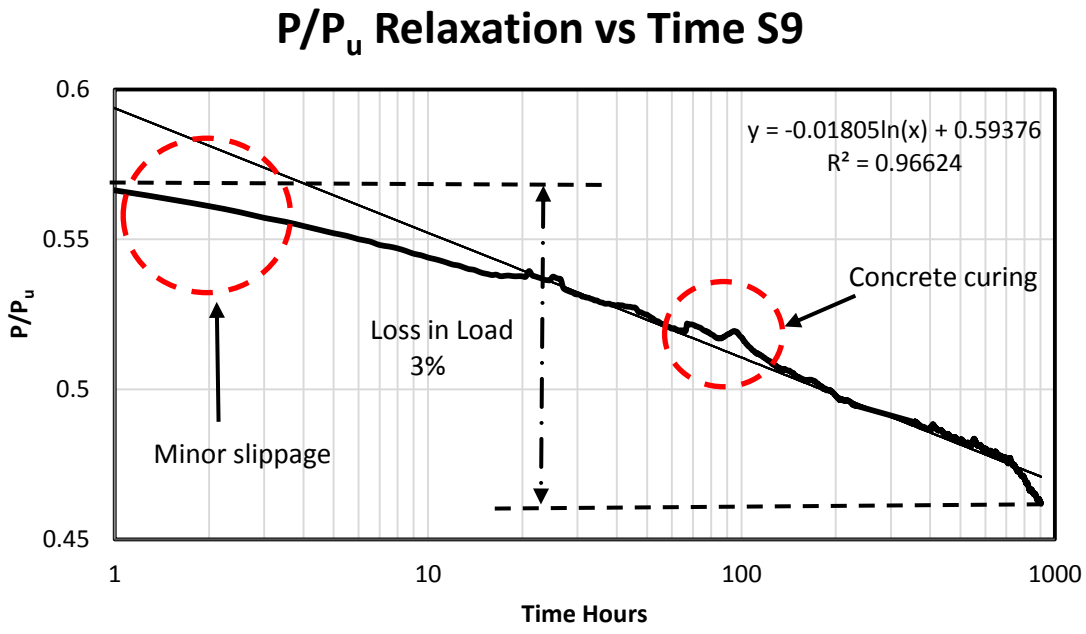

Figure 84 Relaxation stress level 60% specimen 9

The tenth specimen tested was prestressed to 60% of ultimate stress of AFRP bar. Shown in Figure 85 is the relaxation curve for specimen 10. The stress in the bar was determined using load cell reading and adding LVDT displacement by converting to strain and using modulus of elasticity to convert to stress in order to compensate for losses in load due to slippage. The bar was tested for roughly 1000 hours. The relaxation curve is also illustrated in Figure 86 in log scale clearly showing that the bar experienced 11% prestress loss in roughly 1000 hours. From this experiment, it was noted that curing of the concrete caused the rate of relaxation to accelerate.

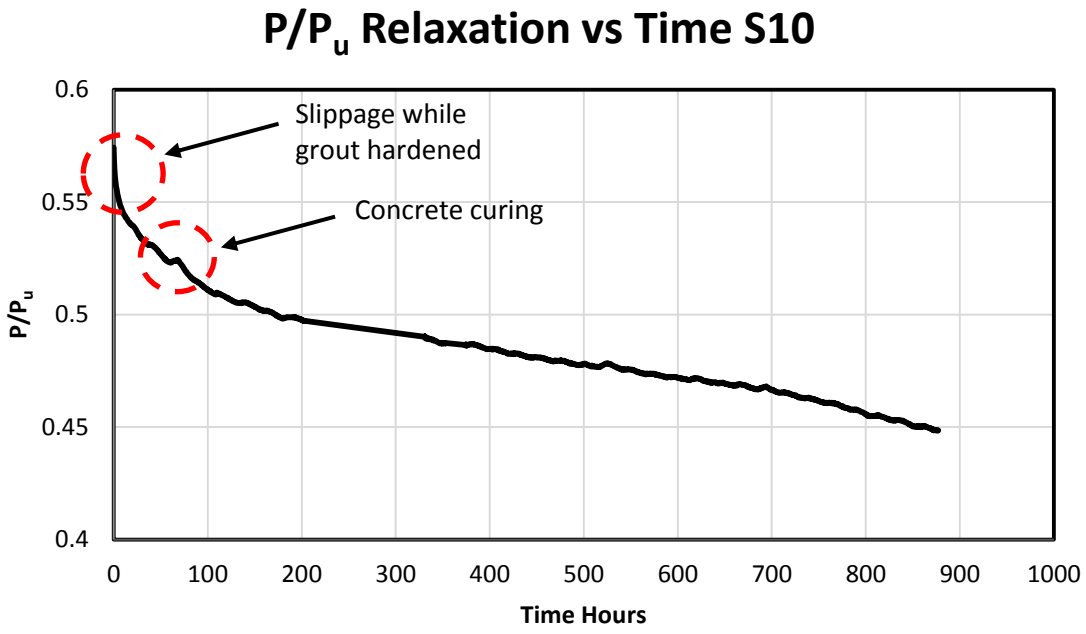

Figure 85 Relaxation stress level 60% specimen 10

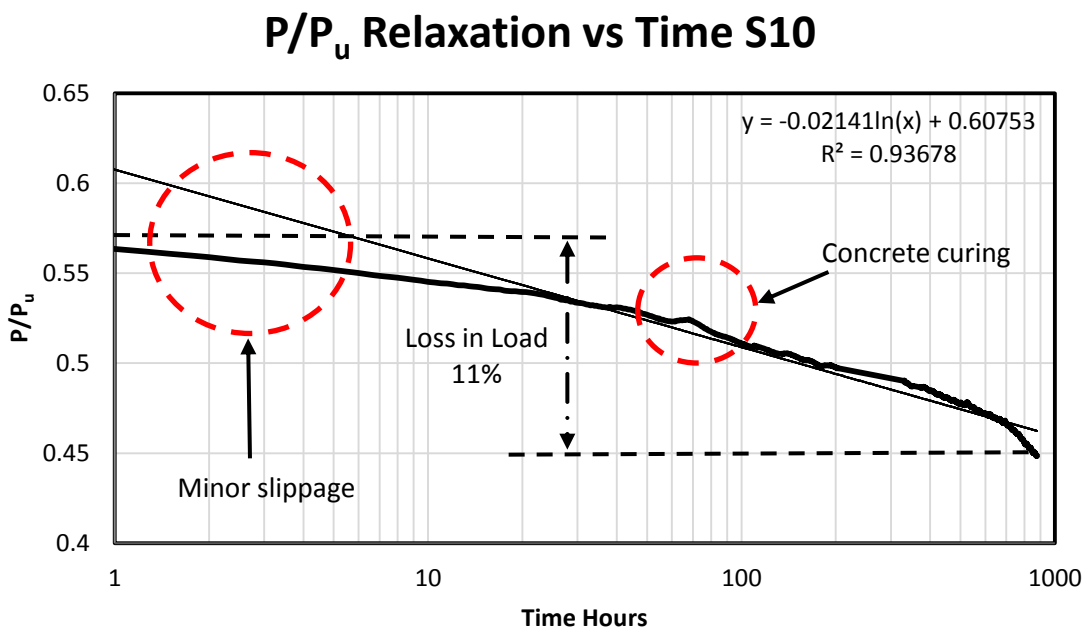

Figure 86 Relaxation stress level 60% specimen 10

The eleventh specimen tested was prestressed to 50% of ultimate stress of AFRP bar. Shown in Figure 87 is the relaxation curve for specimen 11. The stress in the bar was determined using load cell reading and adding LVDT displacement by converting to strain and using modulus of elasticity to convert to stress in order to compensate for losses in load due to slippage. The bar was tested for roughly 1000 hours. The relaxation curve is also illustrated in Figure 88 in log scale clearly showing that the bar experienced 7% prestress loss in roughly 1000 hours. From this experiment, it was noted that curing of the concrete caused the rate of relaxation to accelerate.

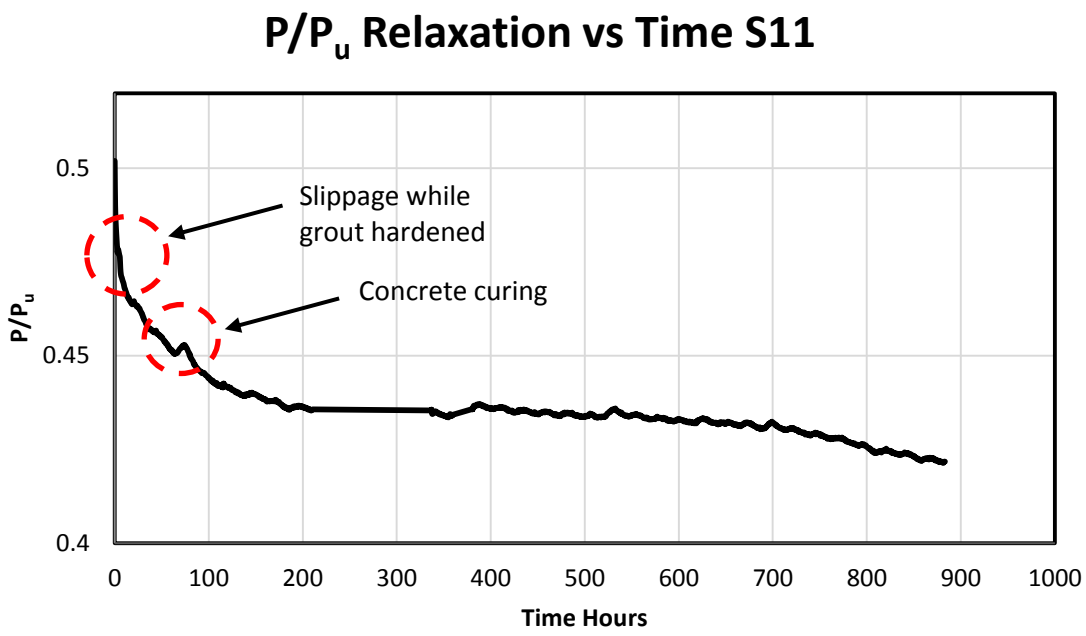

Figure 87 Relaxation stress level 50% specimen 11

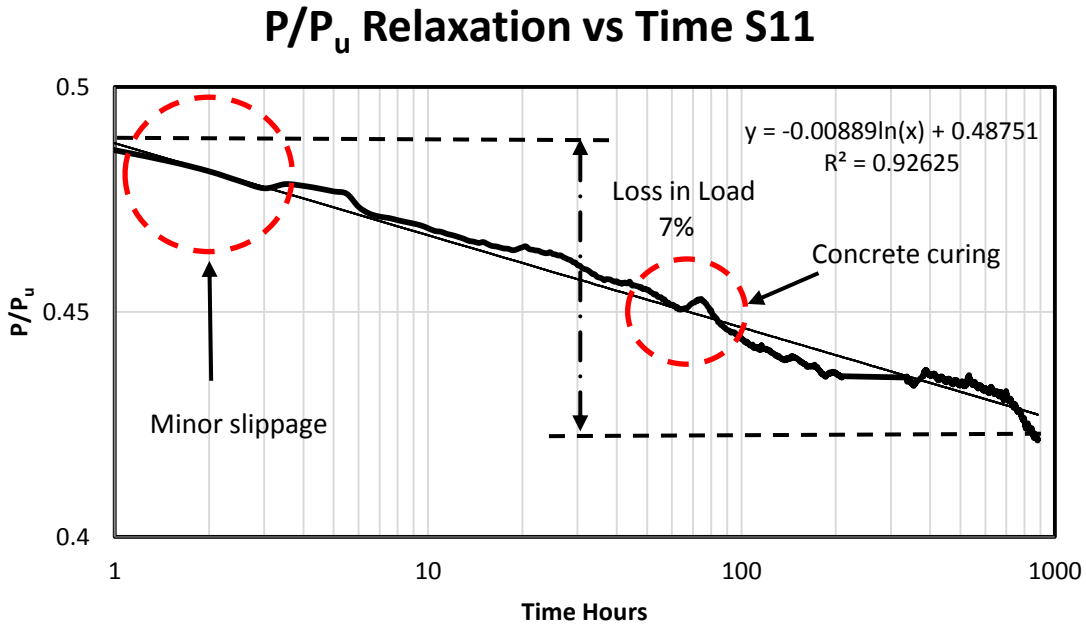

Figure 88 Relaxation stress level 50% specimen 11

The twelfth specimen tested was prestressed to 60% of ultimate stress of AFRP bar. Shown in Figure 89 is the relaxation curve for specimen 12. The stress in the bar was determined using load cell reading and adding LVDT displacement by converting to strain and using modulus of elasticity to convert to stress in order to compensate for losses in load due to slippage. The bar was tested for roughly 1000 hours. The relaxation curve is also illustrated in Figure 90 in log scale clearly showing that the bar experienced 5% prestress loss in roughly 1000 hours. From this experiment, it was noted that curing of the concrete caused the rate of relaxation to accelerate.

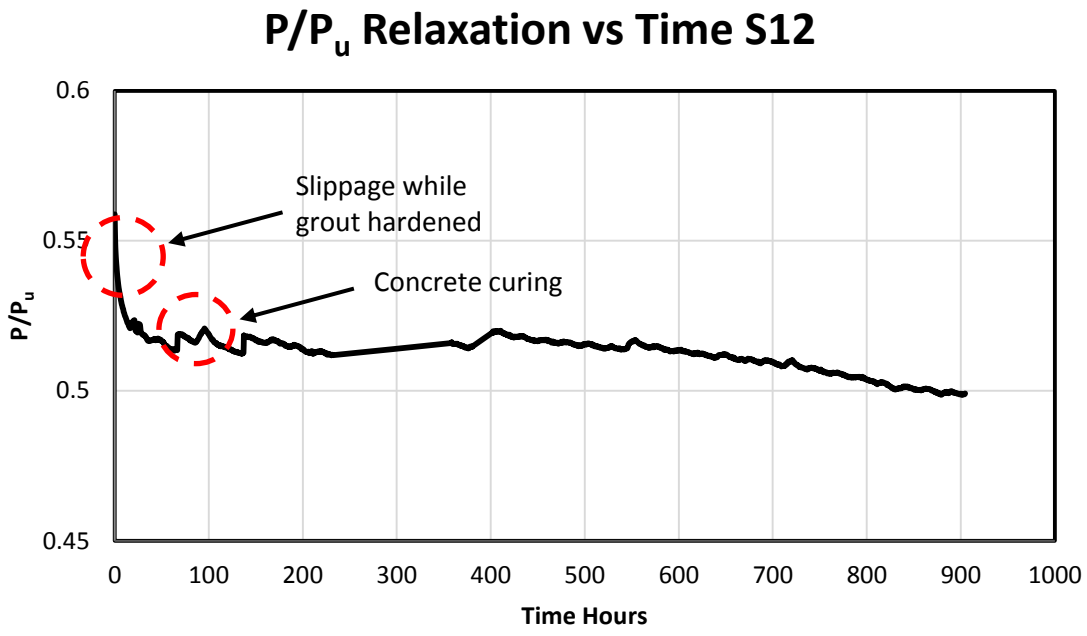

Figure 89 Relaxation stress level 60% specimen 12

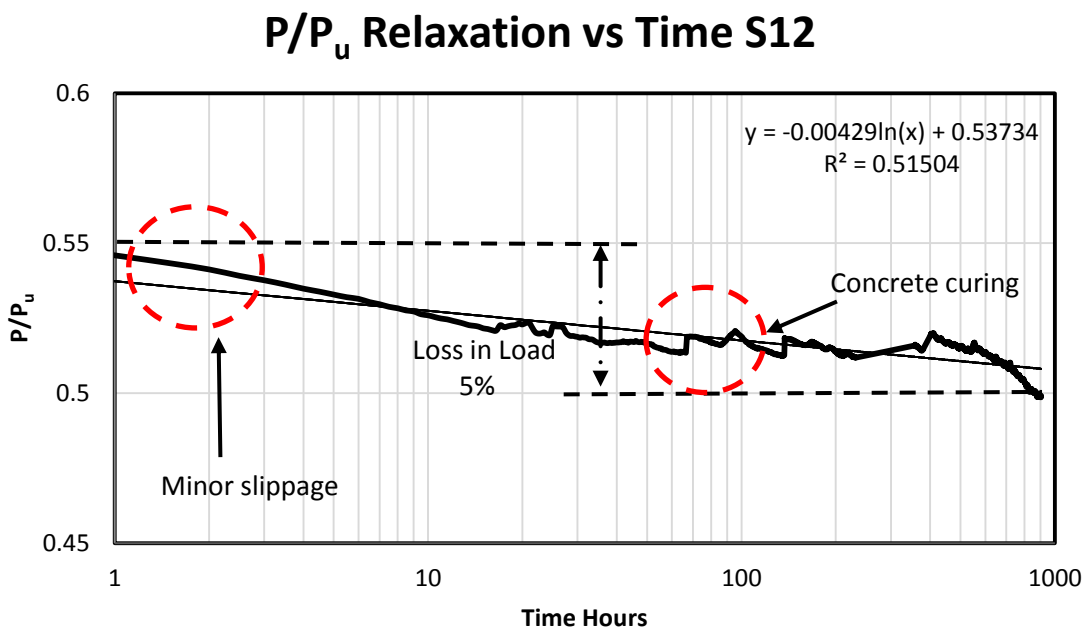

Figure 90 Relaxation stress level 60% specimen 12

4. ANALYSIS OF EXPERIMENTAL RESULTS

4.1 Comparison to Existing Experimental Test Data and Manufacturer's Data

This section focuses on the comparison of the experimental results and other existing results as well as the manufacturer's provided results. The tensile, creep-rupture and relaxation data was compared to other existing experimental data as well as the manufacturer's provided data.

4.1.1 Tensile Test Comparison

The tensile results of this study are listed below in Table 6 below. The manufacture's mechanical properties are also listed for comparison for Arapree®, FiBRA and Technora®.

Table 6 Mechanical properties comparison with manufacturer's data

	Medina et al. 2011	AFRP Manufacture Data		
	Arapree®	Arapree®	FiBRA	Technora®
Tensile Strength	212 ksi (1.46 GPa)	174 to 217 ksi (1.2 to 1.5 GPa)	181 to 203 ksi (1.25 to 1.4 GPa)	246 to 304 ksi (1.7 to 2.1 GPa)
Modulus of Elasticity	10,230 ksi (70.6 GPa)	9,000 to 9,300 ksi (62 to 64 GPa)	9,400 to 10,150 ksi (65 to 70 GPa)	7,800 ksi (54 GPa)
Ultimate Strain	2.10%	2.40%	2 to 3.7%	3.7 to 3.8%

The tensile results of this study have also been compared to other researcher's data. Shown in Figure 91, show that the results that Saadatmanesh et al. (1999) recorded correspond to the lower spectrum for ultimate tensile strength, and modulus of elasticity

was lower than the manufacturer's data as shown in Table 7. The results of strain corresponded well with the results of this study.

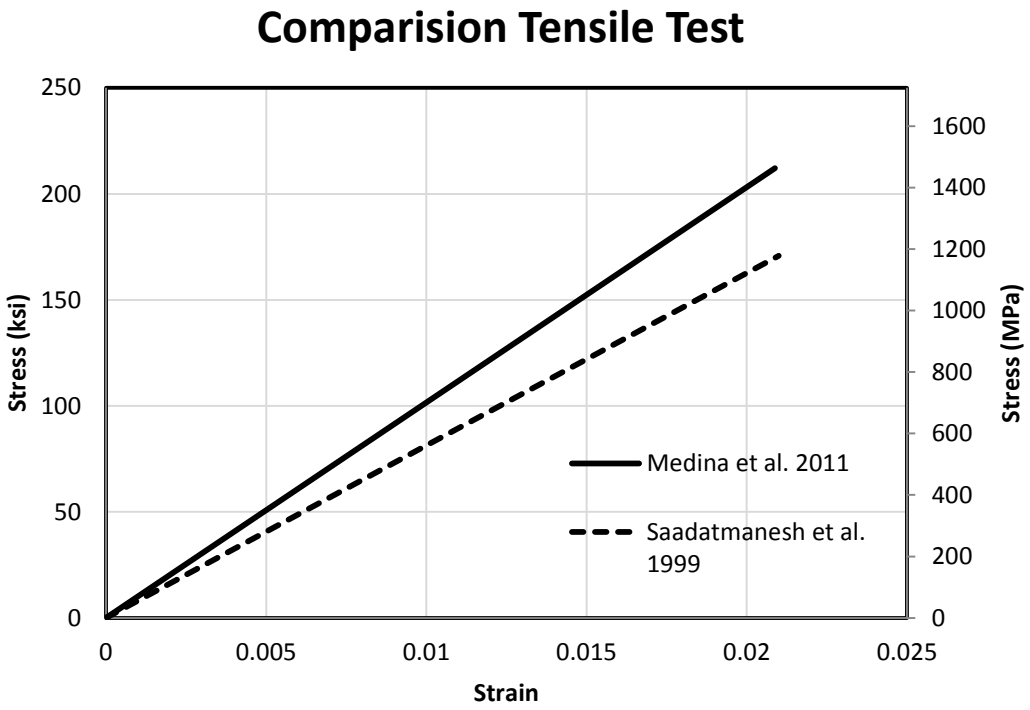

Figure 91 Comparison of experimental tensile test on Arapree® AFRP bars

Table 7 Mechanical properties comparison with Saadatmanesh et al. (1999) data

	Medina et al. 2011 Arapree®	**Saadatmanesh et al. 1999 Arapree®**
Tensile Strength	212 ksi (1.46 GPa)	170.8 ksi (1.18 GPa)
Modulus of Elasticity	10,230 ksi (70.6 GPa)	8134 ksi (56.1 GPa)
Ultimate Strain	2.10%	2.1%

4.1.2 Creep-Rupture Comparison

The creep-rupture results of this study have also been compared to other researcher's data. Shown in Figure 92, are the results that Saadatmanesh et al. (1999) recorded for a specimen exposed to air and room temperature at 40% stress level compared to a specimen tested in this study also in air and room temperature, but embedded in concrete with a load level of 50%. The results show that the overall behavior of creep is the same however, the total creep differs by 1%.

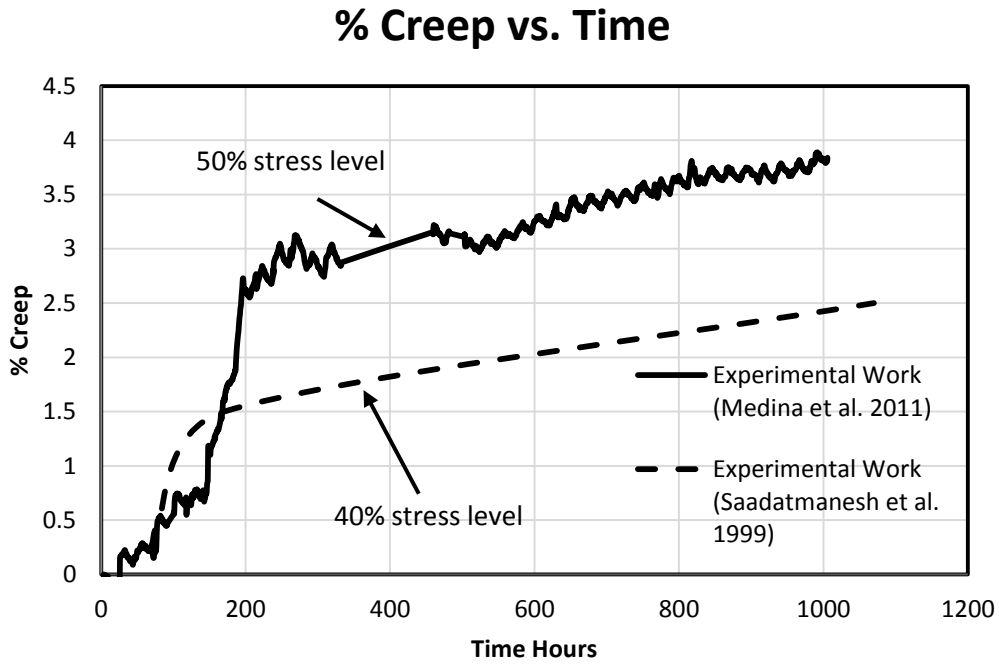

Figure 92 Comparison of experimental creep-rupture on Arapree® AFRP bars

4.1.3 Relaxation Comparison

The relaxation results of this study have also been compared to other researcher's data. Shown in Figure 93, are the results that Saadatmanesh et al. (1999) recorded for a specimen exposed to air and room temperature at 56% stress level compared to a specimen tested in this study also in air and room temperature with a load level of 63%. The results show that the relaxation rate is nearly identical as the percent relation at 100 hours is 3% for both tests.

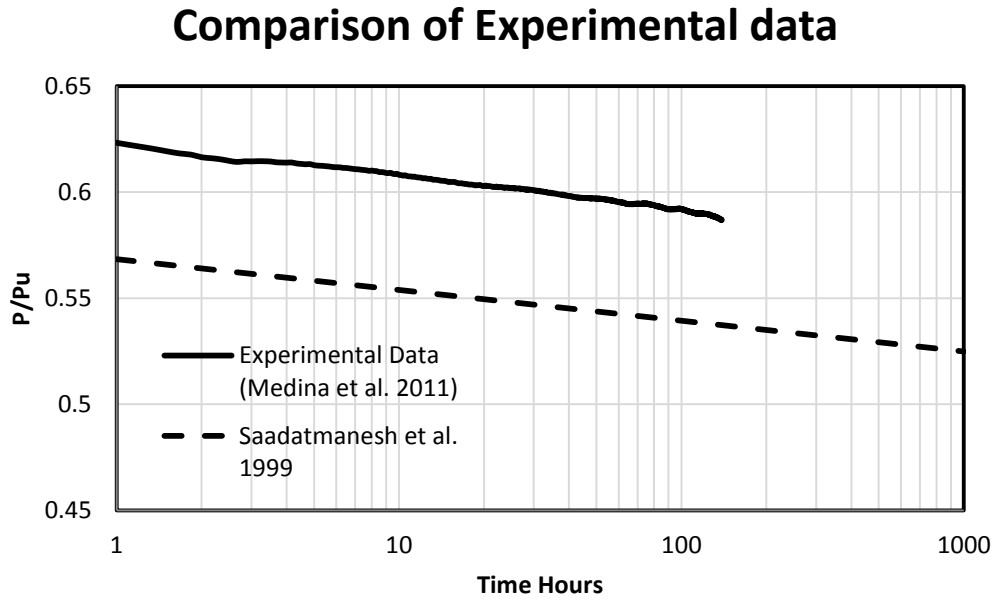

Figure 93 Comparison of experimental relaxation test on Arapree® AFRP bars

4.2 Developing Relationships of Rate of Relaxation

To be able to develop an equation that represented the data trend lines were used to absorb a relationship between the terms involved for relaxation tests for both the

short-term test exposed to air at room temperature, and long-term test embedded in concrete at room temperature. From the observations, a general equation was depicted for each specimen in the form found in Eq. (2).This general equation was then used to develop a unique equation by finding a relationship between m, relation rate or slope with either T, time or P/P_u, initial load over ultimate load. In the following section a relationship between the two will be discussed.

$$Relaxation = -(m)Ln(T) + \left(\frac{P}{P_u}\right)_i \quad (2)$$

4.2.1 Relationship of Rate of Relaxation vs. Load Level Exposed to Air

After analyzing all the data it was obvious that a relationship between m and P/P_u existed and it was also found that this relationship was also dependent on the environment the AFRP bar was exposed to. In Figure 94, it is shown that there is a linear relationship between m and P/P_u for the case of AFRP bar exposed to air and room temperature.

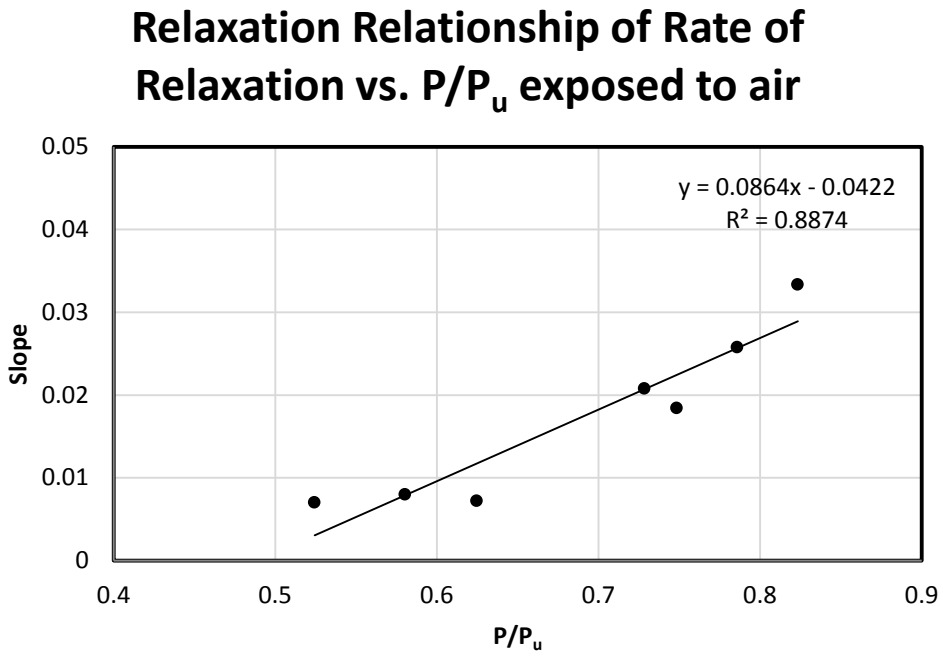

Figure 94 Relaxation relationship of Rate of Relaxation vs. P/P_u for specimens exposed to air

4.2.2 Relationship of Rate of Relaxation vs. Load Level Exposed to Concrete

As stated in the previous section, the relationship of m and P/P_u which is dependent on the environment was also considered for AFRP bar embedded in concrete. In Figure 95, shows the linear relationship between m and P/P_u for the case of AFRP bar embedded in concrete. These relationships can be used to determine m in the trend line equation and the introduction to relaxation loss equation will be done in the next section.

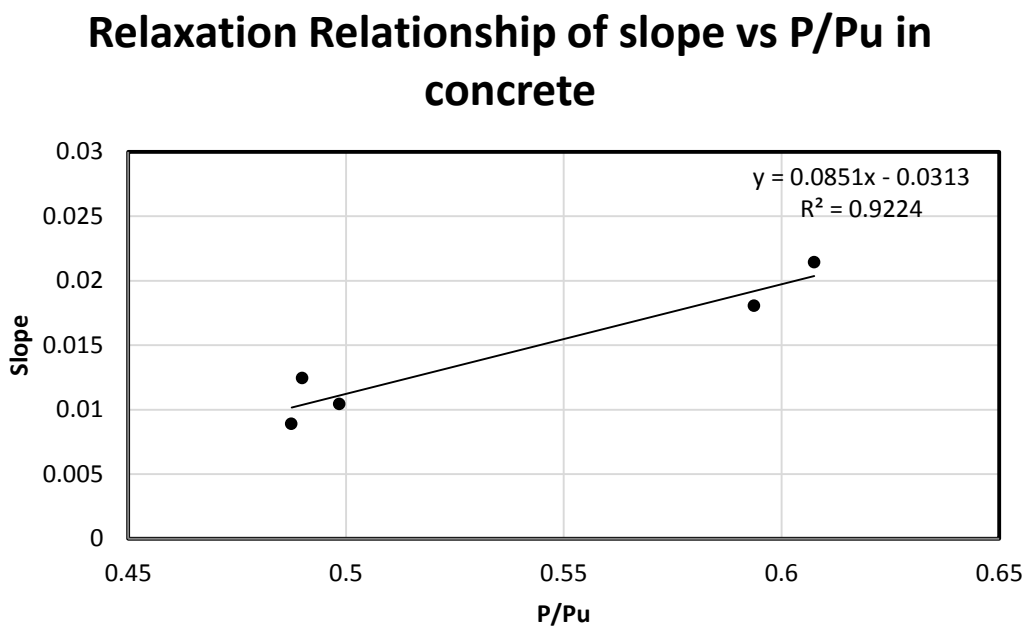

Figure 95 Relaxation relationship of Rate of Relaxation vs P/P_u for specimens in concrete

4.3 Newly Proposed Equation for Relaxation

4.3.1 Relaxation Test Equations

The general equation that is expected to determine the percent relaxation loss at T, time follows the format found in Eq. (3). The parameters needed to determine the relation loss in this equation are P, the prestressing load, P_u the ultimate load capacity, T time, and m the rate of relation or slope. Since in the previous section, a relationship was found for m, we can substitute that relationship to predict % relaxation loss. In the next two sections, the equation will be determined for case of AFRP bar exposed to air and embedded in concrete respectively.

$$\left(\frac{P}{P_u}\right)_F = \left(\frac{P}{P_u}\right)_i + Ln(T^m) \qquad (3)$$

4.3.1.1 Exposed to Air Equations

The proposed relaxation equation for AFRP bar exposed to air is shown in Eq. (4). The only parameter needed to determine the percent relaxation loss is P/P_u and the desired time. This equation will be evaluated in the proceeding section against the experimental data gathered in this study as well as with other experimental data and other equations.

$$\left(\frac{P}{P_u}\right)_F = \left(\frac{P}{P_u}\right)_i + Ln\left(T^{0.0422-0.0864\left(\frac{P}{Pu}\right)_i)}\right) \quad (4)$$

4.3.1.2 Embedded in Concrete Equation

The proposed relaxation equation for AFRP embedded in concrete is shown in Eq. (5). Again in this case only parameter needed to determine the percent relaxation loss is P/P_u and the desired time. This equation will also be evaluated in the proceeding section against the experimental data gathered in this study as well as with other experimental data and other equations. Also it is clear that from Eq. (4) and Eq. (5) that m, rate of relation, it is significantly more for concrete case than exposed to air.

$$\left(\frac{P}{P_u}\right)_F = \left(\frac{P}{P_u}\right)_i + Ln\left(T^{0.0313-0.0851\left(\frac{P}{P_u}\right)_i}\right) \quad (5)$$

4.4 Comparison of Proposed Equations to Experimental Work and JSCE (1997) Equation

This section focuses on the comparison of the proposed equation to experimental results for both AFRP bar exposed to air and embedded in concrete as well as the JSCE (1997) equation (Eq.6).

$$\%\ Relaxation = \left(\frac{P}{P_u}\right)_F = \left(0.9962\left(\frac{P}{P_u}\right)_i + Ln\left(T^{-0.0125\left(\frac{P}{P_u}\right)_i}\right)\right) \quad (6)$$

4.4.1 Comparison of Equation Exposed to Air Compared to Experimental Work

The first specimen compared was an experiment tested at 80% prestress load and exposed to air. Shown in Figure 96 are the relaxation curve for specimen 1 and the predicted results using Eq. (4) and Eq. (6). The experimental results and equation for this case are well matched and the result can be predicted with accuracy.

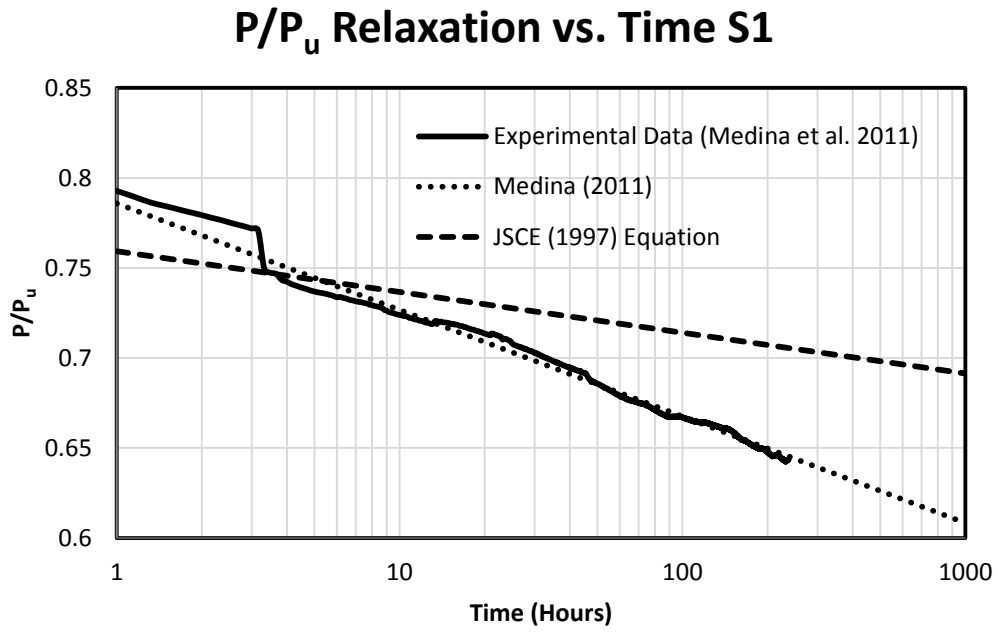

Figure 96 Proposed equation exposed to air compared to specimen 1 data

The second specimen compared was an experiment tested at 60% prestress load and exposed to air. Shown in Figure 97 are the relaxation curve for specimen 2 redo and

the predicted results using Eq. (4) and Eq.(6). The experimental results and equation for this case are not very well matched; however, the equation overestimates the relaxation loss by 2%. It is acceptable to overestimate the relaxation for design purposes however; the biggest issue with this specimen was the fact that it failed in slippage too early (170 hours) to effectively be monitored.

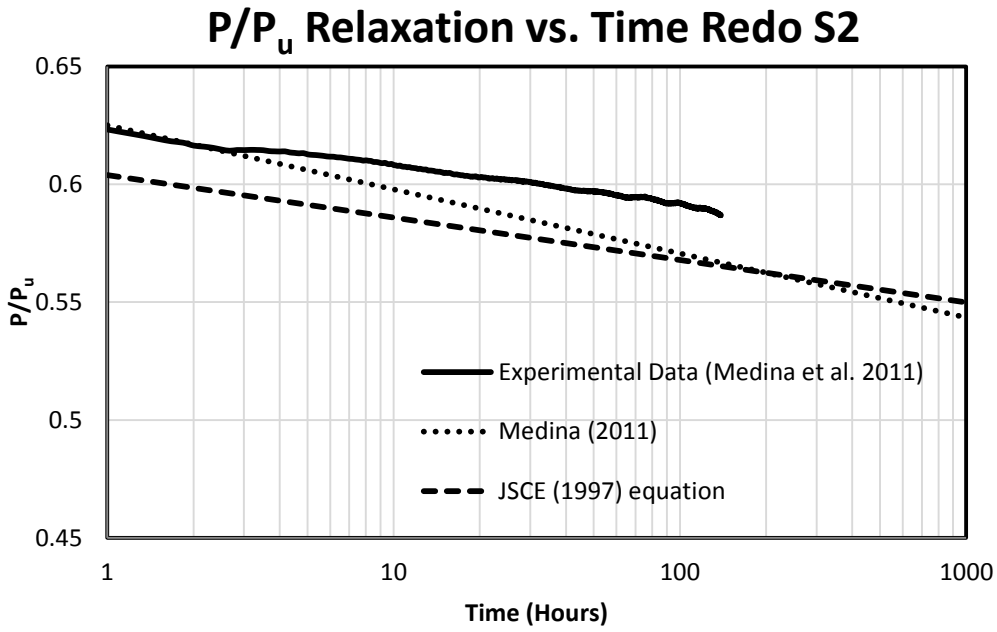

Figure 97 Proposed equation exposed to air compared to specimen 2 data

The third specimen compared was an experiment tested at 75% prestress load and exposed to air. Shown in Figure 98 are the relaxation curve for specimen 3 and the predicted results using Eq. (4) and Eq. (6). The experimental results and equation for this case are well matched and only a 1% relaxation difference at 200 hours. It is acceptable

to overestimate the relaxation for design purposes as we expect the losses in prestressing to be slightly larger.

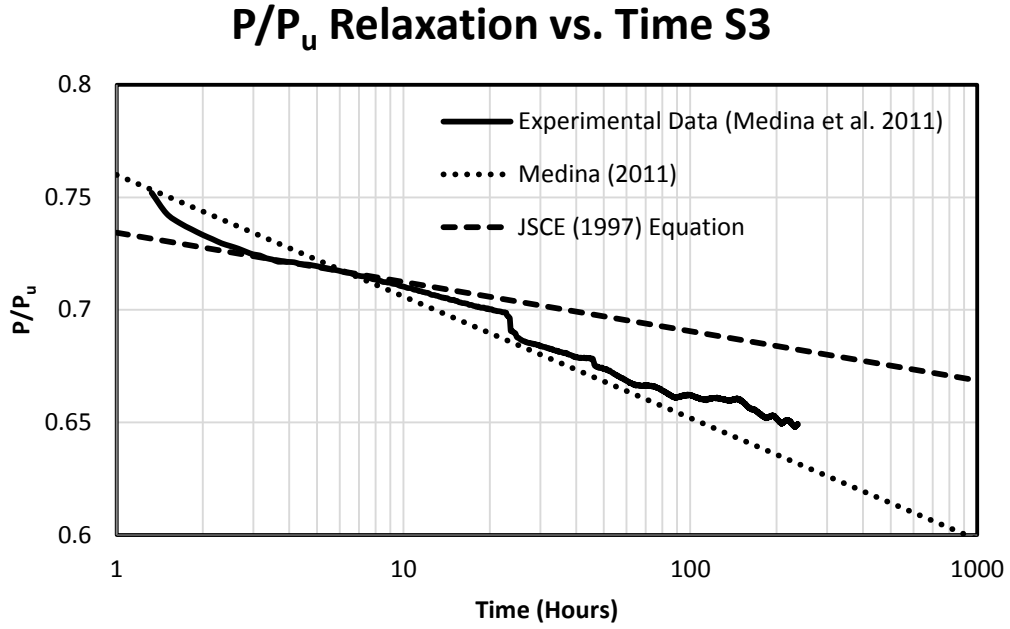

Figure 98 Proposed equation exposed to air compared to specimen 3 data

The fourth specimen compared was an experiment tested at 75% prestress load and exposed to air. Shown in Figure 99 are the relaxation curve for specimen 4 and the predicted results using Eq. (4) and Eq. (6). The experimental results and equation for this case are well matched except for the large slippage in experiment at the beginning of test.

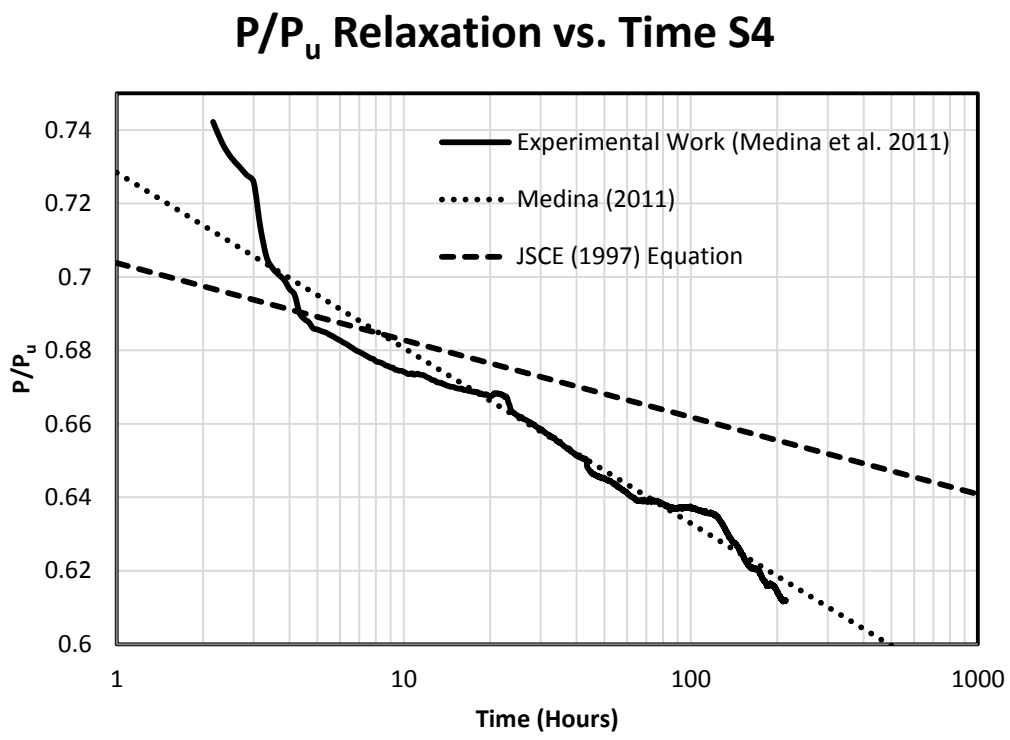

Figure 99 Proposed equation exposed to air compared to specimen 4 data

The fifth specimen compared was an experiment tested at 80% prestress load and exposed to air. Shown in Figure 100 are the relaxation curve for specimen 6 and the predicted results using Eq. (4) and Eq. (6). The experimental results and equation for this case are well matched, some slippage near the end of test lead to a 1% underestimation by the equation.

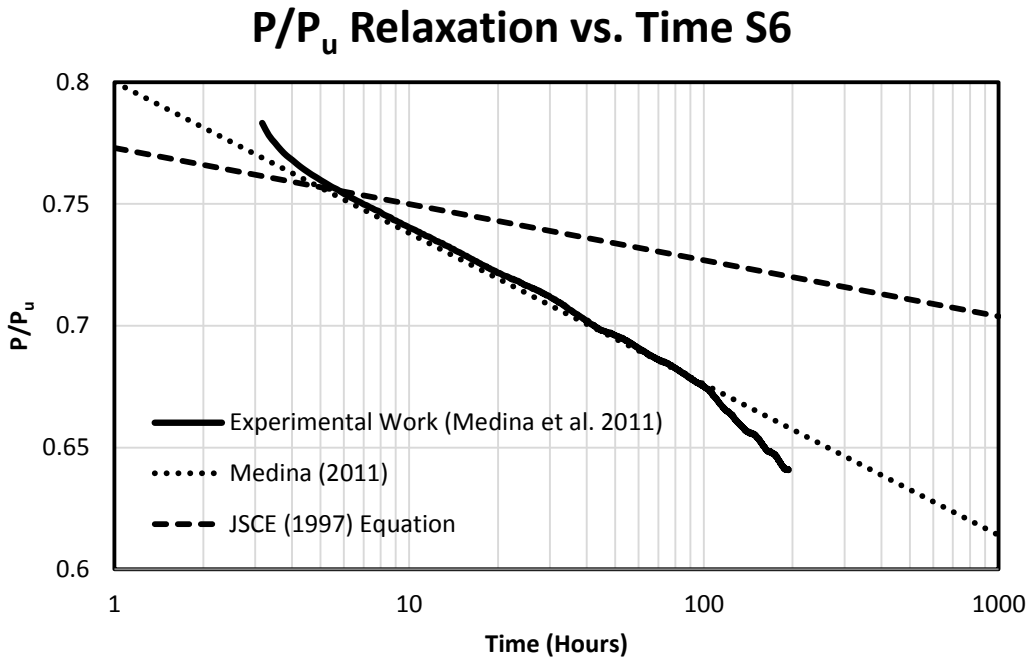

Figure 100 Proposed equation exposed to air compared to specimen 6 data

4.4.2 Comparison of Equation Exposed to Concrete Compared to Experimental Work

The first specimen compared was an experiment tested at 50% prestress load and embedded in concrete. Shown in Figure 101 are the relaxation curve for specimen 7 and the predicted results using Eq. (5) and Eq. (6). The experimental results and equation for this case are well matched.

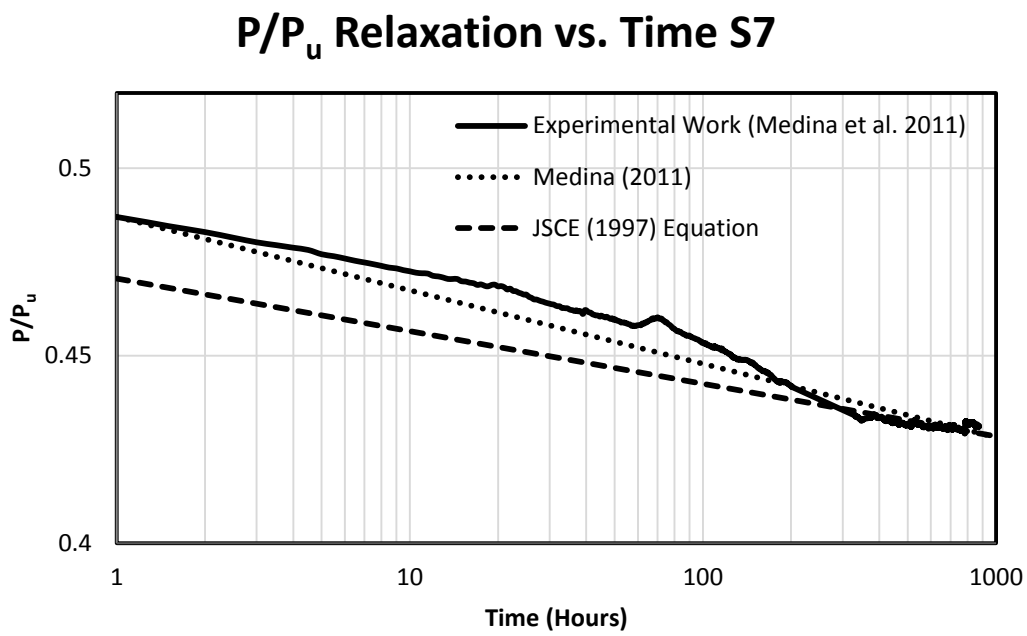

Figure 101 Proposed equation exposed to concrete compared to specimen 7 data

The second specimen compared was an experiment tested at 50% prestress load and embedded in concrete. Shown in Figure 102 are the relaxation curve for specimen 8 and the predicted results using Eq. (5) and Eq. (6). The experimental results and equation for this case are well matched for the initial 100 hours; however, the equation underestimates the results for 1000 hours by only 2%. It is acceptable to overestimate the relaxation for design purposes as we expect the losses in prestressing to be slightly larger.

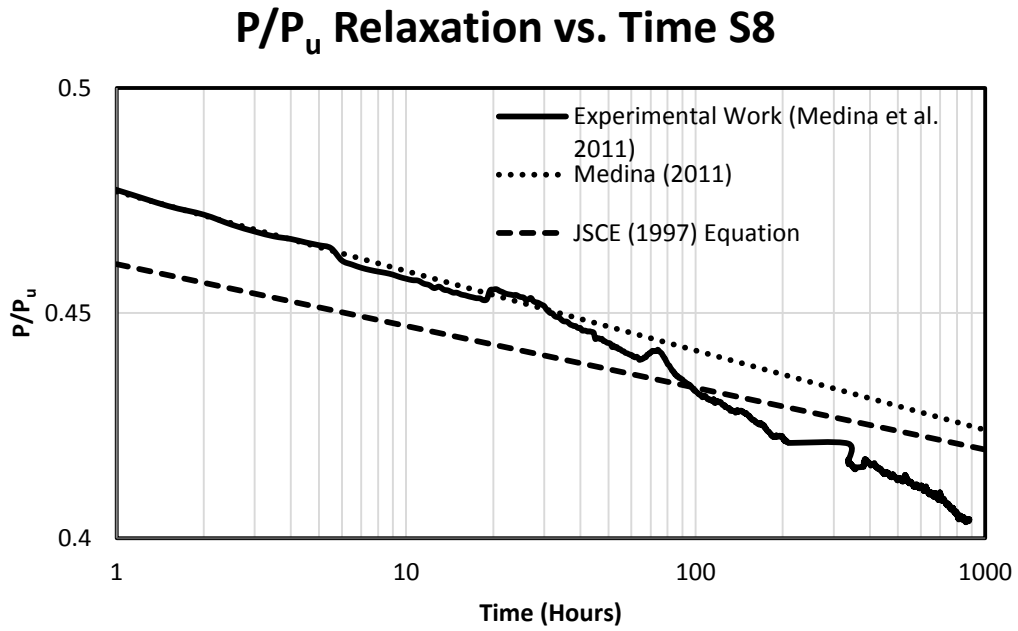

Figure 102 Proposed equation exposed to concrete compared to specimen 8 data

The third specimen compared was an experiment tested at 60% prestress load and embedded in concrete. Shown in Figure 103 are the relaxation curve for specimen 9 and the predicted results using Eq. (5) and Eq. (6). The experimental results and equation for this case are well matched as the predicted value for 1000 hours is less than .05% overestimated. It is acceptable to overestimate the relaxation for design purposes as we expect the losses in prestressing to be slightly larger.

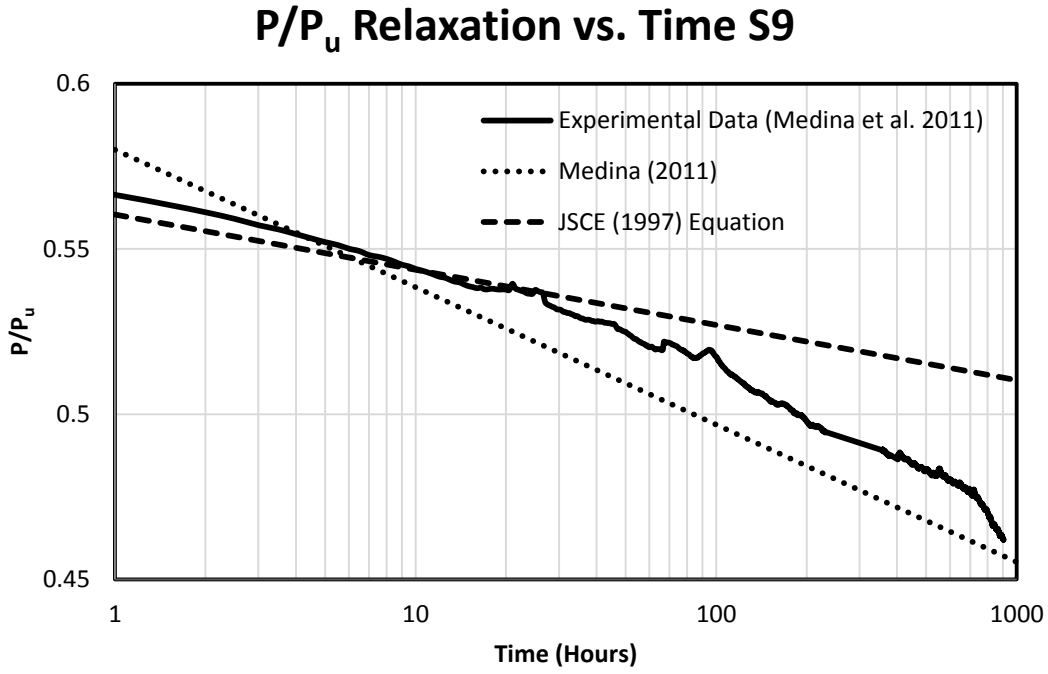

Figure 103 Proposed equation exposed to concrete compared to specimen 9 data

The fourth specimen compared was an experiment tested at 60% prestress load and embedded in concrete. Shown in Figure 104 are the relaxation curve for specimen 10 and the predicted results using Eq. (5) and Eq. (6). The experimental results and equation for this case are well matched and the results at 1000 hours are overestimated by less than 2%. It is acceptable to overestimate the relaxation for design purposes as we expect the losses in prestressing to be slightly larger.

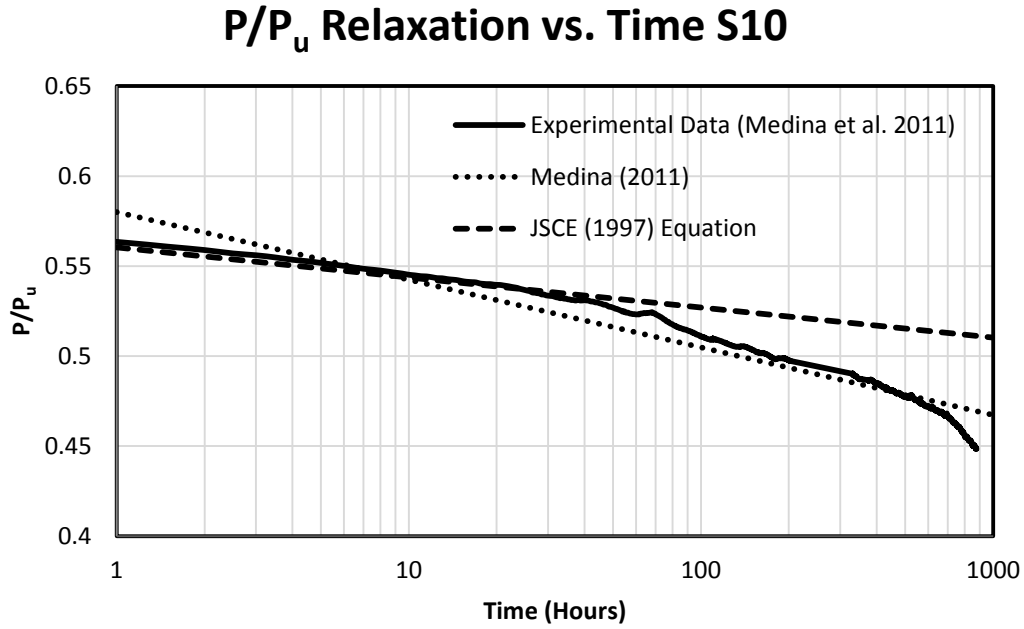

Figure 104 Proposed equation exposed to concrete compared to specimen 10 data

The fifth specimen compared was an experiment tested at 50% prestress load and embedded in concrete. Shown in Figure 105 are the relaxation curve for specimen 11 and the predicted results using Eq. (5) and Eq. (6). The experimental results and equation for this case are well matched and the results at 1000 hours are overestimated by less than 2%. It is acceptable to overestimate the relaxation for design purposes as we expect the losses in prestressing to be slightly larger.

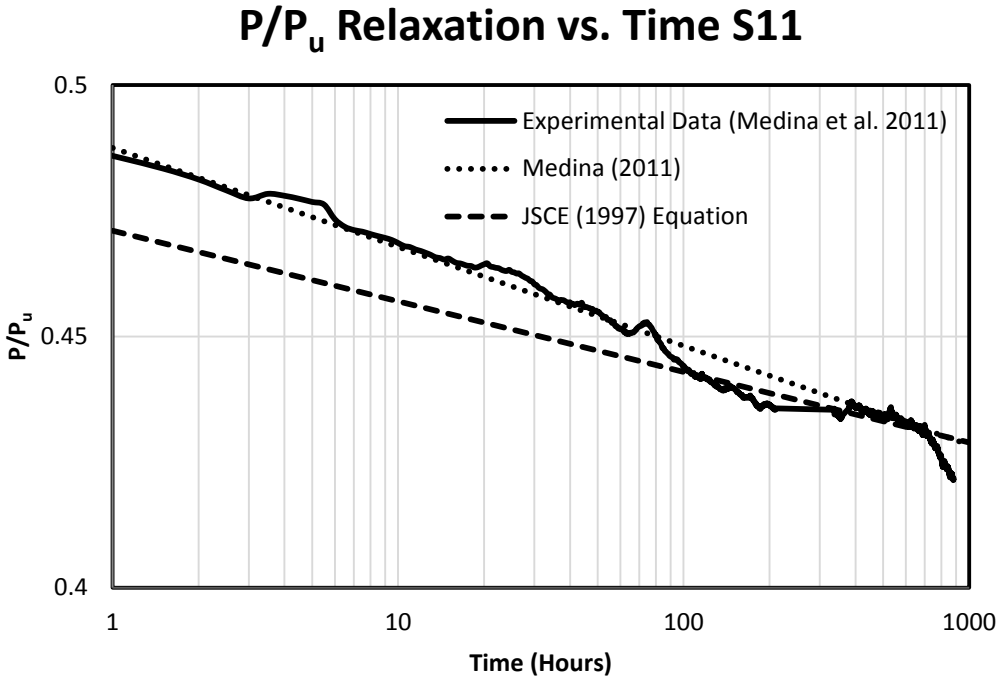

Figure 105 Proposed equation exposed to concrete compared to specimen 11 data

The sixth specimen compared was an experiment tested at 60% prestress load and embedded in concrete. Shown in Figure 106 are the relaxation curve for specimen 12 and the predicted results using Eq. (5) and Eq. (6). The experimental results and equation for this case are not well matched and there is a 4.5% overestimation for this case. It is acceptable to overestimate the relaxation for design purposes as we expect the losses in prestressing to be slightly larger.

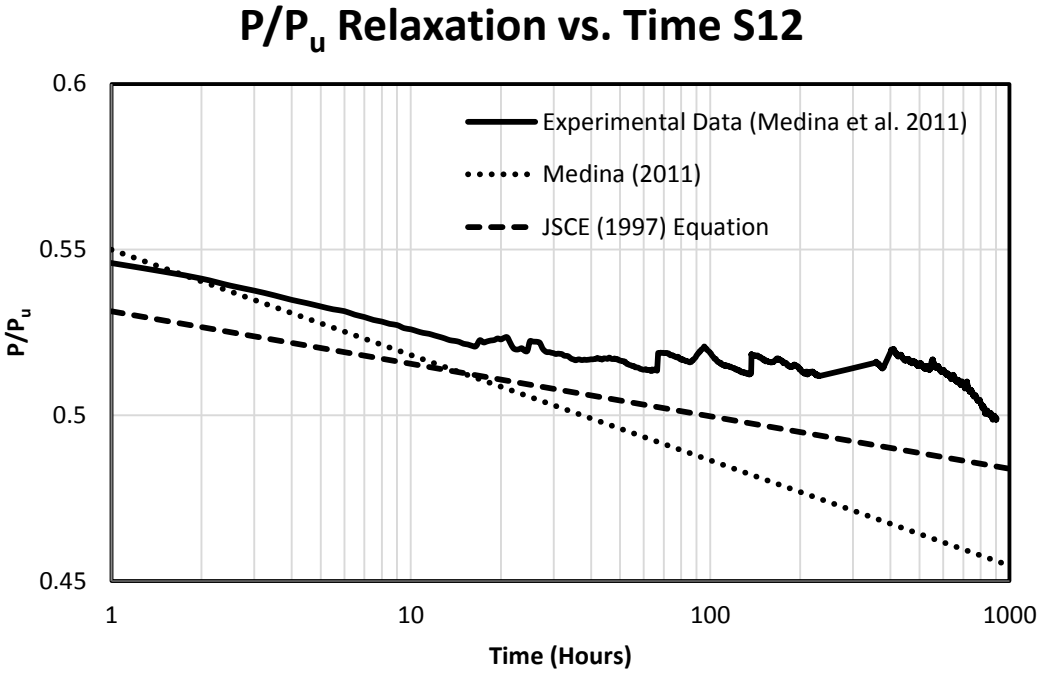

Figure 106 Proposed equation exposed to concrete compared to specimen 12 data

4.5 Comparison of Proposed Equation to Other Experimental Work

The relaxation equation in this section is compared to Japanese Society of Civil Engineers (JSCE) 1997 equation prediction for the experimental result of Saddatmanesh et al. (1999) and will as the proposed equation for this study. Shown in Figure 107, illustrates the prediction by the proposed equation and JSCE (1997) equation. Both have good predictions however, the proposed equation overestimates the relaxation loss by a smaller margin. There were no equations found for case of AFRP bar in concrete to compare equation so the only comparison for this case was to the experimental data gathered in this study.

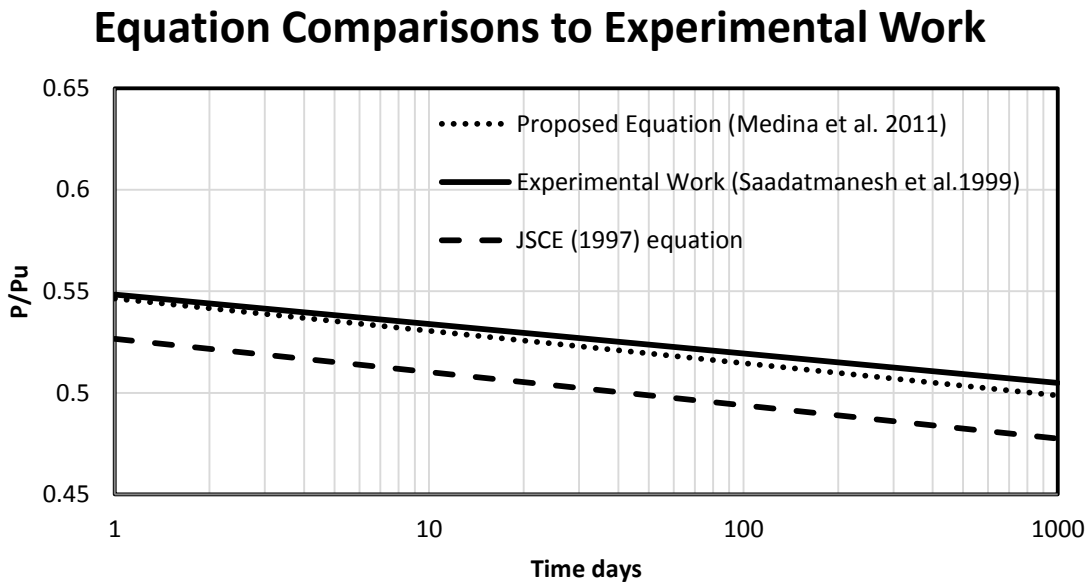

Figure 107 Equation prediction of the experimental data in Saadatmanesh et al. (1999) using proposed equation and JSCE (1997) equation

4.6 Summary

Tensile properties were found to be at the higher end of the spectrum when compared to the manufacturer's mechanical properties. As per the experiments conducted in this study the mechanical properties are 212 ksi (1.46 GPa) for ultimate tensile strength compare to 174 to 217 ksi (1.2 to 1.5 GPa), 10,230 ksi (70.6 GPa) compared to 9,000 to 9,300 ksi (62 to 64 GPa) modulus of elasticity and 2.1% ultimate strain compared to 2.4% ultimate strain provided by Arapree®. Furthermore, when compare to other existing experimental work it was found that variability in mechanical properties may exist as Saadatmanesh et al. (1999) found the following mechanical properties while also test Arapree® AFRP bars with 0.39 in. (10mm) diameter 170.8 ksi

(1.18 GPa) ultimate tensile strength, 8,134 ksi (56.1 GPa) modulus of elasticity and 2.1% ultimate strain.

Creep-rupture behavior was found to be comparable to other researchers' experimental work. Saadatmanesh et al. (1999) test Arapree® AFRP bars for 3000 hours and at 40% prestressing level and the comparison to the creep-rupture test conducted in this experiment at 50% prestressing level show that the creep for 40% was 2.5% and the creep for 50% was 4% after 1000 hours. From these tests it can be concluded that the creep-rupture data between the two tests as the creep-rupture data for 60% load level revealed to be 6.5% at 500 hours.

Relaxation behavior showed a clear relationship between rate of relaxation and initial prestressing level (P/P_u). As a results and equation was developed that model the experimental data with good accuracy and also compared will with other experimental data. Furthermore, it predicted behavior was better than that of JSCE (1997) equation.

5. CONCLUSIONS AND FUTURE WORK

5.1 Conclusions

After testing the conventional anchorage in tensile and prestressing operation it was clear that the conventional anchorage would fail the Arapree® AFRP bar in the range of 55-65% of ultimate tensile capacity. As a result, it is recommended to use 2-18 in. (45.7 cm) 1.9 in. (4.8 cm) diameter grouted pipes at each end to conduct a tensile test. Also the recommended prestressing method consist of using 3-18 in. (45.7 cm) 1.9 in. (4.8 cm) diameter pipes. One will serve as the dead end, the second pipe will be used as an anchorage and the third pipe which is on the live end will be grouted and once cured (2 hours) the jack is released.

Using the recommended anchoring mechanism, tensile tests were conducted to determine the mechanical properties of the Arapree® AFRP bars used for this study. The tensile properties were found to be at the higher end of the spectrum when compared to the manufacturer's mechanical properties. It is very common for manufacturers to provide a product with higher capacity than their specification in order to ensure that the materials meet their claim. As per the experiments conducted in this study, the mechanical properties were found to be 212 ksi (1.46 GPa) for ultimate tensile strength compare to 174 to 217 ksi (1.2 to 1.5 GPa), 10,230 ksi (70.6 GPa) compared to 9,000 to 9,300 ksi (62 to 64 GPa) modulus of elasticity and 2.1% ultimate strain compared to 2.4% ultimate strain provided by Arapree®. Furthermore, when compared to other existing experimental work, it was found that variability in mechanical properties may exist as Saadatmanesh et al. 1999 found the following mechanical properties while also

test Arapree® AFRP bars with 0.39 in. (10 mm) diameter 170.8 ksi (1.18 GPa) ultimate tensile strength, 8,134 ksi (56.1 GPa) modulus of elasticity and 2.1% ultimate strain.

Using the recommend anchorage for creep-rupture it was found that the anchorage was suitable for 50% prestressing level. However, for 60% prestressing level slippage occurred after roughly 500 hours of testing. Therefore, it is recommended to use longer pipes for creep-rupture tests when testing the long-term creep-rupture between 55-70% prestressing levels. Creep-rupture behavior was found to be comparable to other researchers' experimental work. Saadatmanesh et al. 1999 test Arapree® AFRP bars for 3000 hours and at 40% prestressing level and the comparison to the creep-rupture test conducted in this experiment at 50% prestressing level show that the creep for 40% was 2.5% and the creep for 50% was 4% after 1000 hours. From these tests, it can be concluded that the creep-rupture data between the two tests, follows the expected behavior as the creep-rupture data for 60% load level revealed a creep increase of 6.5% at 500 hours. Finally it was found that 60% load level showed 6-8 days in primary stage with 4-5% creep followed by 20 + days of secondary stage with 2-3% creep. For 50% load level showed 8-10 days in primary stage with 2-3% creep followed by 30 + days of secondary stage with 1-2% creep.

Relaxation behavior showed a clear relationship between rate of relaxation and initial prestressing level (P/P_u). As a results and equation was developed that model the experimental data with good accuracy and also compared will with other experimental data. Furthermore, it predicted behavior was better than that of JSCE (1997) equation. From the prestressing level, it was found that 80% load level resulted in 12-15%

prestress loss in 250 hours, 70% load level resulted in 10-13% prestress loss in 250 hours, 60% load level resulted in 8-11% prestress loss in 1000 hours, and for 50% load level resulted in 4-8% prestress loss in 1000 hours.

5.2 Summary and Design Implications

Two relaxation equations have been proposed for calculating the relaxation prestress losses: Equations 4 and 5. These equations can be used in design by inversely determining the initial prestressing force when given the desired level of prestressing forced specified in the design. For example, if the design prestressing level is 45% of the ultimate load, then the equation can be used to determine the required initial prestressing that will result in 45% when concrete is poured.

In short, AFRP materials behave in a linearly elastic manner and do not show any signs prior to failure (e.g. yielding, rusting, and spalling), and can fail in a catastrophic way (Shahaway et al. 2007). Therefore, the design of prestressed concrete members with AFRP bars should be carefully reviewed where the design shall be based on a serviceability limit state in order to prevent failure under service loads. Moreover, the design under ultimate load will require significant deformability as these materials fails in brittle manner, which is important in order to have a ductile system.

5.3 Future Work

The evaluation of long-term performance for relaxation and creep-rupture for which AFRP bars are exposed to more aggressive environments such as to alkaline solution, acidic solution and marine environment is needed. Evaluation in these harsh environments can prove this material to be useful in marine structural applications. More

work is also need to fully characterize fatigue performance and effects of temperature that can lead to delamination of the bars given the difference between the coefficients of thermal expansion of concrete compared to AFRP. Furthermore, more experimental data is need for creep-rupture in the stress range of 65-90% that produces failure, to better predict the 100 year life of the material under constant load.

REFERENCES

ASTM (D 638-2008). "Standard Test Method for Tensile Properties of Plastics," *ASTM Standard*, D 638-08.

Bakis, C. E. (2001). "Flexure of Concrete Beams Prestressed with FRP Tendons," *Pennsylvania State University*. MS Thesis.

Budelmann, H. and Rostasy, F. S. (1993). "Creep Rupture Behavior in FRP Elements for Prestressed Concrete Phenomenon, Results and Forecast Models," *Fiber Reinforced Plastic Reinforced ment for Concrete Structures International Symposium, ACI*, 138-6, 87-101.

Dolan, C. W. (1989). "Prestressed Concrete Using Kevlar Reinforced Tendons," *PhD Dissertation, Cornell University, Ithaca, NY.*

Dolan, C. (1990). "Developments in Non-Metallic Prestressing Tendons," *PCI Journal,* 35(5), 80-88.

Dolan, C. W., Hamilton III, H.R. and Nanni, A. (2001). "Design Recommendations for Concrete Structures Prestressed with FRP Tendons," *Rep. No. DTFH61-96-0019*, *Prepared for the Federal Highway Administration*, Univ. of Wyoming, Pennsylvania State Univ., and Univ. of Missouri-Rolla.

Epoxy Interest Group. (2010). "Use and Installation of Epoxy-Coated Reinforcing Bars," *Epoxy Interest Group*, July, 2010.

Erki, M.A. and Rizkalla, S.H. (1993). "Anchorages for FRP Reinforcement," *ACI Concrete International*, 15(6), 54-59.

Grace, N. F. and Abdel-Sayed, G. (1998). "Ductility of Prestressed Bridges using CFRP Strands," *Concrete International*, 20(6), 84-191.

Griffith, A. and Laylor, H. M. (1999). "Epoxy Coated Reinforcement Study," *Oregon Deparment of Transportation Research Group*, State Research Project #527, June, 1999.

JSCE (1997). "Recommendation for Design and Construction of Concrete Structures Using Continuous Fiber Reinforcing Materials," *Concrete Engineering Series*, No. 23, JSCE, Tokyo.

Lees, J. M. and Burgoyne, C.J. (2000)."Rigid Body Analysis of Concrete Beams Pre-Tensioned with Partially-Bonded AFRP Tendons," *Department of Civil Engineering, University of Cambridge*. Cambridge, United Kingdom, MS Thesis.

McKay, K. S. and Erki, M. A. (1992). "Flexural Behavior of Concrete Beams Pretensioned with Aramid Fiber Reinforced Plastic Tendons," *Canadian Journal of Civil Engineering*, 20(4), 688-695.

Mukae, K. (1993). "Characteristics of Aramid FRP Rods," *Fiber-Reinforcement for Concrete Structures International Symposium*, ACI, Detroit, MI, 35-49.

Okelo, R. and Yuan, R. L. (2005)."Bond Strength of Fiber Reinforced Polymer Rebars in Normal Strength Concrete," *ASCE Journal of Composites for Construction*, 9(3), 203-213.

Pincheria, J. A. (2008). "Corrosion Performance of Epoxy-Coated Reinforcement Bars," *Minnesota Department of Transporation*, September, 2008.

Rafi, M. M. and Nadjai, A. (2009). "Evaluation of ACI 440 Deflection Model for Fiber-Reinforced Polymer Reinforced Concrete Beams and Suggested Modification," *ACI Structural Journal*, 106(6), 762-771.

Rashid, M. A., Mansur, M. A. and Paramasivam, P. (2005). "Behavior of Aramid Fiber-Reinforced Polymer Reinforced High Strength Concrete Beams Under Bending." *ASCE Journal of Composites for Construction*, 9(2), 117-127.

Saadatmanesh, H., and Tannous, F. E. (1999). "Long-Term Behavior of Aramid Fiber Reinforced Plastic (AFRP) Tendons." *ACI Materials Journal*, 96(99), 297-305.

Sagues, A. A. (1994). "Corrosion of Epoxy Coated Rebar in Florida Bridges," *Florida Department of Transportation*, WPI No. 0510603, State Job No. 99700-7556-010, 1994.

Shahaway, M. A. and Beitelman, T. (2007). "Static Flexural Response of Members Bars Pretensioned with Multiple Layered Aramid Fiber Tendons," *Composites*: Part B27B(96), 253-261

Scheibe, M. and Rostasy, F. S. (1996). "Prediction of Stress-Rupture Behavior of AFRP Bars in Concrete Elements," *Fiber Composites in Infrastructure*, Second International Conference on Composites in Infrasture, 138-151.

Scheibe, M. and Rostasy, F. S. (1998). "Stress-Rupture Behavior of AFRP-Bars in Concrete and Under Natural Enviornment," *Fiber Composites in Infrastructure*, Second International Conference on Composites in Infrasture, 41-53.

Toutanji, H. and Saafi, M. (1999). "Performance of Concrete Beams Prestressed with Aramid Fiber-Reinforced Polymer Tendons," *Elsevier Science*. Composite Structures, 44(1999), 63-70.

Wolf, L. M. and Sarcinella, R. L. (1999). "Use of Expoxy-Coated Reinforcing Steel and Other Corrosion Protection Philosophy in Texas: The Belts and Suspenders Approach," *Texas Department of Transportation*, 1999.

APPENDIX I

Test	Testing Output & Sensors	Procedure
1.Tensile ASTM D638-08; D3916 (how to measure diameter with a micrometer)	1.Modulus of elasticity 2.Ultimate tensile strength 3.Ultimate strain 1.Temperature sensor 2.Relative humidity sensor 3.Extensometer (LVDT) 4. Extensometer (LVDT) for slippage	1. Condition test specimen (ASTM D618) at the testing environment (23±2°C (73.4 ±3.6 ° F) and 50±10% relative humidity) for at least 48 hours. 2. Measure the diameter of rod specimens (at least five specimens must be tested), to the nearest 0.025 mm (0.001 in.) at a minimum of two points 90° apart (and/or at three points along the test length with the average value recorded – Dolan [2001, p. 21]). 3. Place the specimen in the grips of the testing machine, taking care to align the long axis of the specimen and the grips with an imaginary line joining the points of attachment of the grips to the machine. 4. Attach the extension indicator (extensometer, i.e. LVDT). a. For modulus of elasticity a class B-2, or better extensometer is required. Set the speed of testing at the proper rate (100 to 500 N/mm^2 per minute or failure at 1/2 to 5 min). b. Record the load-extension curve of the specimen. c. Record the load and extension at yield point (if one exists) and the load and extension at the moment of rupture. d. Plot load versus strain (to eliminate need for cross-sectional dimensions). 5. The loading shall be completed until tensile failure, and the measurements shall be recorded until the strain reaches at least 60% of the tensile capacity or the guaranteed tensile capacity.
2.Creep Rupture ASTM D2990	1.Curve of stress-at-rupture versus time-to-rupture "Creep-rupture envelope"	1. Condition test specimen at the testing environment (23±2°C (73.4 ±3.6 ° F) and 50±10% relative humidity) for at least 48 hours. 2. Mount a properly conditioned and measured specimen (at least three specimens per stress level) in the grips.

		3. Attach the deformation measuring devices to the specimen (extensometer, i.e. LVDT).
	1.Temperature sensor	4. Apply full load rapidly and smoothly to the specimen, preferably in 1 to 5s (In no case shall the loading time exceed 5s.)
	2.Relative humidity sensor	a. At each test temperature, make a creep-rupture test at a minimum of seven load levels that will produce rupture at approximately the following times: 1 10 30 100 300 1000 and 3000 h (1/24, 30/24, 4 1/6, 12 ½, 41 2/3, 125 days)
	3.Time recorder	5. Measure the extension at the following approximate times 1, 6, 12, and 30 min; 1, 2, 5, 20, 50, 100, 200, 500, 700, and 1000h.
	4.Extensometer (LVDT)	6. Measure temperature, relative humidity, and other environmental variables and deformation of control specimen at the same times.
	5. Extensometer (LVDT) for slippage at the head of machine.	
	6.Load indicator	
3. Relaxation	1.Initial stress and strain data	1. Condition test specimen at the testing environment (23±2°C (73.4 ±3.6 ° F) and 50±10% relative humidity) for at least 48 hours.
ASTM E 328-02 (2008)	2.Final stress and strain data	2. Measure the diameter of rod specimens (at least five specimens must be tested), to the nearest 0.025 mm (0.001in) at a minimum of two points 90° apart.
		3. Anchorage, extensometer and strain gauge same as tensile test.
	1.Temperature sensor	4. If a strain gauge is to be set to the test piece, the test piece shall first be stretched taut by applying a load of 10-40% of the prescribed initial load; thereafter the strain gauge shall be attached and correctly calibrated.
	2. Extensometer	5. The initial load shall be either 70% of the guaranteed tensile capacity, or 80% of the million hour creep failure capacity, whichever is the smaller.

	(LVDT) 3. Extensometer (LVDT) for slippage. 4. Load indicator.	6. The initial load shall be applied at a rate of 200±N/mm^2 per minute and the strain on the test piece shall be fixed after the initial load is applied. It will be maintained for 120±2 seconds. This will be the start time for test. 7. Load reduction shall generally be measured over a period of at least 1000 hours. 8. Load reduction shall be recorded automatically and recorded for 1,3,6,15,30,45 min.;1, 1.5, 2, 4, 10, 24, 48, 72, 96, 120 hours and in general every 24 hours thereafter with a minimum of one measurement in every 120 hours.

APPENDIX II

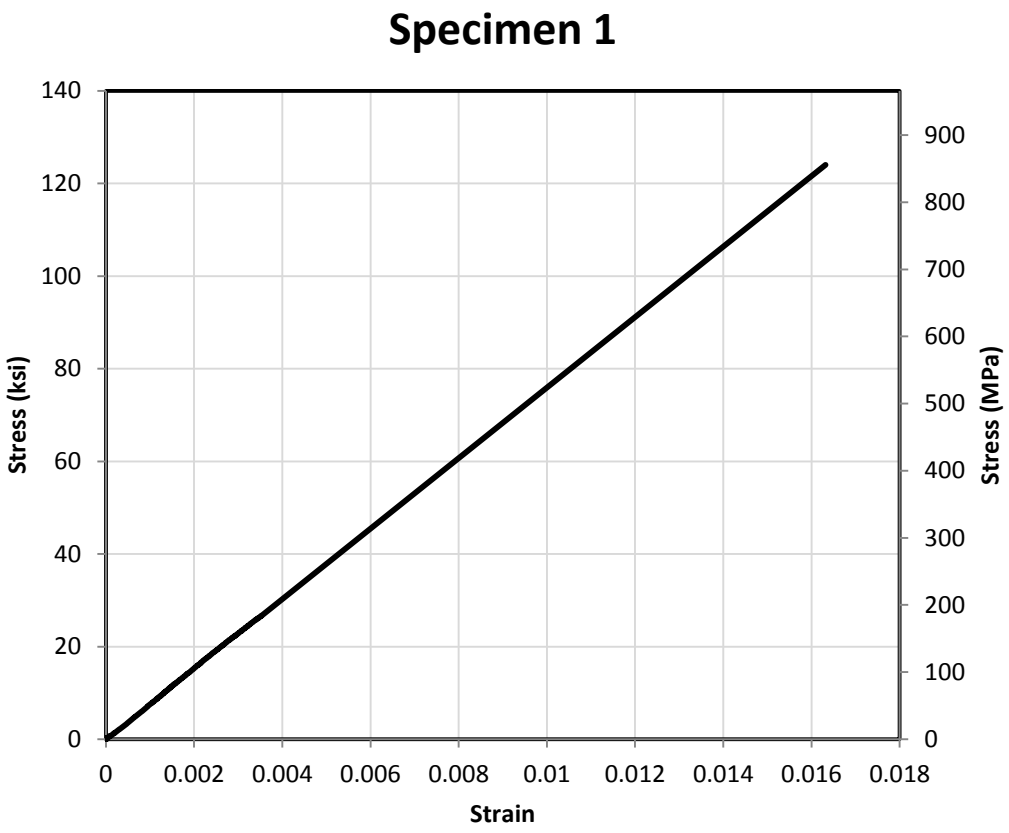

Figure 108 Specimen 1 anchorage system tensile test

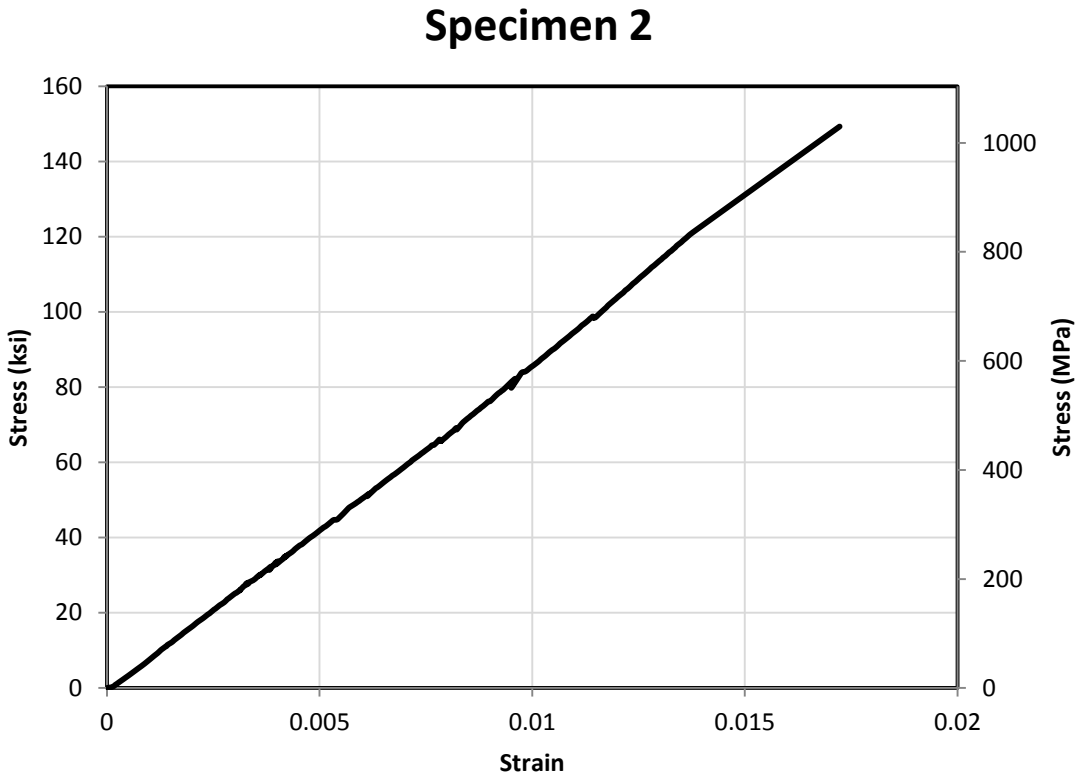

Figure 109 Specimen 2 anchorage system tensile test

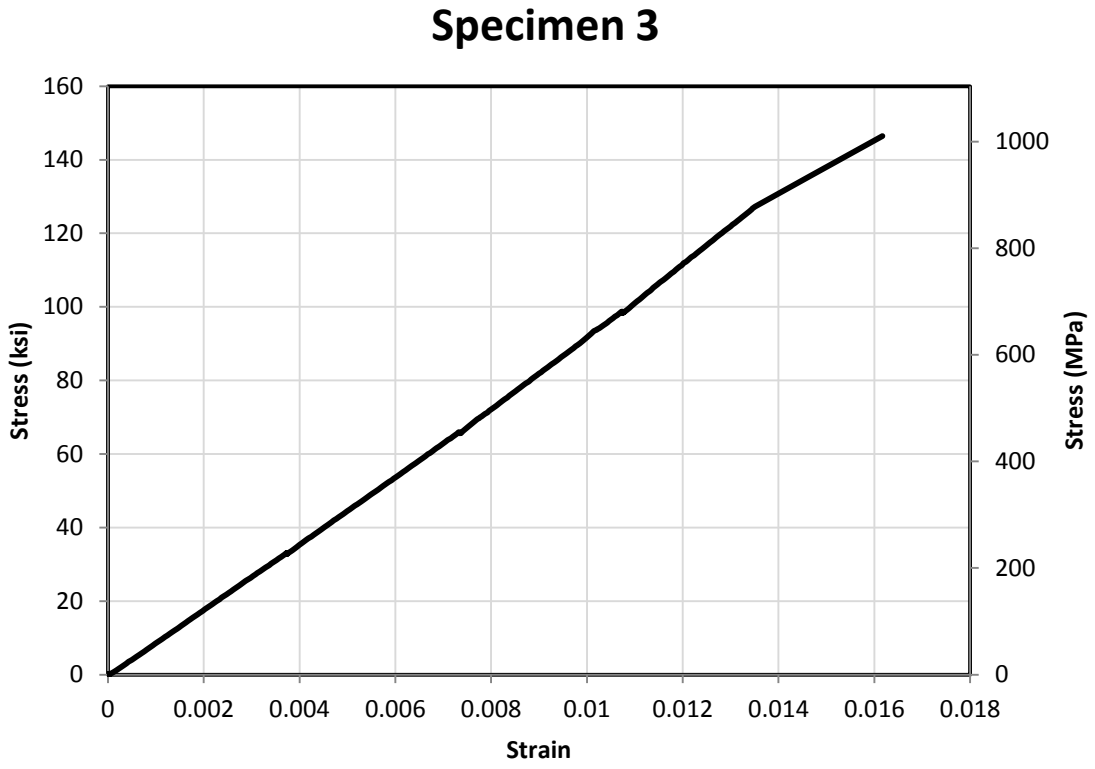

Figure 110 Specimen 3 anchorage system tensile test

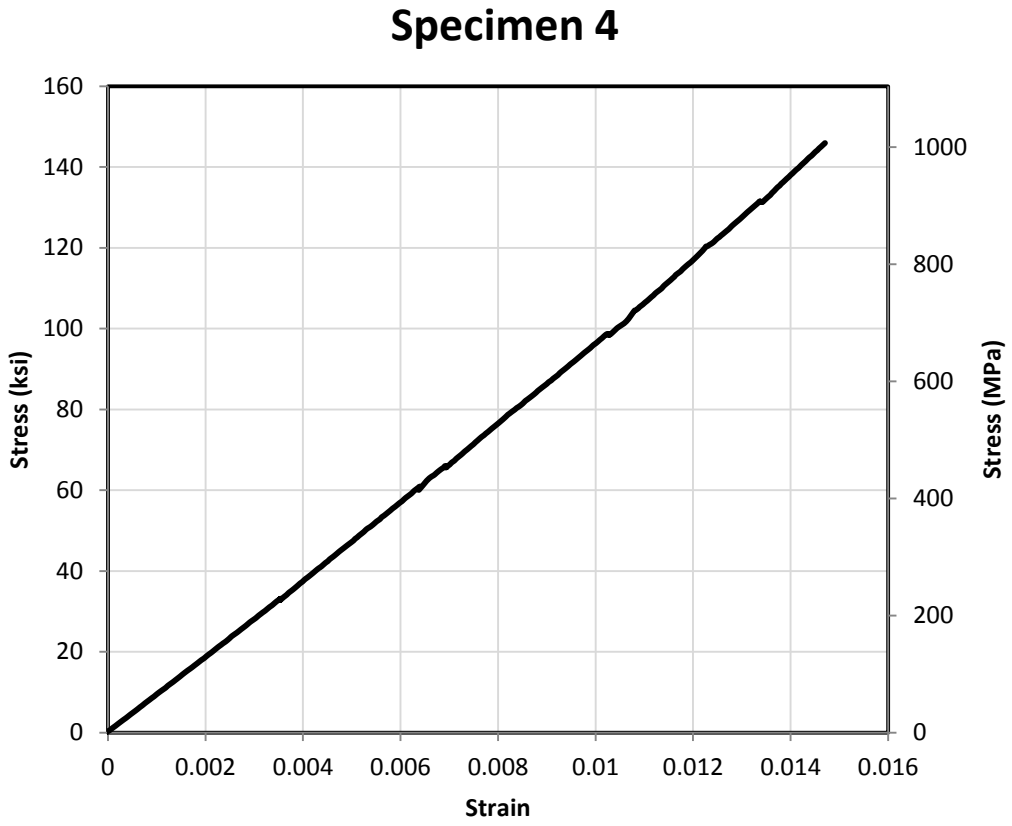

Figure 111 Specimen 4 anchorage system tensile test

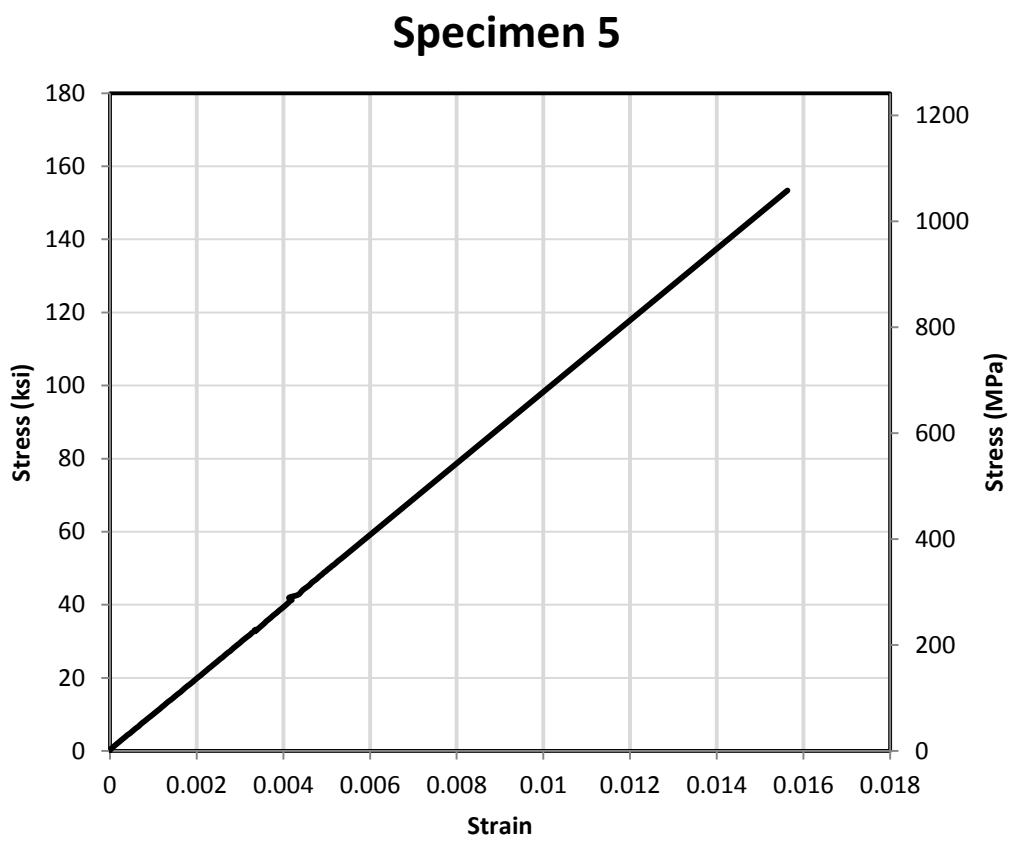

Figure 112 Specimen 5 anchorage system tensile test

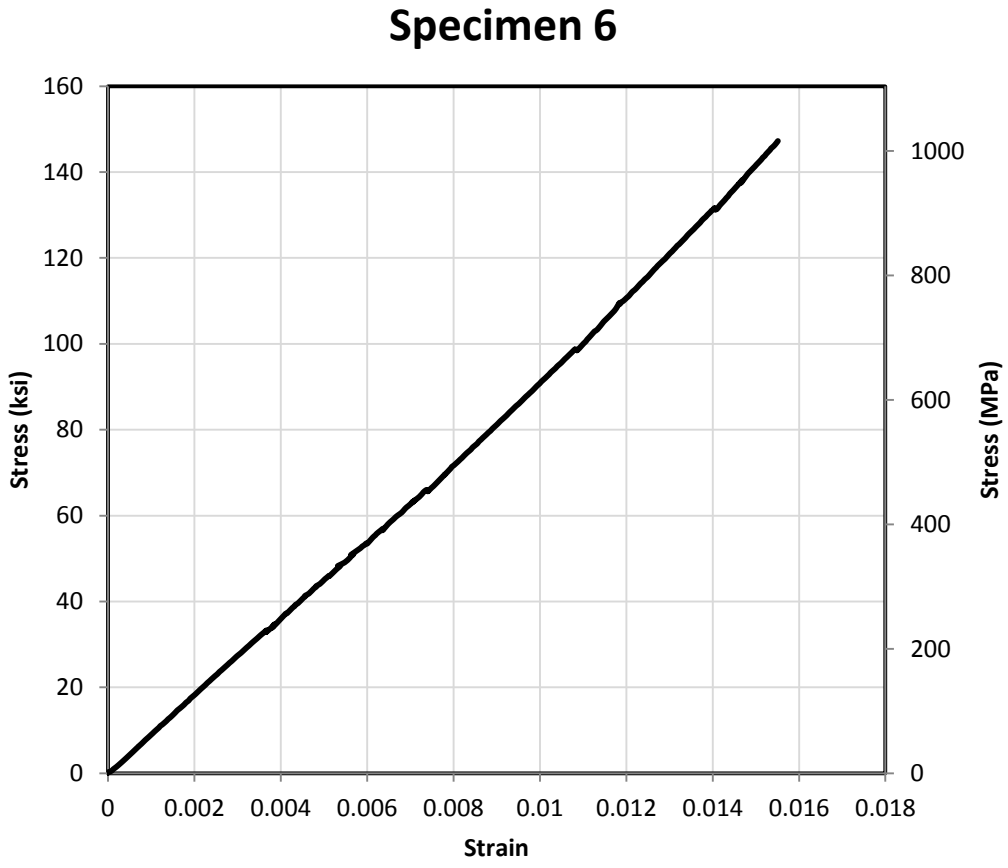

Figure 113 Specimen 6 anchorage system tensile test

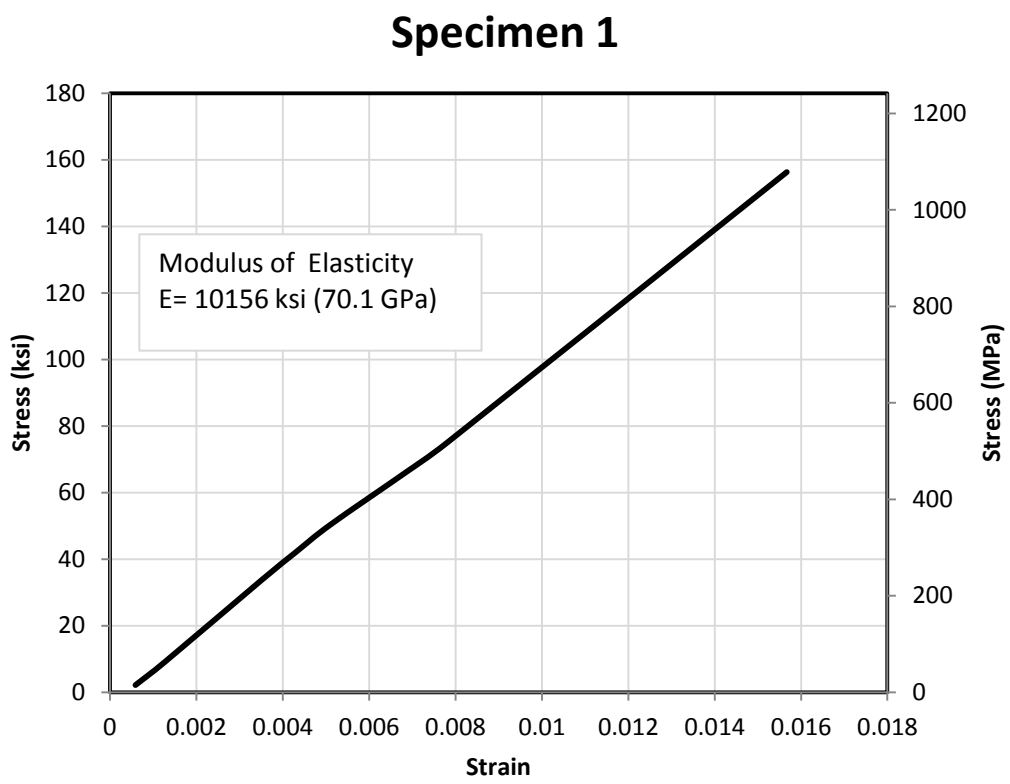

Figure 114 Specimen 1 grouted steel pipe anchorage system tensile test

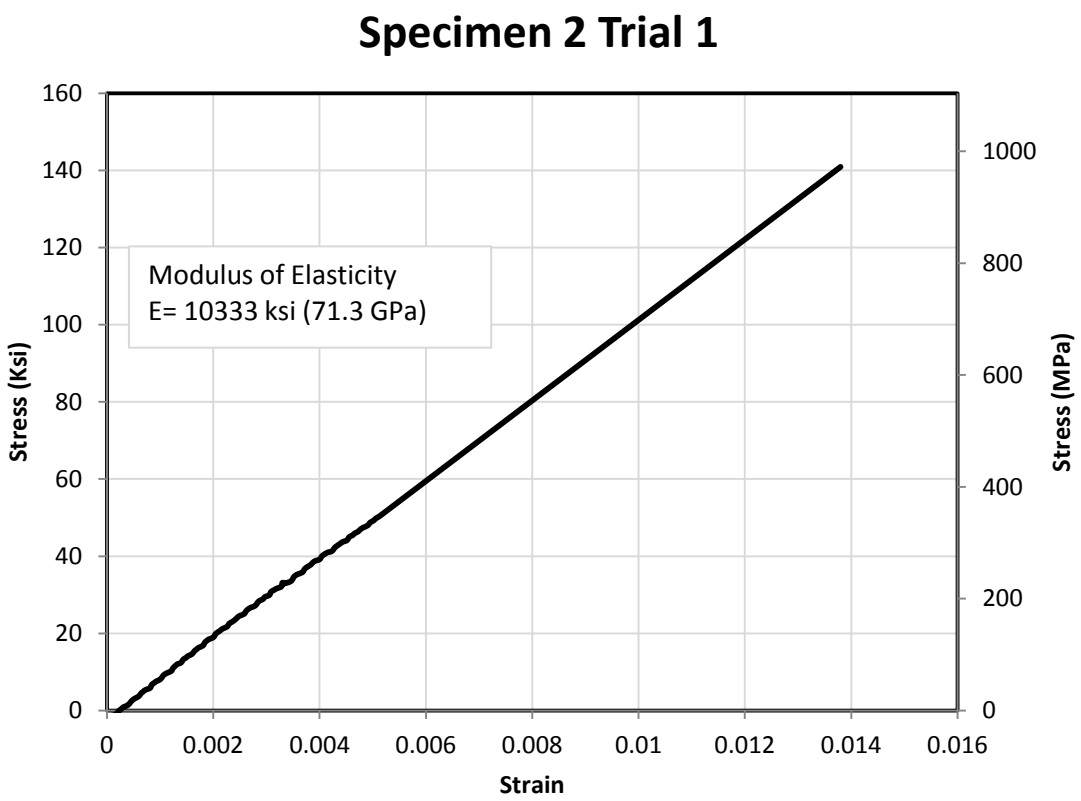

Figure 115 Specimen 2 trial 1 grouted steel pipe anchorage system tensile test

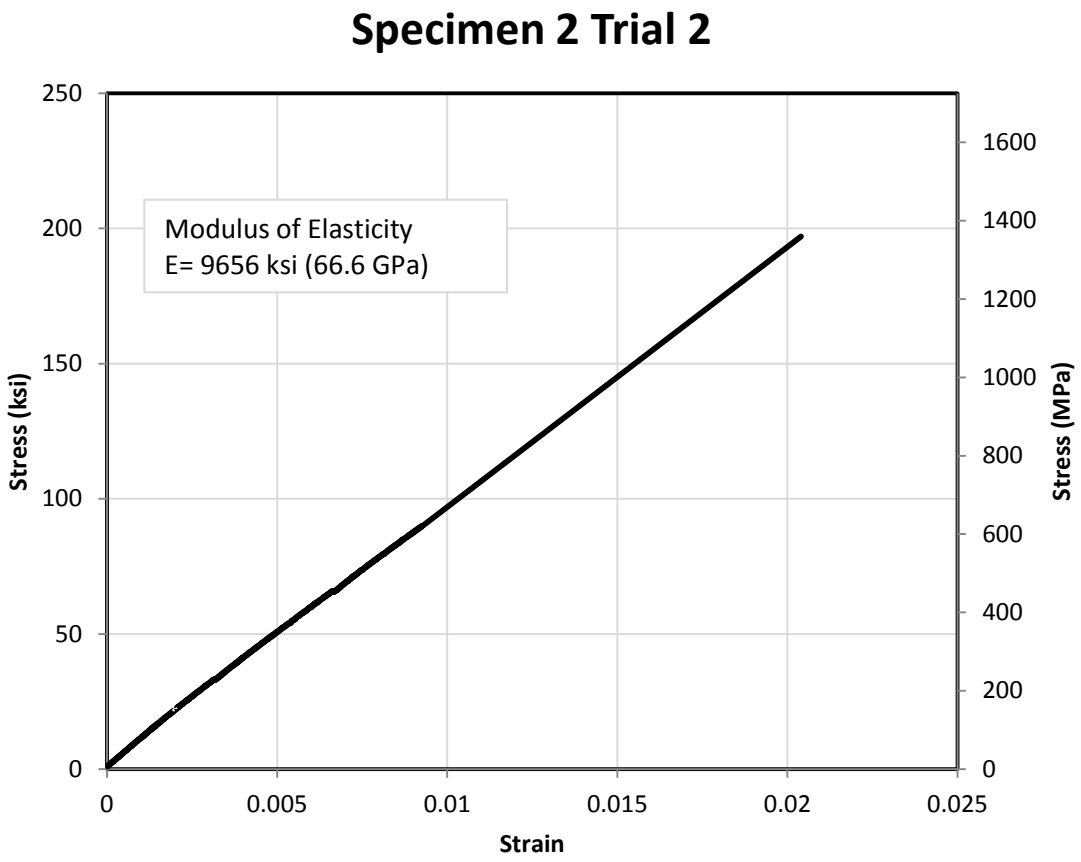

Figure 116 Specimen 2 trial 2 grouted steel pipe anchorage system tensile test

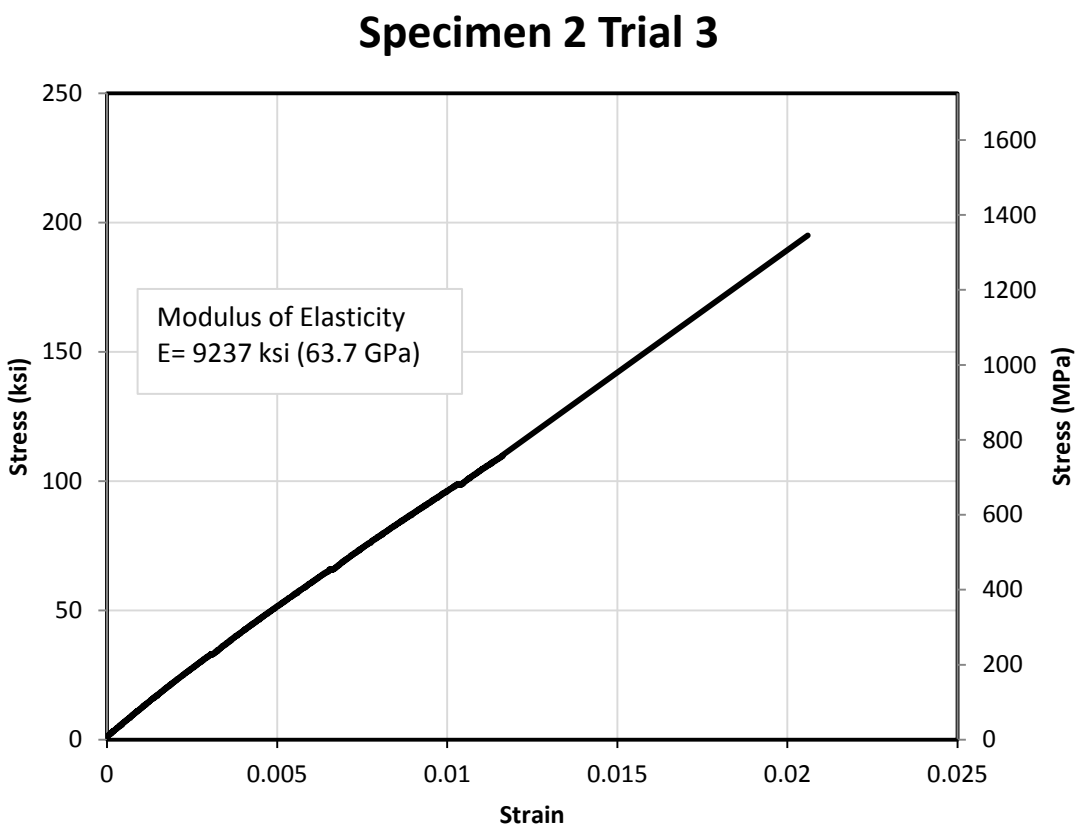

Figure 117 Specimen 2 trial 3 grouted steel pipe anchorage system tensile test

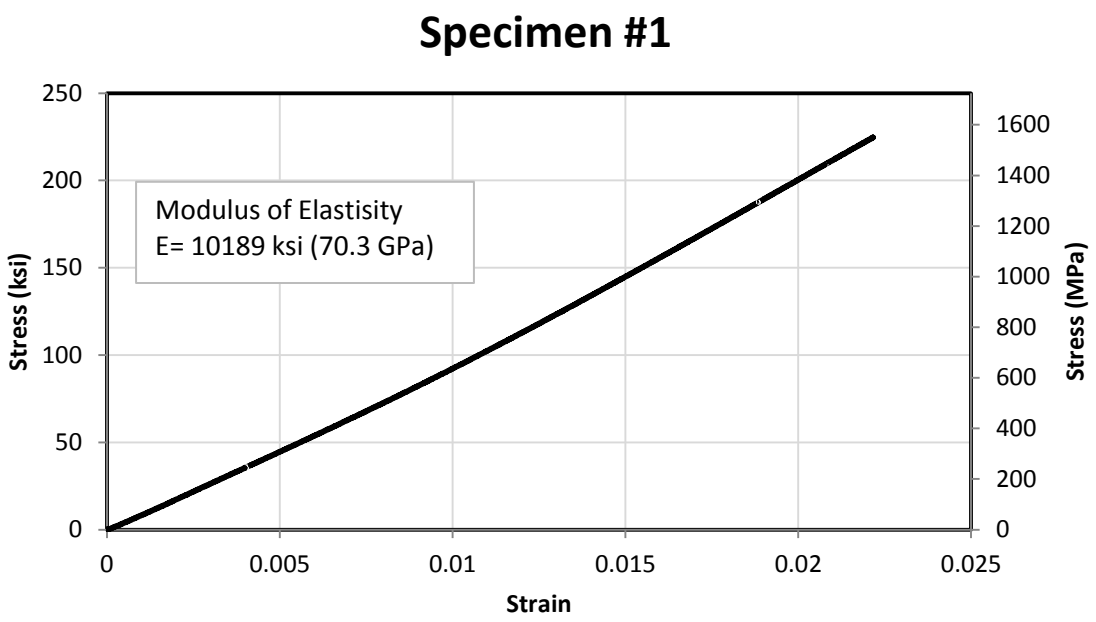

Figure 118 Arapree® AFRP tensile test specimen 1

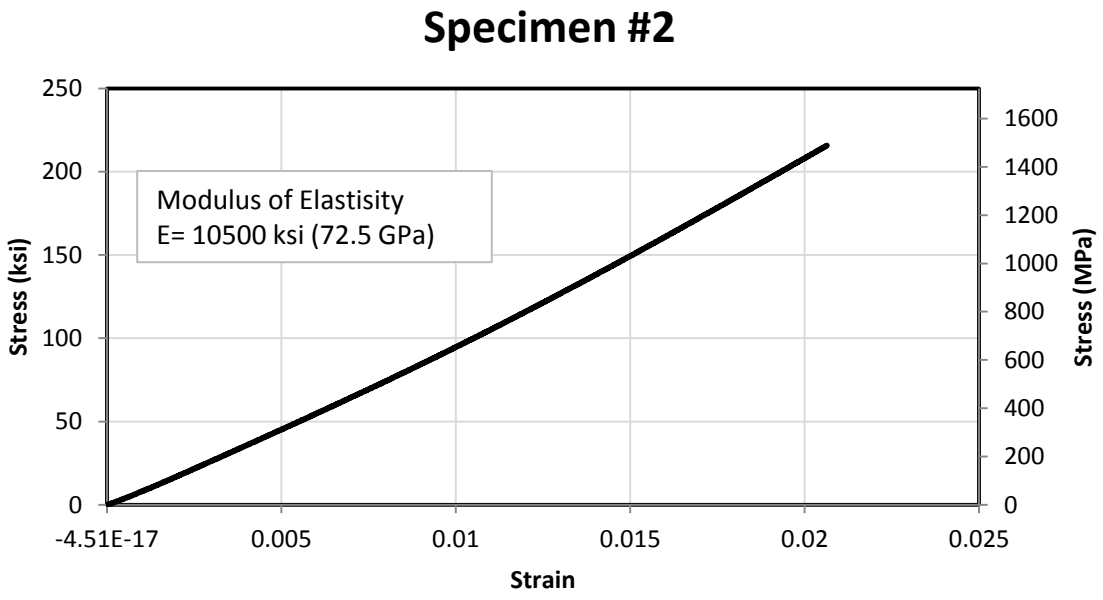

Figure 119 Arapree® AFRP tensile test specimen 2

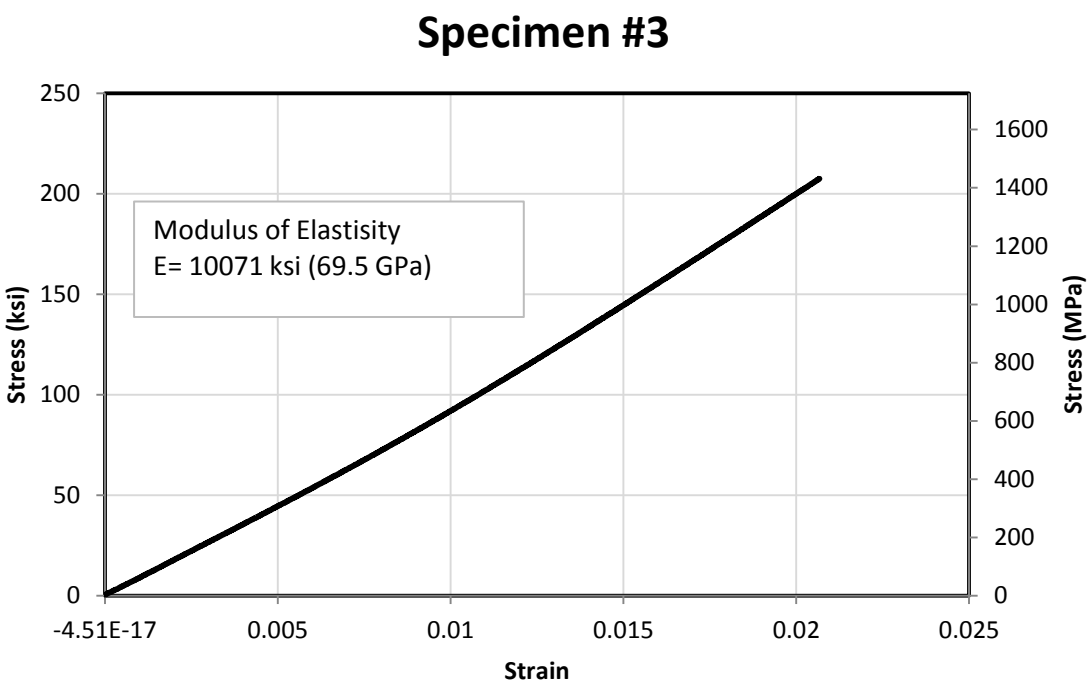

Figure 120 Arapree® AFRP tensile test specimen 3

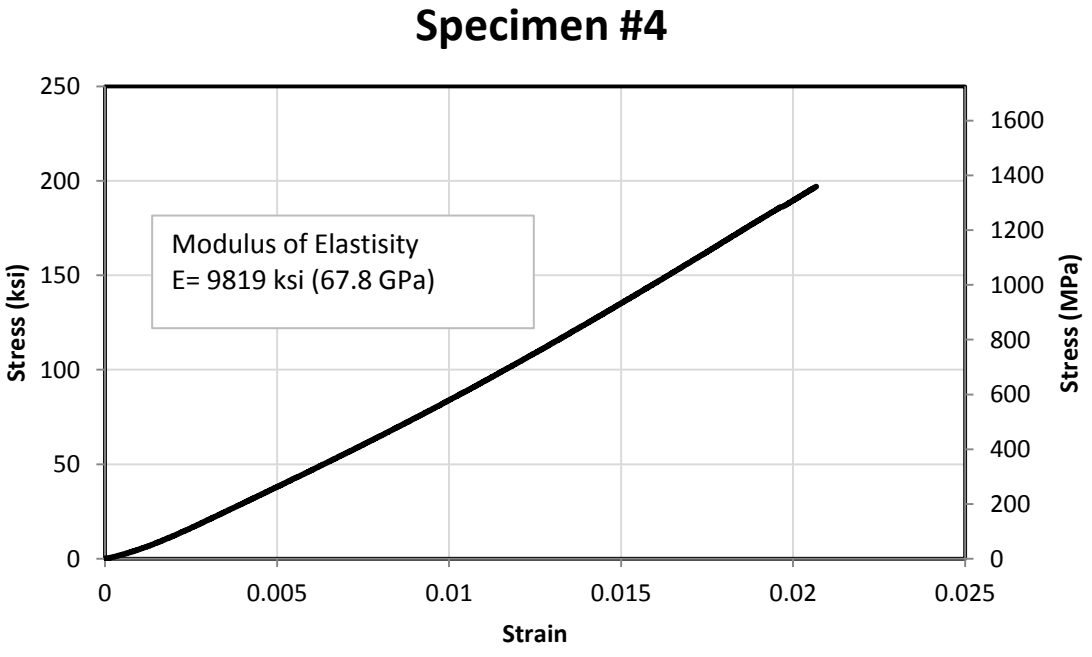

Figure 121 Arapree® AFRP tensile test specimen 4

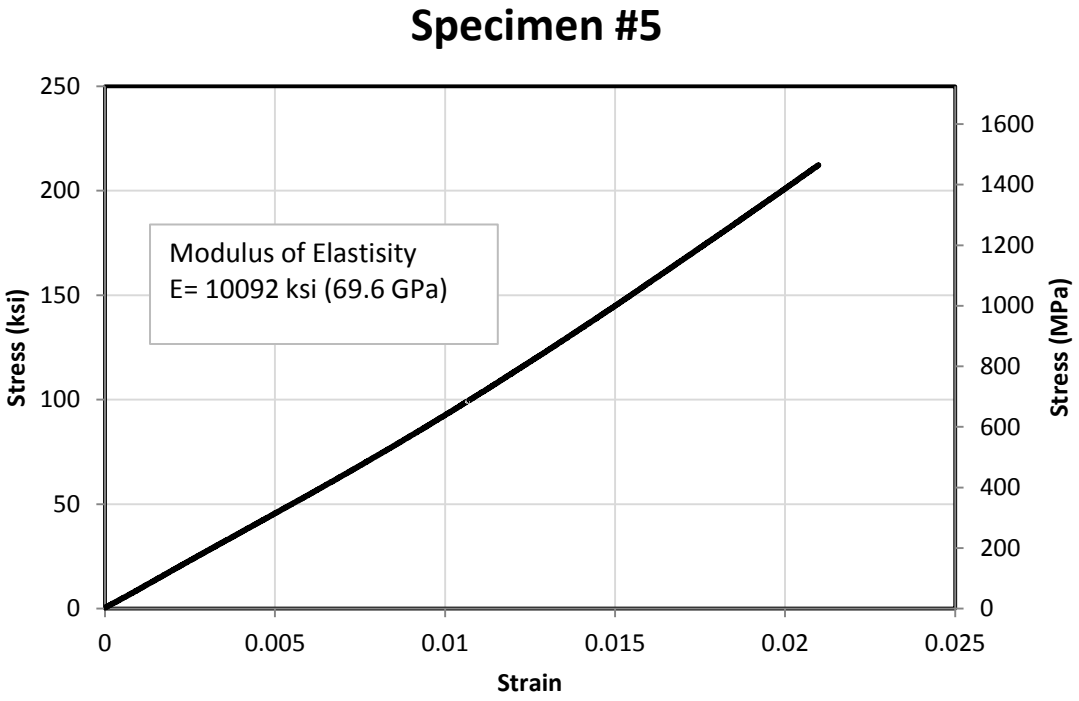

Figure 122 Arapree® AFRP tensile test specimen 5

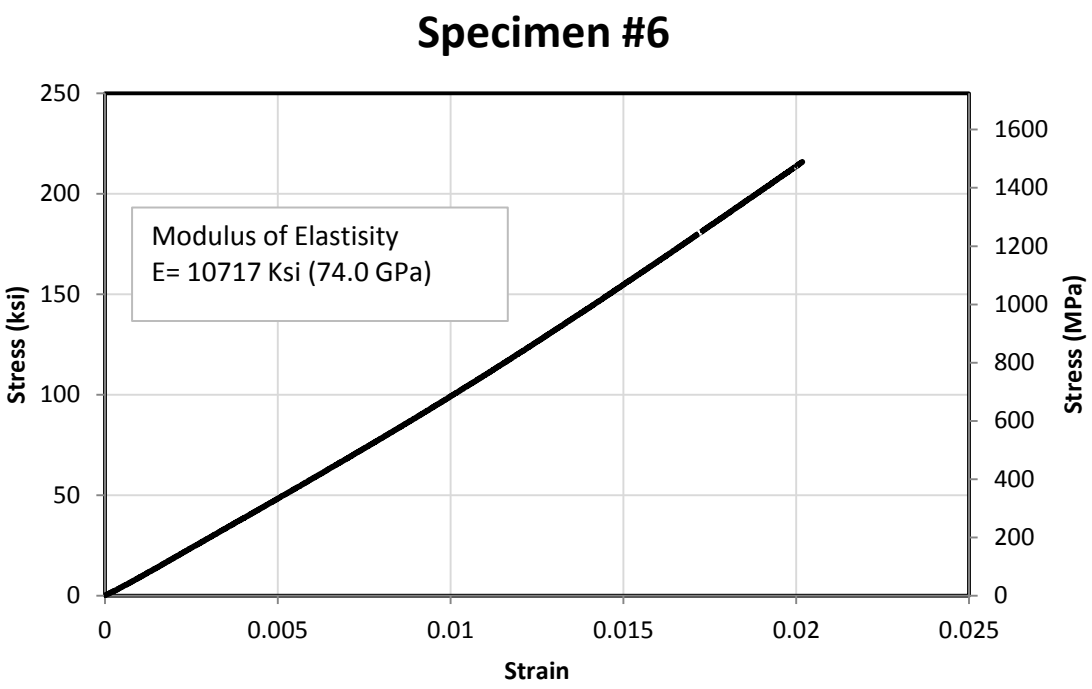

Figure 123 Arapree® AFRP tensile test specimen 6

APPENDIX III

Figure 124 Arapree® AFRP bar spool

Figure 125 Steel rotating wheel

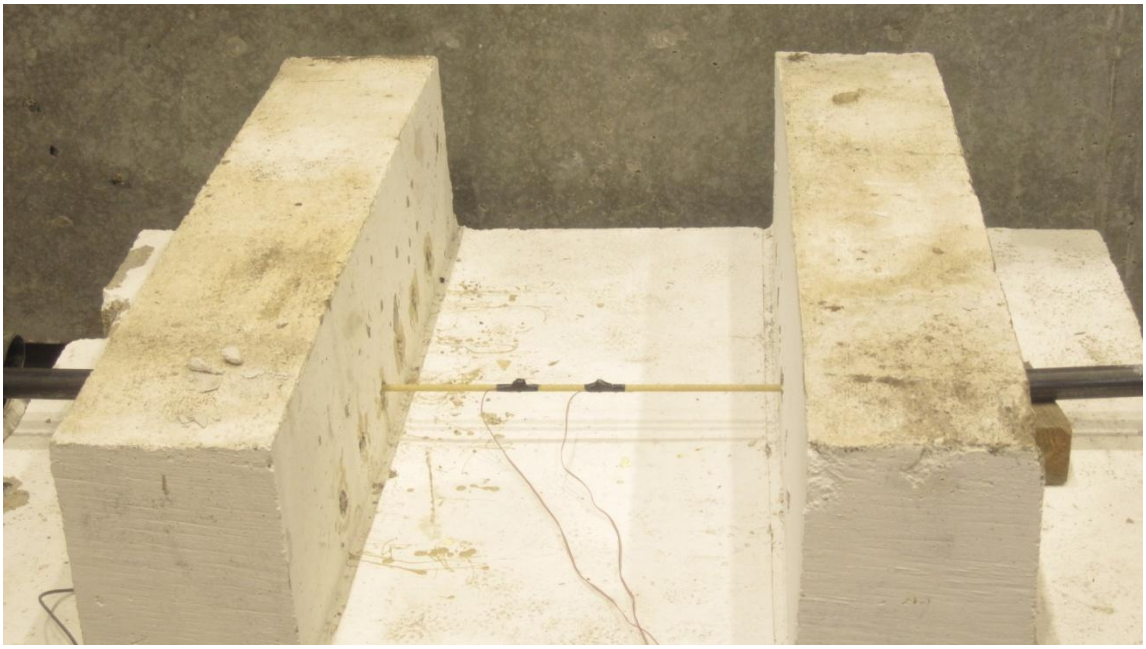

Figure 126 AFRP bar under test

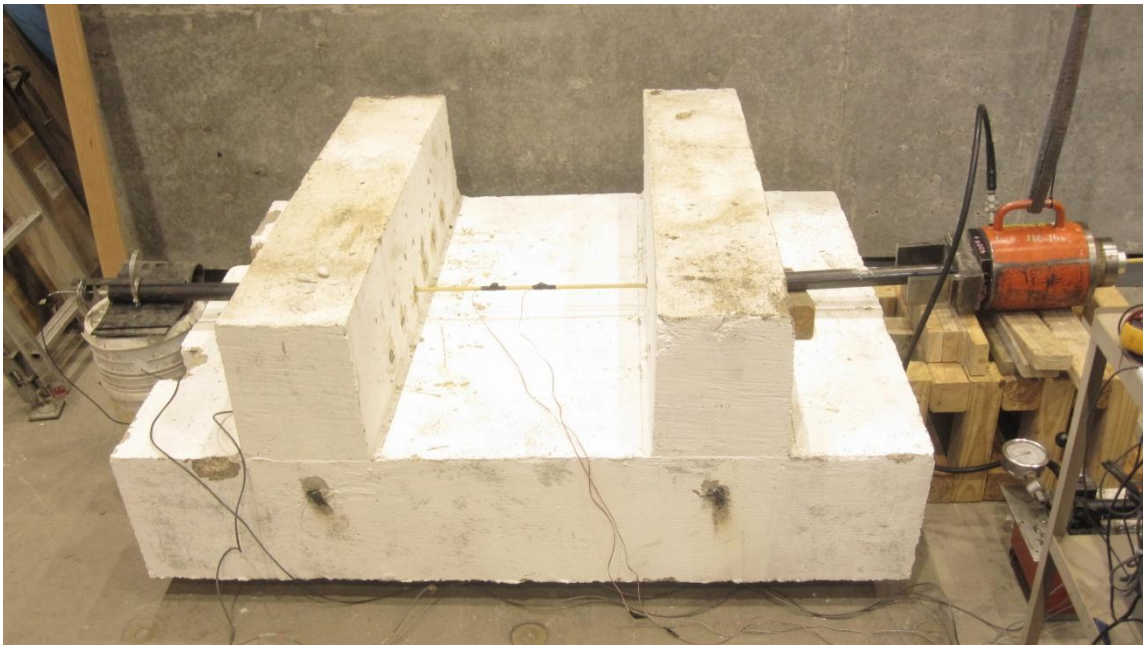

Figure 127 Prestressing operation

VITA

Name: Jose Carlos Medina Jr.

Address: Intecsea Worley Parsons Group
Structural Engineer Subsea Systems
575 N. Dairy Ashford
Houston, TX 77079

Email Address: jose.medina@intecsea.com

Education: B.S., Civil Engineering (Structures), Texas A&M University, 2009
M.S., Civil Engineering (Structures), Texas A&M University, 2011